Chemical Ionization Mass Spectrometry Study of Sulfuric Acid and Amine Chemical Nucleation Processes Pertinent to the Atmosphere

A DISSERTATION
SUBMITTED TO THE FACULTY OF
UNIVERSITY OF MINNESOTA
BY

Coty N. Jen

IN PARTIAL FULFILLMENT OF THE REQUIREMENTS
FOR THE DEGREE OF
DOCTOR OF PHILOSOPHY

Peter H. McMurry

June, 2015

Acknowledgements

I acknowledge funding support from UMN Graduate School Fellowship, Achievement Rewards for College Scientists, National Science Foundation Graduate Research Fellowship, and UMN Doctoral Dissertation Fellowship. The National Science Foundation Awards AGS1068201, AGS0943721, and CDI1051396 provided funds for measurements and model development. Field measurements and data analysis were supported by Atmospheric Radiation Measurement Climate Research Facility and the Office of Biological and Environmental Research of the U.S. Department of Energy Grant Nos. DE-SC0006861 and DE-SC0011780.

I thank my advisor, Peter McMurry, for being the best advisor a student could want. Peter has given me an unparalleled graduate experience by providing me space to independently develop my own ideas and arguments while challenging me to think carefully about every aspect and every written word of our research. I strive to be as patient, nurturing, creative, and intelligent as Peter in my future career. I also thank my pseudo co-advisor, Professor Dave Hanson at Augsburg College, for providing invaluable insights on mass spectrometry and nucleation. Dave taught me to think deeply about every detail in an experiment and data analysis. Without Dave, my thesis research would not have been nearly as successful.

I also acknowledge help from Drs. Fred Eisle and Jim Smith at National Center for Atmospheric Research for assisting in trouble shooting my mass spectrometer. I thank Professor Jun Zhao for his help in improving the Cluster CIMS and Dr. Mari Lee for passing on the most organized set of instructions for a custom built instrument. I thank Derek O., Modi C., Ranga G., Julien B., Mark S, and Roxy K. for providing daily support in the lab and in the field. I thank Professor V. Faye McNeill, Neha S., Allie S., and Sophie C. from Columbia University who gave me useful tips throughout my graduate career.

I am grateful for the unwavering support from my friends including, but not all, Tessie P., Yogesh D., Chris T., Alex M., Brian M., Drew C., Cloud Dragon H., Max E., Jeff T., Sid C., Jeff P., Matt I., Heather L., Megan H., Simon T., Gunnar A., Nick C., Julia C., Jamie Y., Teresa L., Alex C., Jake S., and Luke F. I finally thank my mother, father, and brother for inspiring me to be better person my whole life.

Dedication

This dissertation is dedicated to all the graduate students suffering from mental illness. Do not suffer alone.

Abstract

Clouds influence climate and cool the planet by reflecting incoming sunlight away from Earth's surface. The extent and brightness of these clouds depend on the composition and concentration of atmospheric particles, the starting point for cloud droplet formation. The majority of atmospheric particles originate from a process known as nucleation, whereby low volatility, gaseous precursors react to form stable clusters (~1 nm diameter). Sulfuric acid (H_2SO_4 or SA) is essential for atmospheric nucleation and in continental regions originates primarily from anthropogenic activities. However, atmospheric nucleation remains difficult to study due to the challenges of measuring incipient particles <1 nm (cluster containing ≤4 SA molecules plus water and other stabilizing compounds) and at atmospherically relevant concentrations of 1 part per quadrillion.

The purpose of my thesis work is (1) to better understand the technique of chemical ionization mass spectrometry (CIMS) for measuring SA and its clusters and (2) to measure and model how various atmospherically relevant basic gases, such as ammonia and amines, affect SA nucleation. The main instrument, the Cluster CIMS, uses nitrate (NO_3^-) to chemically ionize SA vapor and clusters at atmospheric pressure. My measurements and subsequent modeling of the chemical ionization processes show that nitrate is unable to ionize chemically neutral SA clusters, i.e. clusters that contain near equal numbers of acid and base molecules. In contrast, the acetate ion ($CH_3CO_2^-$) is capable of ionizing more cluster types, thereby providing more accurate measurements of cluster concentrations. These findings imply that a large fraction of clusters may have gone unobserved in ambient measurements due to inefficient nitrate chemical ionization.

To ensure that the Cluster CIMS accurately measures concentrations of larger SA clusters using acetate chemical ionization, I developed a method for comparing cluster concentrations measured by mass spectrometry with particle number concentrations measured by mobility classification/vapor condensation particle counter in the size range around 1 nm where they overlap. I used computational chemistry, particle dynamics, and

the diffusing transfer function of a mobility classifier to reconcile these two very different measurement techniques. Comparisons show good agreement between the instruments for ~1 nm clusters produced in a sulfuric acid/dimethylamine (DMA) environment.

The Cluster CIMS and a diethylene glycol scanning mobility particle sizer were also used to study how ammonia and amines react with SA vapor to form clusters and particles in a very clean flow reactor. Results show that DMA and diamines produce higher cluster and particle concentrations than methylamine and ammonia, which implies that they form less volatile clusters leading to higher nucleation rates. Diamines, including compounds such as cadaverine and putrescine, are a previously unstudied class of atmospherically relevant compounds that originate from industrial and natural sources. I observed that diamines+SA can produce 10 times more particles than DMA. Field measurements of diamines in Lamont, OK from spring, 2013 show gas phase diamine concentrations are equal to or greater than DMA concentrations. Thus, diamines are potent nucleating agents that likely contribute significantly to atmospheric nucleation. Overall, my thesis work improved nucleation instrumentation and increased knowledge on the chemical mechanisms behind atmospheric nucleation.

Table of Contents

List of Tables

List of Figures

Chapter 1. Introduction

1.1 Atmospheric Nucleation

Atmospheric particles are vital for cloud formation as they serve as seed particles for water condensation. The composition and concentration of atmospheric particles influence the extent and brightness of clouds and ultimately their cooling effect on the planet. The majority of atmospheric particles over land are produced from a process known as nucleation [*IPCC*, 2014], whereby gaseous sulfuric acid vapors condense and form stable particles. However, both laboratory and computational chemistry models have shown that the nucleation rate (i.e., the rate of particle production) by sulfuric acid and water alone is orders of magnitude lower than observed atmospheric nucleation rates [*Weber et al.*, 1996]. The chemical mechanisms behind atmospheric nucleation are poorly understood, resulting in large uncertainties in quantifying the extent to which atmospheric aerosols influence global climate [*IPCC*, 2014]. Thus, a better understanding of processes behind atmospheric nucleation is vital in improving global climate models.

Nucleation can be modeled as a series of reactions that lead to the net formation of clusters and, eventually, larger particles. The classical nucleation theory approach to single-component nucleation accounts only for vapor condensation or evaporation from clusters of a given size. For example in a system containing only compound *A*, the reaction scheme for the formation of a dimer (A_2), a cluster composed of two monomers (A_1), occurs at a forward rate constant of k_{11}. However, A_2 can also evaporate at a rate of E_1. This is described in Reaction 1 and can be extended to larger clusters/particles.

$$A_1 + A_1 \underset{E_1}{\overset{k_{11}}{\rightleftarrows}} A_2 \qquad \textbf{Reaction 1}$$

The evaporation rates serve as bottlenecks to nucleation by limiting the rate at which particles form. The maximum number of particles that can be produced in a system will occur if all the evaporation rates are zero. This upper limit is known as the collision-controlled limit [*Kürten et al.*, 2014; *McMurry*, 1980; *McMurry*, 1983] and implies that every cluster and particle is stable.

At equilibrium, the evaporation rate constant can be determined from the standard Gibbs free energy change of the reaction (ΔG^o), the Boltzman constant (k_B), and the temperature (T). For Reaction 1, the equilibrium constant, K_{eq}, is defined as

$$K_{eq,11} = \frac{k_{11}}{E_1} = \exp\left(\frac{-\Delta G^o}{k_B T}\right) \qquad \textbf{Equation 1}$$

where the forward rate constant, k_{11}, is the monomer collision rate. Classical nucleation theory combined with the liquid droplet model [*Becker and Döring*, 1935] has been applied to the sulfuric acid system to estimate free energies for the cluster formation reactions, and therefore evaporation rates. This model uses bulk vapor pressure and surface energy to balance the change in free energy of adding one molecule to a cluster with the change of free energy in expanding the surface of the cluster. The size at which free energy is maximized is known as the critical size and is where a cluster will have equal probability of evaporating or growing. Particles larger than the critical size grow faster than they evaporate, while evaporation rates for smaller particles exceed vapor condensation rates.

Since the atmosphere contains numerous other compounds, classical nucleation theory with sulfuric acid has been expanded to include two common compounds: water (binary system) and ammonia (ternary system). Nucleation rates predicted for the sulfuric acid-water system are up to 10 orders of magnitude lower than rates observed in the atmosphere [*Weber et al.*, 1996]. Furthermore, observations show that nucleation rates vary approximately in proportion to [sulfuric acid]^2, while classical theory predicts a much stronger dependence ([sulfuric acid]^p, $7<p<10$) [*Weber et al.*, 1996]**.** Including ammonia at 5 pptv in the sulfuric acid-water system dramatically increases predicted nucleation rates (likely even higher if ammonia concentrations match observed concentrations in the ppbv range) [*Coffman and Hegg*, 1995] but are up to 20 orders of magnitude higher than predicted sulfuric acid-water nucleation rates and up to 10 orders higher than observed rates [*Weber et al.*, 1996]. These ternary nucleation rates are

unrealistically too high as they exceed the collision-controlled rate by 2-3 orders of magnitude [*Zhang et al.*, 2010].

The classical theory for atmospheric nucleation fails for several reasons. First, the model assumes bulk properties of the liquid component, such as its density and vapor pressure, can be extended to the 1 nm size scale, the approximate size of stable clusters in the atmosphere. These clusters contain only a few (2-4) sulfuric acid molecules. Such extrapolations are highly inaccurate because they neglect quantum mechanical interactions between molecules such as proton transfers. In addition, classical theory assumes clusters of size *g* (i.e., clusters that contain *g* sulfuric acid molecules) will have the same composition and physical properties. We now know this is inaccurate as clusters of size *g* also contain varying numbers of other molecules (see Chapter 3). Each of these cluster types will have its own thermodynamic properties and will therefore exhibit different evaporation rates. This reality needs to be taken into account.

Alternatively to classical nucleation theory, the evaporation rates and free energies can be estimated from a kinetic perspective where the accumulation of a cluster/particle of a specific size, *g*, is described by its formation and destruction. This is detailed in the cluster balance equations. Equation 2 provides the cluster balance equation for a single component system where the concentration of clusters containing *g* molecules of *A*, [A_g], as a function of time equals its formation and loss rates.

$$\frac{d\left[A_g\right]}{dt} = \sum_{i+j=g} k_{ij}\left[A_i\right]\left[A_j\right] + E_{g+1}\left[A_{g+1}\right] - E_g\left[A_g\right] - \kappa\left[A_g\right] - \eta\left[A_g\right] \qquad \textbf{Equation 2}$$

where κ is the coagulation loss rate with other clusters/particles and η is the loss rate to surfaces. E_g is the evaporation rate of *A* from A_g, and E_{g+1} is the evaporation rate of *A* from a cluster size g+1 to form A_g.

The kinetic model must be expanded to include multiple components as recent research has shown that sulfuric acid vapors and cluster react with various compounds to form stable cluster that evaporate less. These stabilizing compounds include ammonia

[*Chen et al.*, 2012; *Hanson and Eisele*, 2002; *Weber et al.*, 1998], amines [*Almeida et al.*, 2013; *Chen et al.*, 2012; *Glasoe et al.*, 2015; *Jen et al.*, 2014; *Kürten et al.*, 2014; *Zhao et al.*, 2011], oxidized organics [*Schobesberger et al.*, 2013], and water [*Hanson and Eisele*, 2002]. The multi-component reaction model must then take into account formation of clusters by the combination of these various compounds.

To illustrate, consider the two component system containing compounds *A* (sulfuric acid) and *B* (stabilizing compound). The classifications of cluster size are defined by the number of *A* molecules in the cluster but may also contain any number of *B* molecules. We use the term "dimer" to denote clusters that contain two *A* molecules and ≥0 molecules of B. The formation of a dimer in this two component system can then be described the reaction scheme detailed in Reaction 2. This scheme predicts three types of dimer (A_2, A_2•B and A_2•B_2) and two types of monomer (A_1 and A_1•B), each with its own evaporation rate.

$$A_1 + A_1 \underset{E_2}{\overset{k_{11}}{\rightleftarrows}} A_2$$

$$A_1 + B \underset{E_1}{\overset{k_B}{\rightleftarrows}} A_1 \bullet B$$

$$A_1 \bullet B + A_1 \underset{E_{2,A}}{\overset{k_{2,B}}{\rightleftarrows}} A_2 \bullet B \qquad \textbf{Reaction 2}$$

$$A_2 + B \underset{E_{2,B}}{\overset{k_B}{\rightleftarrows}} A_2 \bullet B$$

$$A_1 \bullet B + A_1 \bullet B \underset{E_{2,B2}}{\overset{k_{1,B}}{\rightleftarrows}} A_2 \bullet B_2$$

Cluster balance equations can be written for each cluster type. For example, the cluster balance equation for A_2•B is

$$\frac{d[A_2 \bullet B]}{dt} = k_B[A_2][B] + k_{2.B}[A_1 \bullet B][A_1] - [A_2 \bullet B](E_{2,A} + E_{2,B}) - [A_2 \bullet B](\kappa + \eta) \qquad \textbf{Equation 3}$$

Overall, six cluster balance equations are needed to describe Reaction 2, including one to describe the consumption of *B*. More equations will be needed if additional cluster types are added, such as A_2•B_3, or if more compounds are added to the system. Once the concentration of precursor gases (e.g. sulfuric acid and stabilizing compounds) and the

evaporation rates are known, then the cluster balance equations can be solve to predict nucleation rates of particles of a certain size.

Previous research has determined evaporation rates using two distinct but complementary methods. Computational chemistry, specifically density functional theory, has been used by the Vehkamäki group to calculate the free energy of each cluster type. Evaporation rates can be extracted from the energies following equilibrium thermodynamics (Equation 1) [*Ortega et al.*, 2012]. In addition, the Vehkamäki group has developed a program to simulate time-evolved cluster concentrations by solving the balance equations with their calculated evaporation rates [*McGrath et al.*, 2012]. Our group uses the second approach and solves the cluster balance equations for evaporation rates from experimental observations that were measured using recently developed instrumentation. Jiang et al. [2011c] presented first measurements of the complete atmosphere particle distribution down to one molecule of sulfuric acid. However, cluster concentrations measured by mass spectrometry are not comprehensive and do not include every type of sulfuric acid cluster that may exist. In addition, solving the interdependent cluster balance equations for evaporation rates likely leads to large uncertainties. Thus to model atmospheric nucleation, our group has developed a simplified hybrid model that focuses on the key bottleneck steps in the chemical nucleation and identifies atmospherically relevant stabilizing compounds. This heuristic model, known as the acid-base chemical reaction model, calculates evaporation rates based upon measureable quantities .

1.2 Heuristic Acid-Base Chemical Reaction Model for Atmospheric Nucleation

First published in Chen et al. [2012], the acid-base reaction model groups clusters with g number of sulfuric acid molecules (but varying numbers of B stabilizing compounds) into one group labeled N_g. Examples are given in Table 1.

Table 1 Examples of cluster types for each cluster size, where A=sulfuric acid and B=stabilizing compound

Label, cluster size	**Possible cluster types**
Monomer, N_1	A_1, A_1•B
Dimer, N_2	A_2, A_2•B, A_2•B_2
Trimer, N_3	A_3, A_3•B, A_3•B_2, A_3•B_3

The cluster formation reactions then follow the single component reaction scheme (c.f. Reaction 1) in that each cluster size can grow via condensation or evaporation of N_1. However unlike the single component system, the acid-base model also explicitly infers key stabilizing reaction steps from observations. For example, a dimer may evaporate or react with a basic compound to form a lower volatility dimer that does not evaporate. These two types of dimers are indistinguishable to the mass spectrometer (for reasons discussed below) but the total [N_2] will show a positive dependency on [B]. This trend will be captured by including the reaction of the dimer with *B*. Depending on the data available, these stabilizing reactions can be general or target specific cluster types. Due to instrument limitations, previous experimental observations resulted in only including generalized stabilizing reactions, such as N_2 reacting with *B* to form a lower volatility N_2 [*Chen et al.*, 2012]. Experimental results presented here combined with computational chemistry results have refined these reactions to include more specific reactions such as A_1 reacts with *B* to form A_1•B.

Unlike the full, multi-component model where each cluster formation pathway must be taken into account, this acid-base reaction model uses measured cluster concentrations and computational chemistry to chart out most likely cluster formation pathways. Fitted evaporation rates then represent an average over the rate limiting steps to form clusters of that specific size. Furthermore, additional components can be added to the acid-base model without significantly complicating the cluster balance equations by including only their significant reaction steps to the cluster formation pathways. Overall, this heuristic chemical reaction model for nucleation provides a useful tool for identifying

potential stabilizing compounds, calculating average evaporation rates, and determining which generalized cluster formation steps are the bottlenecks to nucleation.

Chen et al. [2012] used the acid-base model to explain experimental observations and determined that sulfuric acid dimers and trimers (with some number of attached stabilizing molecules) evaporate to some extent, implying that evaporation from the dimer and trimer sizes were the primary bottlenecks to nucleation. Kürten et al. [2014] found that the dimer, with two sulfuric acids and one or two dimethylamine molecules, is the first cluster size to not evaporate. Taken together, these results suggest that the identity of the stabilizing compound affects the evaporation rates of sulfuric acid clusters. Furthermore, these observations demonstrate that nucleation rates are limited by the formation of clusters that contain fewer than four sulfuric acid molecules. Since nucleation rates are determined by the formation of such small clusters, the problem is more tractable than would otherwise be the case.

I have focused my research on pinpointing specific stabilizing agents and quantifying the relative extents to which they enhance nucleation. This is challenging for two reasons:

1) Atmospheric nucleation involves reactions between gases that are present at exceeding low concentrations. Creating an environment where sulfuric acid only interacts with a specific stabilizing compound entails reducing the impurity levels below 0.1 pptv.

2) Measuring vapors, clusters, and freshly formed particles (~1 nm in diameter) at atmospherically relevant concentrations (≥1 ppqv) requires very sensitive instrumentation. While an instrument for measuring sulfuric acid vapor concentrations as low as 1 ppqv has been available since 1993 [*Eisele and Tanner*, 1993], methods to measure other trace compounds that might react with and stabilize sulfuric acid clusters has only recently been developed [*Hanson and Eisele*, 2002; *Hanson et al.*, 2011].

The work presented in the following chapters uses an extraordinarily clean and repeatable flow reactor to produce a constant source of sulfuric acid vapor. Various basic gases were injected into the flow reactor and, depending on the experiment, given 3 or 40 s to react with sulfuric acid. The resulting cluster concentrations were measured using the Cluster Chemical Ionization Mass Spectrometer (Cluster CIMS) [*Titcombe*, 2012; *Zhao et al.*, 2010], and particle number distributions were monitored using a Diethylene Glycol Scanning Mobility Particle Sizer (DEG SMPS) [*Jiang et al.*, 2011b]. Results from these measurements provide solid experimental evidence that atmospheric nucleation can be described by an acid-base chemical reaction model and use this framework to explore possible compounds that could stabilize sulfuric acid clusters and enhance nucleation rates to levels observed in the atmosphere.

1.3 Nanoparticle and Cluster Instrumentation

The DEG SMPS is capable of detecting particles down to ~1 nm in diameter (geometric size) [*Jiang et al.*, 2011b]. Neutral particles are first charged in a bipolar charger (Po-210 alpha source) then size separated in a nano-mobility classifier. Classified particles are then grown to detectable sizes via DEG and butanol condensation. However, the DEG SMPS only provides size and concentration data with no clues on particle composition. The concentration measurements of the DEG SMPS are also uncertain as particle composition influences measurement to an extent that remains to be quantified [*Jiang et al.*, 2011b]. My research provides some insights into those uncertainties.

Atmospheric pressure chemical ionization mass spectrometers (CIMS) have very recently been deployed to provide vapor and cluster information including cluster size, composition, and concentration. These instruments include the Cluster CIMS [*Titcombe*, 2012; *Zhao et al.*, 2010] and the Chemical Ionization Atmospheric Pressure Interface-Time of Flight mass spectrometer (CI-APi-ToF) [*Jokinen et al.*, 2012]. Both instruments use a soft ionization technique known as chemical ionization (CI) to charge neutral clusters at atmospheric pressure. Soft ionization reduces cluster fragmentation, and atmospheric pressure ionization allows for greater sensitivity in measuring low concentrations of neutral vapors and clusters [*Gross*, 2010]. Specifically, the University

of Minnesota Cluster CIMS is capable of measuring concentrations down to 10^5 cm^{-3} (~40 ppqv).

Chemical ionization can be conceptualized as an acid-base reaction. To produce negative ions, the neutral cluster must have lower proton affinity (i.e., must be more acidic) than the reagent ion. Traditionally, nitrate (NO_3^- with ligands) is used to charge sulfuric acid vapor and its clusters. An example CI reaction of the sulfuric acid dimer is given below.

$$(H_2SO_4) \bullet X + HNO_3 \bullet NO_3^- \rightarrow H_2SO_4 \bullet HSO_4^- + X + 2HNO_3 \qquad \textbf{Reaction 3}$$

X describes compounds that are attached to the sulfuric acid dimer but evaporate upon chemical ionization or entering the vacuum region of the mass spectrometer. Since the nitrate reagent ion ($HNO_3 \bullet NO_3^-$) is a very weak conjugate base (low proton affinity), only a few compounds are acidic enough to donate a proton to it; this limits the number of compounds that nitrate CI is able to detect. In the atmosphere, sulfuric acid is one of the few compounds that undergoes CI by nitrate ions. Therefore, using nitrate reduces interferences from non-sulfuric acid signals relative to those that would occur if a more basic reagent ion were used. For clusters that are more basic, we use protonated water clusters (H_3O^+ with water ligands) to positively charge electrically neutral clusters.

The Cluster CIMS uses an electric field to draw the reagent ions (e.g. nitrate or protonated water clusters) perpendicularly across the flow containing the neutral clusters. The mobility of the reagent ion is known, so the time they have to react with neutral clusters depends on their cross-flow velocity, which can be varied by adjusting the electric field (i.e., the voltage across the inlet). The CI reaction time dictates the amounts of ionized clusters formed (which translates to signal intensity) and controls the extent to which ionized sulfuric acid vapors can combine with neutral vapors/clusters to form charged clusters, a process known as ion-induced clustering (IIC) [*Hanson and Eisele*, 2002]. IIC leads to false ion counts for larger clusters and higher than predicted neutral cluster concentrations. IIC can be suppressed by reducing the CI reaction time, however

this also decreases overall signal. My work examines the effects of IIC on the accuracy of Cluster CIMS measurements.

IIC is just one source of uncertainty for the Cluster CIMS (and CI-APi-ToF). Overall, the process of measuring clusters with these mass spectrometers remains poorly understood. For example, chemically ionizing neutral clusters likely leads to changes in cluster composition (see X in Reaction 3), with basic molecules evaporating from the resulting ion cluster [*Kurtén et al.*, 2011]. Furthermore, neutral clusters containing near equal numbers of acid and base molecules may have too high of a proton affinity (too basic) to be chemically ionized by nitrate. This would cause measured concentrations to be less than true values. Thus, to better map out the acid-base chemical reactions, I carried out experiments aimed at exploring these sources of uncertainty. This work has led to a better understanding of cluster concentration and composition data obtained with the Cluster CIMS.

1.4 Outline of Research

This dissertation addresses two key gaps in knowledge: the chemical reactions behind atmospheric nucleation and the instruments used to measure freshly formed clusters and particles. In Chapter 2, the Cluster CIMS was used to measure sulfuric acid dimer concentrations in the presence of various atmospherically relevant basic compounds. The measured concentrations present clear evidence that basic gases react with sulfuric acid to form more stable sulfuric acid dimers and support the acid-base chemical reaction model for atmospheric nucleation. The study also identifies which basic gases stabilize sulfuric acid dimers and reduce evaporation rates the most. The measured monomer and dimer concentrations were then used to fit cluster evaporation rates from the acid-base reaction model and predict atmospheric nucleation rates from measured precursor gas concentrations.

However, the acid-base reaction model developed in Chapter 2 and its fitted evaporate rates rely on several assumptions for the larger clusters that likely affect predicted nucleation rates. Unlike the sulfuric acid dimer, the larger clusters exhibit much

larger sources of uncertainty due to poor understanding of the chemical ionization and ion-molecule interactions. To better understand and quantify these uncertainties, Chapter 3 develops a method to compare number concentrations of sulfuric acid+dimethylamine clusters measured by two fundamentally different instruments in their overlapping size range of 1 nm: Cluster CIMS and a DEG SMPS. The comparison indicates that nitrate reagent ions are unable to chemically ionize clusters with near equal numbers of acid and base molecules. Acetate chemical ionization with the Cluster CIMS measured more clusters and led to significantly improved agreement with the number concentrations measured by the DEG SMPS. Furthermore, the DEG SMPS measured higher than predicted concentrations of particles in the pure sulfuric acid environment, suggesting that 1 nm particles are being produced in the charger (via IIC).

After identifying possible uncertainties that may affect the 1 nm size range of the DEG SMPS, this instrument was used to show that diamines, a previously unstudied group of stabilizing compounds, react with sulfuric acid to produce more particles than dimethylamine. Chapter 4 presents particle measurements that indicate diamines are more effective at stabilizing sulfuric acid clusters and enhancing nucleation rates than dimethylamine. The concentrations of putrescine and cadaverine, both naturally produced diamines, were measured during atmospheric observations in rural Oklahoma. These concentrations (10-100 pptv) were equal to or greater than dimethylamine concentrations at this site, so diamines are likely to significantly contribute to atmospheric nucleation.

Chapter 5 builds upon the discoveries of the previous chapters by exploring the chemistry behind cluster formation for monoamines and diamines based upon observed concentrations of the larger clusters. To understand the observed trends, the acid-base neutral cluster formation model from Chapter 2 is expanded to explicitly include formation of larger clusters and is coupled to models that describe chemical ionization, ion-induced clustering, and ion decomposition. Cluster observations and modeling help identify particular ion cluster behavior in specific time scales. Results also illustrate the challenges in using either nitrate or acetate chemical ionization to detect sulfuric acid

clusters. Future research into cluster chemistry must be done to better extract evaporation rates from measured cluster concentrations. Chapter 6 summarizes the work presented here and outlines potential projects to help answer questions raised in this dissertation.

Chapter 2. Stabilization of Sulfuric Acid Dimers by Ammonia, Methylamine, Dimethylamine, and Trimethylamine[a]

2.1 Overview

This study experimentally explores how ammonia (NH_3), methylamine (MA), dimethylamine (DMA), and trimethylamine (TMA) affect the chemical formation mechanisms of electrically neutral clusters that contain two sulfuric acid molecules (dimers). Measurements were conducted using a glass flow reactor which contained a steady flow of humidified nitrogen with sulfuric acid concentrations of 10^7 to 10^9 cm^{-3}. A known molar flow rate of a basic gas was injected into the flow reactor. The University of Minnesota Cluster Chemical Ionization Mass Spectrometer (Cluster CIMS) was used to measure the resulting sulfuric acid vapor and cluster concentrations. It was found that, for a given concentration of sulfuric acid vapor, the dimer concentration increases with increasing concentration of the basic gas, eventually reaching a plateau. The base concentrations at which the dimer concentrations saturate suggest $NH_3 < MA < TMA \lesssim DMA$ in forming stabilized sulfuric acid dimers. Two heuristic models for cluster formation by acid-base reactions are developed to interpret the data. The models provide ranges of evaporation rate constants that are consistent with observations, and leads to an analytic expression for nucleation rates that is consistent with atmospheric observations.

2.2 Introduction

Atmospheric nucleation is a significant source of cloud condensation nuclei and plays an important role in radiative forcing [*IPCC*, 2014]. Nucleation occurs when trace gases such as sulfuric acid [*Kulmala et al.*, 2004; *Weber et al.*, 1996], various basic compounds [*Almeida et al.*, 2013; *Chen et al.*, 2012; *Hanson and Eisele*, 2002; *Zhao et al.*, 2011], highly oxidized organics [*Schobesberger et al.*, 2013], and water [*Leopold*,

[a] This chapter is reproduced with permission from Jen, C. N., McMurry, P. H., and Hanson, D. R.: Stabilization of sulfuric acid dimers by ammonia, methylamine, dimethylamine, and trimethylamine, Journal of Geophysical Research: Atmospheres, 119, 2014JD021592, 10.1002/2014JD021592, 2014.

2011] react to produce stabilized molecular clusters that subsequently grow by vapor uptake.

Experimentalists and modelers have used multicomponent classical nucleation theory (CNT) to conceptualize the nucleation process and predict nucleation rates based upon calculated and observed concentrations of gaseous precursors [*Seinfeld,* 2006]. CNT assumes that clusters at one size have identical compositions with thermodynamic properties equal to those of equivalent bulk solutions. The nucleation rate is then the net rate at which clusters pass through the "critical size" (i.e., the size that is in equilibrium with the condensing vapors). In actuality, clusters containing a given number of sulfuric acid molecules also likely include varying numbers of water, basic, and/or highly oxidized organic molecules. The thermodynamic properties of such clusters are highly sensitive to cluster compositions [*Hanson and Lovejoy*, 2006; *Leverentz et al.*, 2013; *Ortega et al.*, 2012]; thus, cluster evaporation rates will depend on the cluster's exact makeup. Overall, CNT under predicts atmospheric boundary layer nucleation rates by several orders of magnitude and does not capture the observed functional dependence on sulfuric acid vapor concentration [*Chen et al.*, 2012; *Riipinen et al.*, 2007; *Weber et al.*, 1996]. An alternative approach to CNT is the use of chemical kinetics to explain the formation and growth of nucleating clusters. Both computational chemistry [*Dawson et al.*, 2012; *Olenius et al.*, 2013; *Ortega et al.*, 2012] and empirical observations [*Chen et al.*, 2012] have been exploited to develop kinetics-based nucleation models.

Vehkamäki and coworkers have modeled atmospheric nucleation by using *ab initio* calculations to compute free energies of sulfuric acid clusters (up to 4) with water and base molecules. Their results have shown that adding ammonia [*Kurtén et al.*, 2007], dimethylamine, triemethylamine, or water lower the energies of pure sulfuric acid clusters [*Leverentz et al.*, 2013; *Olenius et al.*, 2013; *Paasonen et al.*, 2012]. These free energies are converted to cluster evaporation rates by assuming the cluster is at equilibrium [*Ortega et al.*, 2012]. They are then able to predict nucleation rates for specific acid-base systems from the calculated evaporation rates [*McGrath et al.*, 2012].

Nucleation rates obtained from their *ab initio* results for several aminated sulfuric acid clusters match those seen in field and laboratory measurements [*Almeida et al.*, 2013; *Paasonen et al.*, 2012].

Our group has focused on the use of measured nucleated cluster concentrations to infer cluster reaction rates. The Cluster Chemical Ionization Mass Spectrometer (Cluster CIMS) measured concentrations of neutral sulfuric acid vapor and neutral clusters that contain up to four sulfuric acid molecules [*Eisele*, 1983; *Hanson and Eisele*, 2002; *Hanson and Lovejoy*, 2006; *Zhao et al.*, 2010]. These size four clusters are ~1 nm in geometric diameter or ~1.3 nm in mobility diameter [*Larriba et al.*, 2011]. For particles larger than this, we use the diethylene glycol scanning mobility particle spectrometer (DEG SMPS) [*Iida et al.*, 2009; *Jiang et al.*, 2011c] in combination with more conventional aerosol instrumentation [*Woo et al.*, 2001] to measure the remaining portion of the particle size distribution. Our observations from field and laboratory experiments indicate that sulfuric acid evaporates to some extent from cluster containing two or three sulfuric acid molecules. Sulfuric acid vapor is taken up at the collision rate for clusters that contain four or more sulfuric acid molecules [*Chen et al.*, 2012]. We have therefore defined the nucleation rate as the formation rate of size four clusters [*Chen et al.*, 2012], although this size may depend on the concentrations of other nucleating gases. Based upon these measurements, we have developed a simplified acid-base atmospheric nucleation model. This model does not rely on the concept of a critical size that is in equilibrium with the condensing vapors. Instead, cluster concentrations are governed by rates of reactions between vapors and clusters. Evaporation from clusters that contain one, two or three sulfuric acid molecules is the primary bottleneck to nucleation.

Chen et al. [2012] assumed that all basic gases enhance nucleation to the same extent, but pointed out that this requires further investigation. In this paper, we describe an experimental study on the effects of various basic gases on the formation of sulfuric acid dimers, one of the major bottlenecks to nucleation in the atmosphere. Our aim was to shed light on chemical processes that may have contributed to the scatter in dimer

concentrations shown in Fig. 2a of Chen et al. [2012]. The greatest experimental challenge for such investigations is the extraordinary cleanliness required to isolate and study particular chemical systems. This study utilizes a previously characterized glass flow reactor at Augsburg College [*Panta et al.*, 2012; *Zollner et al.*, 2012]. This flow reactor has been continuously purged over a period of two years with about two million liters of nitrogen from the head space of a liquid nitrogen tank; a portion of this flow carries sulfuric acid vapor which coats all the surfaces within the reactor. The flow reactor exhibits high repeatability between experiments. Measurements were carried out using four basic compounds: ammonia (NH_3), methylamine (MA), dimethylamine (DMA), and trimethylamine (TMA). This work provides new information on the effects of diverse bases, such as MA and TMA, on dimer concentrations and adds to prior work on the effects of NH_3 and DMA on nucleation rates [*Almeida et al.*, 2013; *Benson et al.*, 2009; *Erupe et al.*, 2011; *Hanson and Eisele*, 2002; *Kirkby et al.*, 2011]. The University of Minnesota Cluster CIMS (MCC) [*Titcombe*, 2012; *Zhao et al.*, 2010] and diethylene glycol scanning mobility particle spectrometer (DEG SMPS) [*Iida et al.*, 2009] measured the resulting neutral cluster and particle concentrations.

2.3 Data and Methodology

Figure 1 shows a schematic of the flow reactor and the locations of the base injection and MCC sampling. The internal flow reactor temperature was maintained at 295-305 K with relative humidity of ~30%. The sulfuric acid concentration inside the reactor was varied by adjusting the clean nitrogen flow over a temperature-controlled sulfuric acid reservoir. The sulfuric acid concentration in the flow reactor ranged from 10^7 to 10^9 cm^{-3}. Since the flow reactor is coated with thin layers of sulfuric acid, the evaporation of sulfuric acid from the reactor walls precluded measurements at sulfuric acid concentrations lower than this. Gaseous NH_3, MA, DMA, and TMA from permeation tubes were separately injected perpendicularly into the flow reactor. The injected base (shown in red) mixed into the sulfuric acid-containing flow along the centerline of the reactor. At the point of injection, the centerline base concentration was ~10 times greater than at the MCC sampling point [*Freshour et al.*, 2014]. A well-mixed

concentration, called no loss dilution concentration (NLD), of basic gas was determined *a priori* [*Zollner et al.*, 2012] from the permeation rate and dilution ratios, assuming no losses to the walls. The MCC in positive ion mode measured the base concentration and is within 20% of NLD (see SI). The reaction time for the majority of the gas was ~3 sec, determined from flow profiles via computational fluid dynamic simulations [*Freshour et al.*, 2014]. The total reactor and base injection flows were kept constant, providing a consistent flow field and high repeatability between experiments.

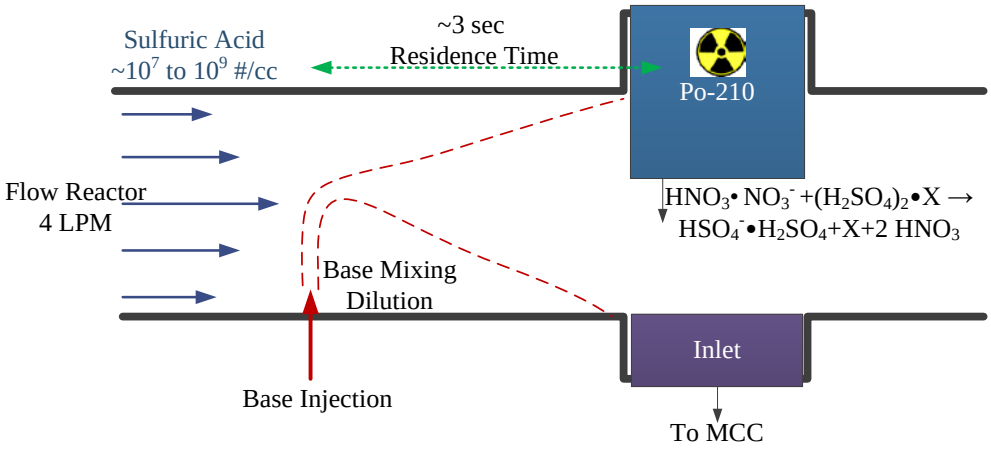

Figure 1 Schematic of the flow reactor including the location of the MCC sampling region. The flow in the reactor is laminar, leading to a reaction time of ~ 3 sec. The base concentration decreases about 10 times due to diffusion mixing (indicated by the red dashed line) by the MCC sampling location. The chemical ionization of the dimer (195 m/z) is shown explicitly with the unknown compound(s) X evaporating from the cluster upon ionization.

The MCC was connected in-line with the flow reactor via a glass manifold followed by a stainless steel sampling tube. This design minimized flow restrictions and allowed the shielded, Po-210 holder to sit inside the reactor flow (see Figure 1). Dilute nitric acid was passed over the radioactive source to produce the nitrate ion (with ligands, $(HNO_3)_{1\text{-}4}\bullet NO_3^-$) which was used to detect sulfuric acid monomer and dimers [*Eisele and Hanson*, 2000; *Hanson and Lovejoy*, 2006; *Titcombe*, 2012; *Zhao et al.*, 2010]. The transport time of the reagent ion across the sampling tube was estimated to be 20 msec, determined from the spacing and electric field in the sampling region and the mobility of

the ions [*Hanson and Eisele*, 2002]. The MCC detects the monomer, A_1, at 160 m/z (HNO_3•HSO_4^-) and the dimer, A_2, at 195 m/z (H_2SO_4•HSO_4^-). These product ion signals provide information only on the sulfuric acid content of the clusters (and HNO_3 ligands). It is likely that neutral monomers and dimers also contain water and base molecules that evaporate upon chemical ionization and entry into the vacuum system [*Hanson and Eisele*, 2002; *Hanson and Lovejoy*, 2006; *Kurtén et al.*, 2011; *Zhao et al.*, 2010]. Thus, the signals at 160 and 195 m/z actually represent H_2SO_4•X and $(H_2SO_4)_2$•X respectively, where X represents unmeasured amounts of water, base, and other compounds. The measured cluster signals at 160 and 195 m/z were converted to sulfuric acid monomer ($[A_1]$) and dimer ($[A_2]$) concentrations and corrected for ion induced clustering (IIC) and mass-dependent sensitivity [*Chen et al.*, 2012; *Zhao et al.*, 2010]. We assumed IIC occurs at the collision rate for all base compounds and concentrations, and therefore the reported $[A_2]$ represent the lower limit (see SI for further discussion on IIC).

Each day, prior to the addition of base, $[A_1]$ and $[A_2]$ were measured to serve as the "baseline" measurement for the flow reactor and MCC (*cf.* Zollner et al. [2012]). The primary origin of the baseline measured $[A_2]$ is due to IIC and is further explained in the SI. Deviations from the baseline would signal a change in the MCC or possible contaminant. Consistent baselines provided confidence that the subsequent experiments were conducted in the same environment as previous experiments. The repeatability of the baseline and data for specified reactant concentrations enabled by this flow reactor have allowed us to systematically probe the relative tendencies of different basic gases to form stabilized sulfuric acid dimers (see SI for more on repeatability).

2.4 Results and Discussion

2.4.1 Observations

Figure 2 shows the measured $[A_2]$ vs. $[A_1]$ for the four bases at various concentrations (denoted generally as [B]). Note that for a given $[A_1]$ (moving vertically up on any graph in Figure 2), $[A_2]$ increase as [B] increase, eventually reaching a limiting value where further increases in [B] do not result in higher $[A_2]$. This observation

suggests two key points. Consider first in the pure sulfuric system where dimer formation occurs by collisions of A_1 and evaporation from A_3; dimers are removed by sulfuric acid evaporation, growth to larger cluster sizes, collisions with larger particles, and deposition on the reactor walls. None of these processes depend on [B]. The fact that measured $[A_2]$ increases with [B] implies that the basic gases must assist in the formation of the dimer. Furthermore, [B] at which the $[A_2]$ reaches saturation differs from base-to-base. For NH_3, this saturation concentration occurs between 1800-2300 pptv, MA at 80-180 pptv, TMA at 30 pptv, and DMA at 20 pptv. To obtain a measured $[A_2]$ of ~10^8 cm^{-3} at $[A_1]$ of ~10^9 cm^{-3}, 100 times more NH_3 or 2-4 times more MA than DMA or TMA are needed. From the observations alone, we conclude that the rate limiting step in stabilizing A_2 must be a reaction with a base with an effectiveness increasing from NH_3< MA< TMA≲DMA.

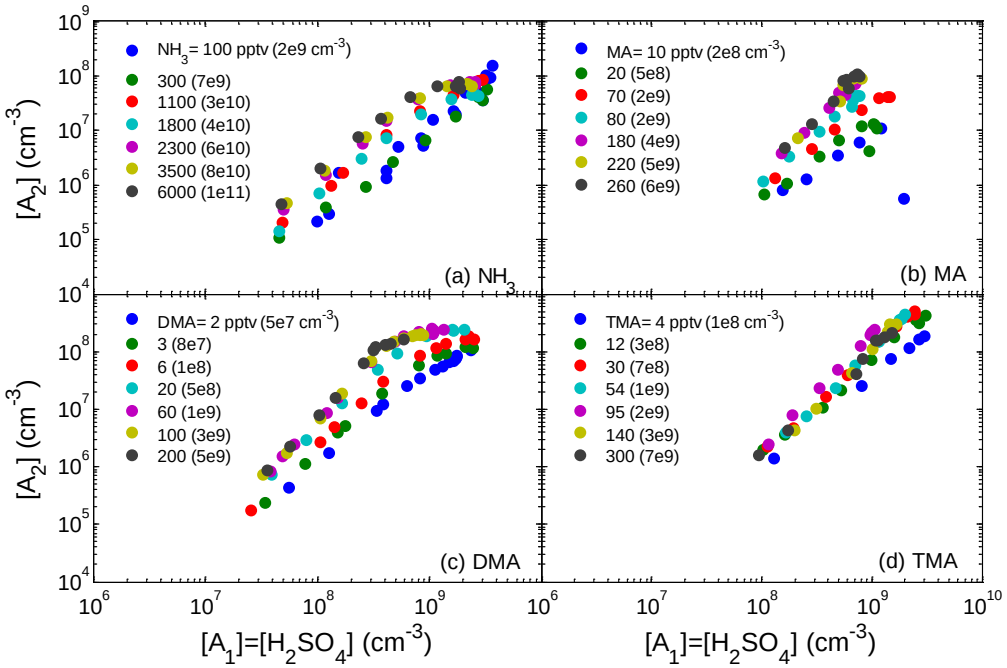

Figure 2 Measured $[A_2]$ vs. $[A_1]$ for the four bases at various concentrations. (a) Ammonia, NH_3; (b) Methylamine, MA; (c) Dimethylamine, DMA; and (d) Trimethylamine, TMA

TMA shows a different pattern than the other bases where the range of $[A_2]$ at a given $[A_1]$ is constricted with perhaps $[A_2]$ decreasing with [TMA] beyond the saturation [TMA]. This could be due to the tertiary nature of TMA: no subsequent hydrogen bonds

are available after it reacts with a sulfuric acid molecule. This would limit further clustering with the (sulfuric acid • TMA) adduct, and lower [A_2] if the adduct is a large fraction of the A_1 population. Steric hindrance by the methyl groups might also block A_1 clustering in the formation of the A_2. These steric effects are not present for NH_3, MA, and DMA (amines with 0 to 2 methyl groups). At [A_1]=2x10^8 cm^{-3}, [A_2] with DMA is higher than [A_2] with TMA. However at [A_1]=2x10^9 cm^{-3}, this trend reverses. The presence of TMA in the monomers and dimers may prevent clusters from coagulating. Then at high [A_1]/[TMA], more sulfuric acid molecules are free of TMA and numerous sulfuric acid collisions would overcome TMA's hindering effect.

The measurements in Figure 2 also show that [A_2] tend to increase with [A_1]. For low [A_1], saturation curves for all bases indicate that [A_2] goes as [A_1]^2. This signifies that at high [B], the formation of A_2 is limited by A_1 collisions. At high [A_1], the saturation curves exhibit a downturn of [A_2] from this squared relationship. As shown in the modeling results below, this can be explained by the depletion of A_2 by collisions with itself. It is also possible that the clusters with high base content cannot undergo efficient chemical ionization by the nitrate ion. The downturn is more pronounced for NH_3, DMA, and TMA than MA but this may be due to smaller [A_1] range for MA. Greater insight into the slope and the shape of the saturation curves requires detailed modeling (see below).

Figure 3 compares the DMA dimer data from this study (without IIC correction for equal comparison) to those reported by CLOUD [*Almeida et al.*, 2013] and from a flow reactor [*Petäjä et al.*, 2011]. The blue squares are the baseline measurements from Petäjä et al. [2011], i.e. those without added base and at a residence time of 32 sec. Their results can be directly compared to our baseline measurement at 40 sec, given as a dashed black line in Figure 3. This residence time is determined from the point of sulfuric acid injection into the flow reactor [*Zollner et al.*, 2012] and is different from the 3 sec reaction time where the base is injected (see Figure 1). The solid black curve is the steady state collision-controlled limit (no cluster evaporation and no base reaction, but with

coagulation and wall losses for the Augsburg flow reactor). The blue squares closely follow the collision-controlled limit. This provides further evidence, as suggested by Almeida et al. [2013], that the flow reactor used in Petäjä et al. [2011] had high levels of a stabilizing compound(s). Figure 3 also depicts the DMA stabilized [A_2] data from Almeida et al. [2013] ([DMA]=3-100 pptv) as green triangles. The range of [A_1] in Almeida et al. [2013] is lower than our work but extrapolating the measured [A_2] reported in Almeida et al. [2013] shows that their [A_2] is slightly higher for a given [A_1] than were seen in this study. This could be due to a lower temperature in their chamber (278 K compared to ~300 K here) or differences in reaction times between the Augsburg flow reactor (~3 sec) and the CLOUD chamber. Also, IIC remains a poorly understood process and varies between the MCC and their CIMS. The reported [DMA] in Almeida et al. [2013] indicate that [A_2] saturates at a [DMA] between 3-5 pptv, below the value shown here of 20 pptv. It may be possible that NH_3, which was also present in the CLOUD chamber at 10 pptv, led to an increase in [A_2] for a specific [DMA].

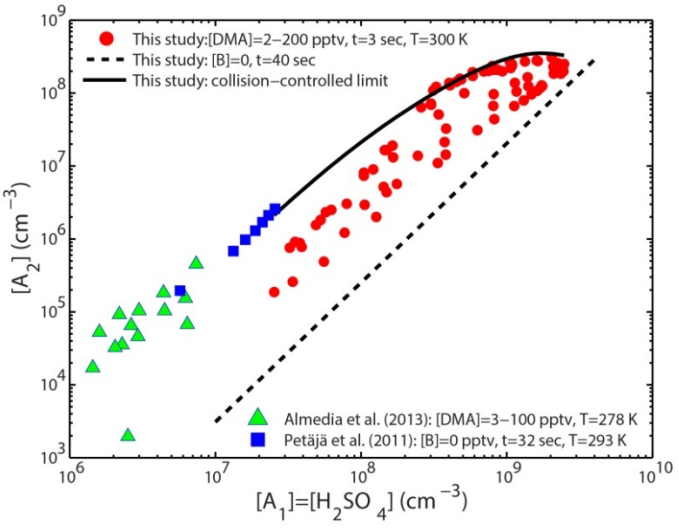

Figure 3 Comparison between the DMA data shown in this study and those given in Almeida et al. [2013]. [A_2] from this study are shown as red points and are not corrected for IIC (actual concentrations will be ~1-100% lower, depending on [A_1]). The green triangles correspond to the DMA experiments (range 3-100 pptv) from CLOUD. The blue squares are the baseline measurements from Petäjä et al. [2011] at a residence time of 32 sec. The dashed black line is the baseline measurements from this study at a residence time of ~40 sec. The solid black cure is the collision-controlled limit where evaporation is negligible and clusters do not react with the base.

We have developed two heuristic models to describe the data in Figure 2. The first scheme is based upon the acid-base reaction model proposed in Chen et al. [2012]. Based on observations, Chen et al. argued that A_2 (i.e., the signal measured at 195 m/z) contains two flavors of dimer: more volatile (A_{2MV}) and less volatile (A_{2LV}). This model assumes that A_1 collides with A_1 to form A_{2MV}. This more volatile dimer either evaporates with a rate constant of E_{2MV} or reacts with a base to form A_{2LV}. A_{2LV} collides with A_1 to form A_3, which then can grow to A_4. This is pictorially explained in Figure 4 on the left hand side. This original acid-base model was modified in two ways to better describe the data presented here. Chen et al. used the Fuch's surface area from the particle distribution (1-10 nm) to approximate monomer loss (κ) to all larger particles/clusters including dimers. This was adequate for that study since the measured [A_2] never exceeded 10% of [A_1]. However in these flow reactor experiments, the measured [A_2] approaches 50% of the measured [A_1]. Thus, a significant loss of A_2 will be to dimer-dimer coagulation. Furthermore, the model was modified to include a base evaporation from A_{2LV}, termed E_{2BLV}. Including this term gives the model flexibility to describe [A_2] behavior for a wide range of [B] (1-6000 pptv). The modifications to the model are shown in red on Figure 4.

As the MCC measures all dimer types at one mass (195 m/z), [A_2] is assumed to be composed of both A_{2MV} and A_{2LV}, thus the modeled [A_2] is the sum of both. Cluster loss to larger particles, κ, was calculated from DEG SMPS measured size distribution at various [A_1] and [B] (see SI). The wall loss rate, η, was estimated based on the diffusion coefficient of sulfuric acid [*Hanson et al.*, 1992; *Murphy and Fahey*, 1987; *Pöschl et al.*, 1998]. The forward rate constants were taken to be the collision rate. See SI for the explicit rate equations.

The second scheme begins with A_1 reacting with B to form an A_1B which dissociates at a rate constant E_1. Since A_1 may already contain water and some base molecules, the notation A_1B represents a monomer that is more neutralized than A_1.We assume A_1 and A_1B can be detected efficiently by MCC at 160 m/z. A_2 is formed from

A_1B by the addition of either A_1 or A_1B and does not evaporate. The lack of dimer evaporation is supported by *ab initio* calculations of various aminated dimers [*Ortega et al.*, 2012]. A_3 is formed in a similar manner but evaporates at E_3 as in scheme 1 and in our previous work [*Chen et al.*, 2012]. Trimer evaporation rate constant was included to test for its effect on modeled [A_2] and [A_1]. All cluster sizes are lost to the wall at η and to larger particles at κ. Scheme 2 is depicted on the right of Figure 4, and the explicit rate equations are given in the SI.

We used two solutions of the differential equations that describe these schemes to interpret the data. The first approach assumes that cluster concentrations at the MCC sampling point have achieved steady state and depend only on measured [A_1] and [B]. This would be valid if characteristic lifetimes of the clusters are short relative to the 3 sec time available for acid-base reactions (Figure 1). The second approach involves a transient solution at 3 sec which defines the time dependencies for the chemical reactions illustrated in Figure 4. This accounts for changes in [B] as it mixes with the carrier gas and depletion of both [A_1] and [B] as they are lost by reactions or to the walls.

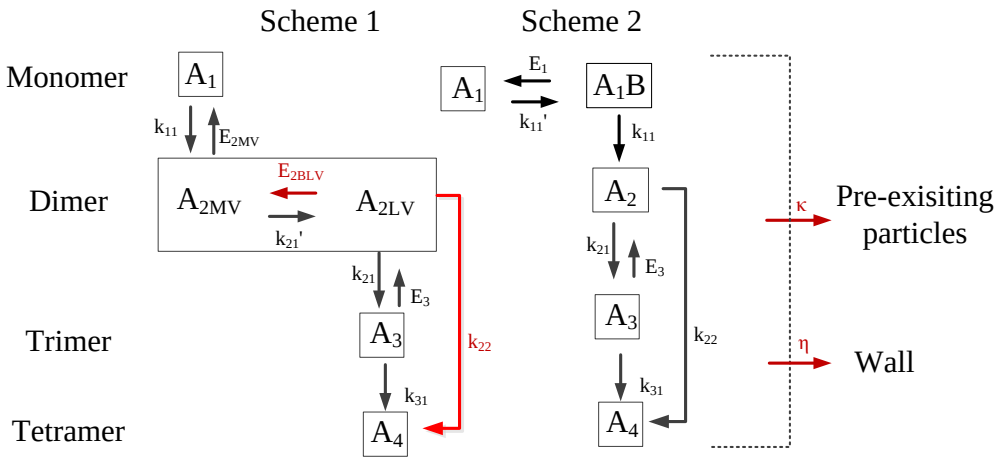

Figure 4 Two conceptual acid-base reaction schemes where moving downwards is a monomer (both A_1 and A_1B for scheme 2) addition and moving to the right is a base addition. Modifications to the acid-base reaction model proposed in Chen et al. [2012] are shown in red. κ and η apply to both schemes.

2.4.2 Scheme 1, Steady State Model

We assume that [B]=NLD and the measured [A_1] are at steady state with all clusters. In addition, since it was found that trimer evaporation contributes negligibly to [A_2], E_3 was set to 0 s^{-1}. This leaves two fitting parameters: E_{2MV} and E_{2BLV}. E_{2MV} allows for evaporation of A_1 from A_2. Including this in the model allows [A_2] to be at or below collision-controlled values, as is observed (see SI). Allowing for the transformation of more volatile to less volatile dimer by reaction with the basic gas helps to explain the observed dependence of [A_2] on [B] (recall, observed [A_2] includes both more and less volatile dimer). We found that for the stronger bases (DMA and TMA), the data could be reasonably explained using only one parameter: E_{2MV}. However, for the weaker bases (NH_3 and MA) it was also necessary to allow for the evaporation of base from A_{2LV} at the rate E_{2BLV}. Figure 5 compares the steady state model predictions (lines) with the observations for the four basic gases. The evaporation rate constants that best fit the model for the full [B] range of the data are shown inside each plot. Fitting to both high and low [B] produces an estimated range for each evaporation rate constant (see Table 2).

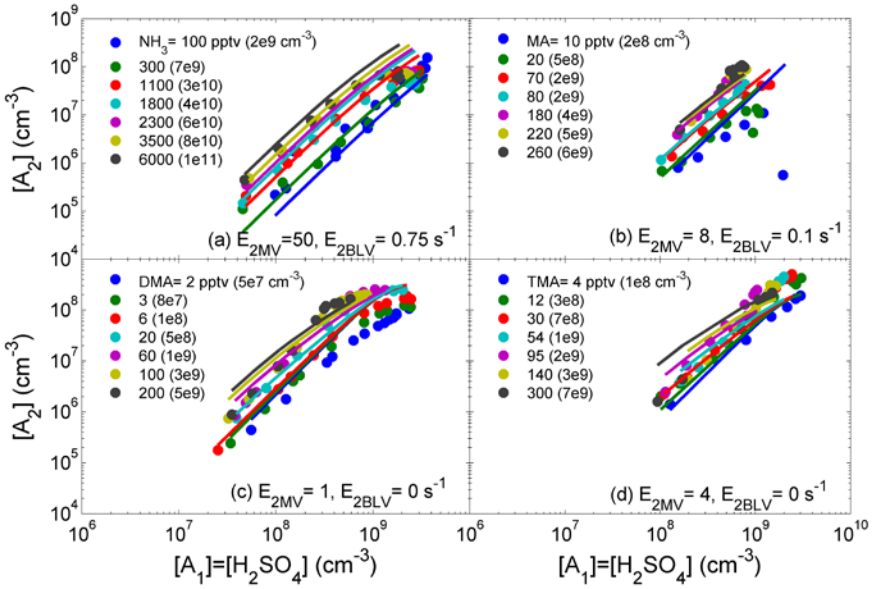

Figure 5 Scheme 1 solved at steady state (lines) is compared to the measured [A_2] and [A_1] (points). Colors for the lines correspond to the same [B] as the points, and fitted evaporation rate constants are given inside each base graph. (a) NH_3, (b) MA, (c) DMA, and (d) TMA

The steady state model captures several key trends of the data. First, the model predicts [A_2] will reach saturation when [B] is sufficiently high, though not always at the same [B] as was experimentally observed. The model also captures [A_2]'s general dependence on [B], even at high [NH_3] (see SI for [A_2] vs. [B] at constant [A_1] plots). The model also predicts the downturn of [A_2] at high [A_1], though to a lesser extent than is seen in the data. This trend is due primarily to dimer-dimer and particle coagulation losses.

For DMA and TMA, scheme 1 steady state model over-predicts [A_2] at high [B] and does not predict the squared dependence of [A_2] on [A_1] for the saturation curve. [A_2] over-prediction may be due to a fault in the steady state assumption. We see from the fitted E_{2MV} that the lifetime of the more stable A_{2MV} is quite long (~1 sec). This is on the order of the reaction time of the flow reactor which raises questions regarding the suitability of a steady state model.

2.4.3 Scheme 2, Steady State Model

The dependence of [A_2] on [B] can also be described by a reaction of A_1 with B. Therefore, we modeled scheme 2 at steady state by assuming [B] = NLD. However, as this reaction model posits two types of monomers, we assume that measured 160 m/z = [A_1]+[A_1B]. We also assume the reaction of A_1 with B is at equilibrium. Unlike scheme 1, E_3 was found to play a significant role in modeling [A_2], thus we use E_3=0.4 s^{-1} from Chen et al. [2012] as [A_3] data from the MCC requires a better understanding of IIC (see SI).

Figure 6 shows the steady state solution of scheme 2 compared to measured [A_2] vs. [A_1]. This reaction model better describes the behavior at high [A_1] but under-predicts [A_2] at high [A_1] except for NH_3. This could be due to an over-estimation of κ. This model also reasonably predicts the saturation [B] and the squared dependence of [A_2] on [A_1]. However, this model and solution method over-predicts [A_2] at high [B] for the lower bound of E_1. We suspect this is due to the short reaction time preventing [A_1] and [B] from reaching equilibrium. Table 2 summarizes the fitted evaporation rate constants

for the two schemes solved at steady state. Both schemes demonstrate that NH_3< MA< TMA≲ DMA in facilitating the formation of stabilized dimers.

Table 2 Summary of the saturation [B] and the fitted evaporation rates constants for both schemes at steady state. Note for scheme 1, E_3=0 s^{-1} and for scheme 2, E_3=0.4 s^{-1} from Chen et al. [2012].

	Observations		Steady State Scheme 1		Steady State Scheme 2
Base Name	**Saturation [B] (pptv)**	**Approximate Slope**	**E_{2MV} (s^{-1})**	**E_{2BLV} (s^{-1})**	**E_1 (s^{-1})**
NH_3	1800-2300	2	20-60	0.5-0.75	500-2500
MA	80-180	2	8-15	0.03-0.1	30-60
DMA	20	2	1-5	0	1-7
TMA	30	2	4-10	0	5-30

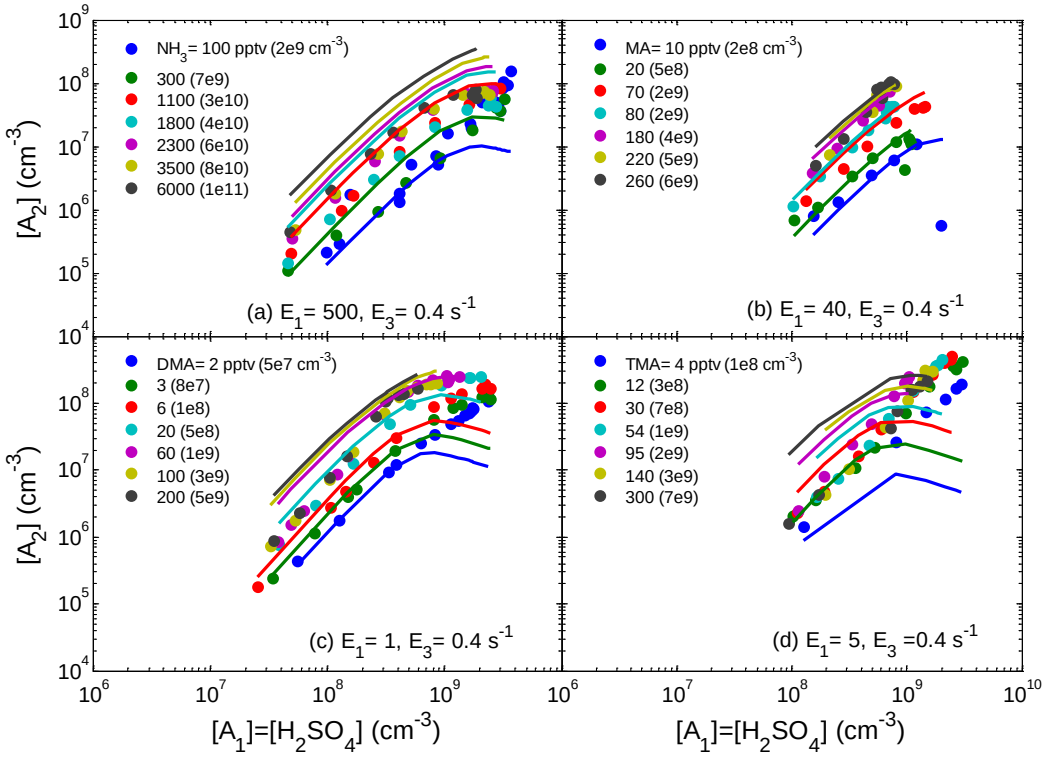

Figure 6 Scheme 2 solved at steady state (lines) is compared to the measured [A_2] and [A_1] (points). Fitted evaporation rate constants are given inside each base graph. (a) NH_3, (b) MA, (c) DMA, and (d) TMA

2.4.4 Scheme 1, Transient Model

When dimer lifetimes are comparable to transport times through the reactor, cluster concentrations will not be at steady state. (This does not preclude the use of the steady state model for describing atmospheric dynamics as those processes occur over timescales of minutes to an hour.) Therefore, we solved the rate equations for species and processes shown in scheme 1 of Figure 4 to more accurately simulate processes that occur during the 3 sec reaction time. This transient model takes into account the dilution of [B] following injection (see Figure 1) as a function of time as well as its reaction with and evaporation from clusters. The base is injected at a concentration ~10 times higher than NLD. Centerline [B] at sampling point is about equal to NLD, confirmed by MCC measurements (see SI) and computational fluid dynamic simulations [*Freshour et al.*, 2014]. The dilution and wall loss of [B] can be approximated as an overall first-order loss rate, μ. The transient model also describes the presence of high concentrations of low volatility clusters that might be formed where [B] are highest. This may then lead to the formation of larger particles (>1 nm) and implies that κ is time dependent. For more discussion on this and solution method, see SI.

Figure 7 compares observations with transient model predictions (solid lines) for $[A_2]$ vs $[A_1]$. The captions inside the graph indicate the fitted evaporation rate constants with their ranges in Table 2. The transient model shown in Figure 7 accounts for η but not κ (see SI). The ranges of fitted evaporation rate constants increase for all bases when compared to the steady state values, with the largest gain for ammonia. The increase in evaporation rate constants is primarily due to high [B] at times shortly after 0 sec. This creates many dimers, leading to significantly higher values of predicted $[A_2]$. A higher E_{2MV} is required to lower the predicted $[A_2]$. Regardless, the trend NH_3< MA< TMA≲DMA in helping the formation of stabilized dimers is also seen here, but with perhaps a larger distinction of TMA<DMA.

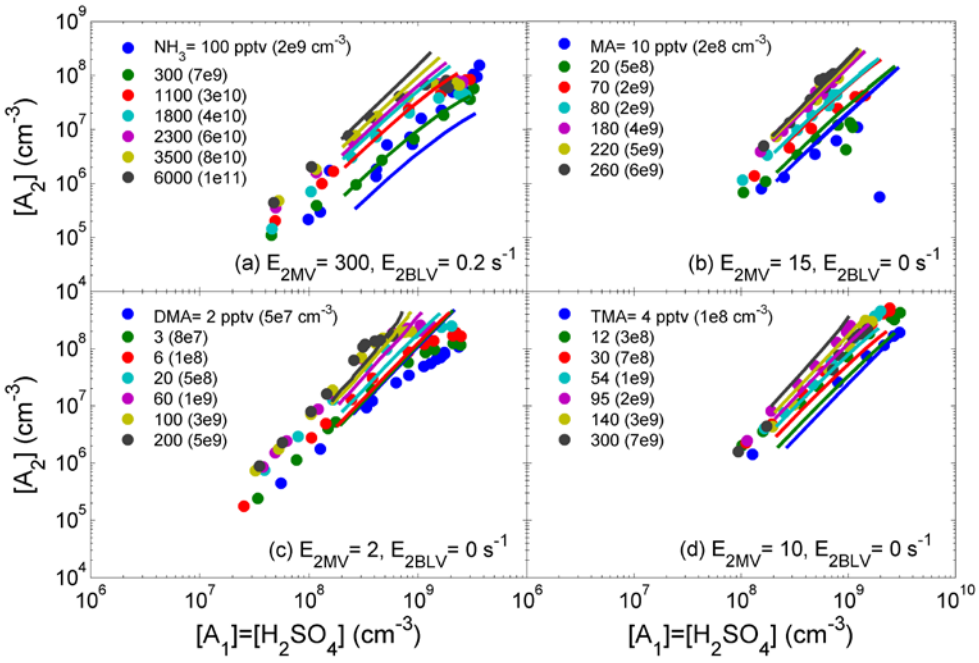

Figure 7 Comparison between transient scheme 1 (lines) to measured $[A_2]$ vs $[A_1]$ at different [B]. The fitted evaporation rates are shown inside the graphs. (a) NH_3, (b) MA, (c) DMA, and (d) TMA

The transient model also captures the saturation curve and the squared dependence of $[A_2]$ on $[A_1]$. This solution method also better describes the behavior of the $[A_2]$ at high [B]. Furthermore, the fitted overall loss rates μ between the four bases are approximately equal. This is consistent with expectations as wall loss and dilution mixing is regulated by fluid transport and depends weakly on the molecular makeup of the base.

Table 3 Fitted evaporation rate constants from the transient solutions. Note for scheme 1, E_3=0 s^{-1} and for scheme 2, E_3=0.4 s^{-1} from Chen et al. [2012].

	Transient Scheme 1			Transient Scheme 2		
Base	**E_{2MV} (s^{-1})**	**E_{2BLV} (s^{-1})**	**μ (s^{-1})**	**E_1 (s^{-1})**	**E_3 (s^{-1})**	**μ (s^{-1})**
NH_3	200-300	0.2-0.5	0.92	400-700	0.4	0.9
MA	15-30	0	0.92	20-40	0.4	0.9
DMA	2-3	0	0.87	0-1	0.4	0.70
TMA	10-15	0	0.90	5-15	0.4	0.75

2.4.5 Scheme 2, Transient Model

The transient solution for scheme 2 follows that given for scheme 1 (see above) with E_3=0.4 s^{-1} taken from Chen et al. [2012]. Figure 8 shows the comparison between transient solution of scheme 2 to the observed [A_2] vs. [A_1]. This model better captures the downturn of [A_2] at high [A_1] than scheme 1, especially for [DMA] at 6 pptv and lower. Furthermore, this scheme is able to describe the range of [A_2] for both small and large ranges of [B], with TMA as the exception. It is possible that steric hindrance minimizes [A_2] dependence on [TMA] and is not captured in this model. Scheme 2 also predicts slightly lower [A_2] for low [B] than is observed for NH_3 and TMA. It also predicts [A_2] saturation at similar [B] as is observed. The ranges of E_1 values are given in Table 2. It should be noted that unlike scheme 1, this model is sensitive to the value of E_3. Future studies that explore E_3 could possibly alter these fitted E_1. Nonetheless, scheme 2 also supports the conclusion that NH_3< MA< TMA$\lesssim$DMA in affecting the formation of stabilized dimers.

Both schemes 1 and 2 are equally valid based upon our data. Computational chemistry simulations of sulfuric acid with DMA or NH_3 suggest that scheme 2 is more likely as calculated sulfuric acid evaporation rates of A_2 containing NH_3 or DMA are much lower than A_1 with the same number of base molecules [*Ortega et al.*, 2012; *Paasonen et al.*, 2012]. Comparing evaporation rates of certain species for specific clusters (Table 3) further indicates that scheme 2 is more likely. The reactions listed are from Ortega et al. [2012] with evaporation rates that most closely match those found in this study. As seen in Table 3, E_{2MV} values do not fall near the computed sulfuric acid evaporation rate constants of Ortega et al. [2012] for most likely dimer compositions. However, E_1 are close to/within the computed range of base evaporation from the monomers. Our rate constants fall within a narrower range than those of Ortega et al. [2012], but our rate constants represent a weighted average over cluster sizes that contain varying number of base molecules where the average is dominated by the most stabilized and abundant cluster composition. The *ab initio* calculations are for specific cluster

compositions with 1-4 DMA or 1-4 NH_3 molecules. In addition, our empirical evaporation rate constants can be influenced by water molecules in the clusters which are not taken into account in the simulations.

Table 4 Comparison of empirical evaporation rate constants from this study to those from Ortega et al. [2012]

Scheme 1	**This Study**	**Ortega et al. (2012)**
$A_2 \bullet NH_3 \rightarrow A_1 \bullet NH_3 + A_1$	E_{2MV}=20 to 300 s^{-1}	10^{-2} s^{-1}
$A_2 \bullet (NH_3) \rightarrow A_2 + NH_3$	E_{2LV}=0.2 to 0.75	10^{-2} s^{-1}
$A_2 \bullet DMA \rightarrow A_1 \bullet DMA + A_1$	E_{2MV}=1 to 2 s^{-1}	10^{-5} s^{-1}
Scheme 2		
$A_1 \bullet NH_3 \rightarrow A_1 + NH_3$	E_1=400 to 2500 s^{-1}	10^{4} s^{-1}
$A_1 \bullet DMA \rightarrow A_1 + DMA$	E_1=0 to 7 s^{-1}	10^{-2} s^{-1}

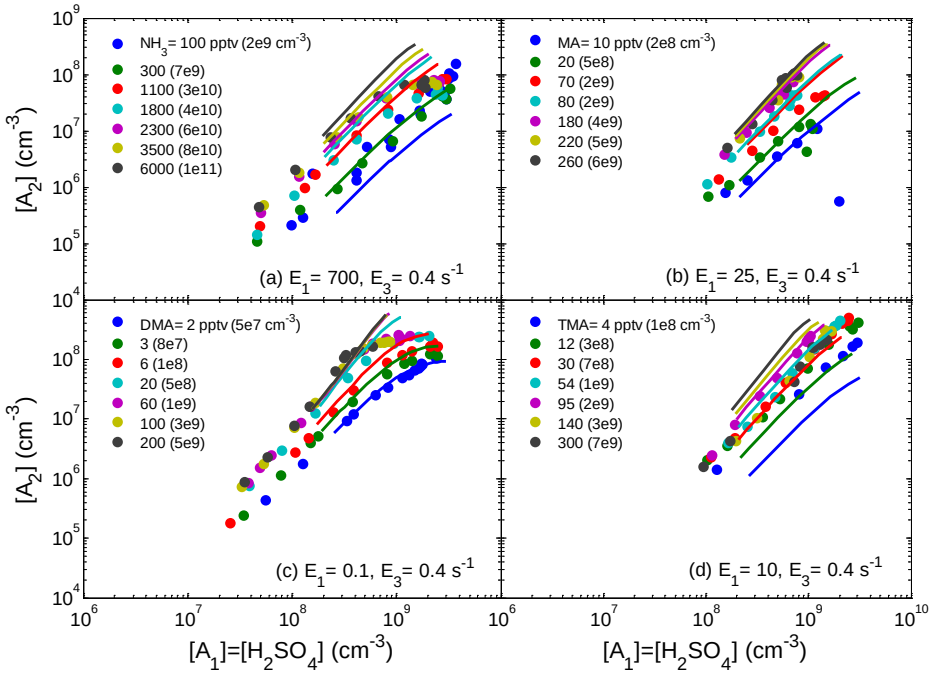

Figure 8 Comparison between transient solution of scheme 2 (lines) to measured $[A_2]$ vs $[A_1]$ at different [B]. The fitted evaporation rates are shown inside the graphs. (a) NH_3, (b) MA, (c) DMA, and (d) TMA

The transient models should more accurately describe processes that occur in the reactor than the steady state model. Therefore, we believe the evaporation rate constants obtained from the transient models should more accurately illustrate the differences between the bases in the production of stabilized dimers. However, it is difficult to quantify uncertainties in these evaporation rates. The transient models undoubtedly oversimplify both the fluid dynamics and chemical reactions taking place in the flow reactor. Furthermore, we assume that chemical ionization by nitrate ions allows the MCC to detect all compositions of sulfuric acid clusters. We are confident that the sulfuric acid clusters are not losing acid molecules [*Chen et al.*, 2012; *Eisele and Hanson*, 2000; *Zhao et al.*, 2010], but it is possible some clusters of the form A_1B_N or A_2B_N, where N is the number of attached bases, are highly neutralized. These clusters may have lower proton affinities and might not react with the nitrate ion. If so, these clusters would not be efficiently detected, leading to an underestimation on the stabilizing effect of B on A_2.

The evaporation rate constants from both solution methods and schemes differ from those previously reported by our group's closely related paper [*Chen et al.*, 2012]. That study involved the analysis of ambient data and Teflon chamber measurements involving the SO_2 photooxidation in the presence of DMA. We inferred evaporation rate constants of E_{2MV}=400 s^{-1} (from the chamber study) and E_3=0.4 s^{-1} (from the ambient data). Using these evaporation rates, predicted nucleation rates were found to be in reasonable agreement with measured rates in Mexico City and Atlanta, assuming that all basic gases (NH_3 plus all measured amines) are equally effective at stabilizing the clusters (i.e., form clusters with equal values of E_{2MV} and E_3). The value of the evaporation rate constant found in this study for DMA (E_{2MV}=2 s^{-1} or E_1=0.1 s^{-1}) is below the value reported in the previous study (E_{2MV} range 100 to 1000 s^{-1}). The flow reactor experiments described in this paper are more repeatable and less prone to contamination than the chamber study described by Chen et al. [2012] and this could explain the differences. Overall, these flow reactor experiments show unambiguously that different bases stabilize clusters to different extents, and that this must be accounted for in nucleation models.

2.5 Atmospheric Implications

The ultimate goal of our work is to predict nucleation rates from the concentration of precursor gases with an accuracy that is adequate for atmospheric modeling. Based upon our measurements and guided by computation chemistry results, we used scheme 2 at steady state to formulate a nucleation rate or the formation rate of the tetramer, J_4. Solving scheme 2 at steady state produces

$$J_4 = P' \bullet \frac{1}{2} k \left[A_{1tot}\right]^2 \qquad \textbf{Equation 4}$$

where $[A_{1tot}]$ is the total concentration of monomers detected at 160 m/z. P' is a prefactor that is defined as

$$P = -\frac{1}{E_3 + \kappa_3 + \eta}\left(k\left[A_{1tot}\right]\left(1 - \frac{E_3}{E_3 + \kappa_3 + \eta}\right) + \kappa_2 + \eta\right) + \frac{1}{E_3 + \kappa_3 + \eta}\sqrt{\left(k\left[A_{1tot}\right]\left(1 - \frac{E_3}{E_3 + \kappa_3 + \eta}\right) + \kappa_2 + \eta\right)^2 + 4k\left[AB\right]^2\left(\frac{E_1}{\left[B\right]} + \frac{k}{2}\right)} \qquad \textbf{Equation 5}$$

[AB] is a fraction of $[A_{1tot}]$ and equals

$$\left[AB\right] = \frac{k\left[B\right]}{E_1 + k\left[B\right]}\left[A_{1tot}\right] \qquad \textbf{Equation 6}$$

This analytical expression for nucleation rate is analogous to Equation 2 of Chen et al. [2012], albeit for scheme 2 rather than scheme 1. The prefactor P' is always less than 1. Equation 4 signifies that the nucleation rate is some fraction of the A_1-A_1 collision rate.

Figure 9 compares atmospheric nucleation rates from a variety of field campaigns with values calculated using Equation 4. The evaporation rate constants E_1 and E_3 used for these calculations are tabulated with Figure 9. The value of E_3 is based on Chen et al. [2012], and E_1 values were obtained from the transient model of scheme 2 (Table 2),

which we believe is likely our most accurate model. We assume these evaporation rate constants, measured at ~300 K and 30% RH, can be applied to atmospheric conditions. The measured [A_1], [DMA], [NH_3], were taken from Atlanta, 2009. During this field campaign, [A_1] ranged from $1x10^7$ to $2x10^8$ cm^{-3}, [NH_3] from 500 to 3000 pptv, and DMA from 1 to 10 pptv. Two enclosed regions overlaying the data represent the predicted nucleation rates: black dots/dashes representing nucleation due only to reactions of sulfuric acid with ammonia and purple dashes for reactions only with DMA. The model shows that J is a function of A_{1tot}^4, due in part to the dependence of P' on A_{1tot}. This dependence is in reasonable agreement with observations overall, but differs with our earlier conclusion that J is proportional to A_{1tot}^2 for individual data sets [*Kuang et al.*, 2008].

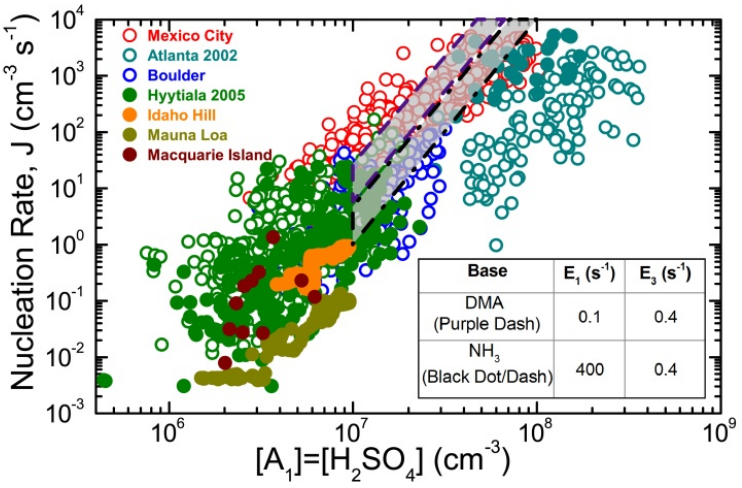

Figure 9 Observed nucleation rates from various locations as a function of [A_1]. Scheme 2 presented here predicts nucleation rates enclosed in purple dashes if nucleation is due to reactions of sulfuric acid with DMA and in black dot/dash if due to reactions with NH_3. The table to the right details the values used to determine the DMA and NH_3 nucleation rates

However, the atmosphere contains numerous compounds that react simultaneously to stabilize sulfuric acid clusters. Computational chemistry has shown that DMA displaces ammonia in sulfuric acid ion clusters [*DePalma et al.*, 2011; *Kupiainen et al.*, 2012]. Furthermore, Yu et al. [2012] have experimentally shown a NH_3/DMA mixture in a sulfuric acid environment enhances the number of particles

formed relative to either NH_3 or DMA alone. To more accurately model atmospheric nucleation, an average E_{2MVmv} or E_1 would capture how all bases affects the formation of stabilized A_2.

2.6 Conclusions

These experiments show that NH_3< MA< TMA≲DMA in helping the production of stabilized sulfuric acid dimers in the presence of water. Two acid-base reaction schemes were used to model the data. Scheme 1 assumes there are more and less neutralized dimer that are respectively less and more volatile. Scheme 2 assumes that there are more and less neutralized monomer, and that stabilized dimer are only formed by collisions between both types of monomer. At steady state, scheme 1 solution reproduced the observation that dimer concentrations reached a saturation level as [B] increased for a fixed $[A_1]$ and over-predicts $[A_2]$ for high [B], whereas scheme 2 more accurately captures the $[A_2]$ trends at high $[A_1]$. Transient solutions to both schemes significantly improve the predicted $[A_2]$ at high [B], reproduce the $[A_2]$ saturation, and the $[A_2]$ α $[A_1]^2$ relationship. As the MCC cannot distinguish between different types of monomer or dimers due to unmeasurable compounds (X) that evaporate during the measurement, the data does not provide evidence that one scheme is more accurate than the other, although previously published theoretical results favor scheme 2. However, modeling the data via the two schemes produces further evidence that NH_3< MA< TMA≲ DMA at facilitating the formation of stabilized A_2.

2.7 Supporting Information[b]

2.7.1 MCC Measurement of NLD

The MCC operated in positive ion mode using charged water clusters to measure [B] (see Hanson et al. [2011] for comparison). Figure S1 shows the measured [B] as a function of measured [A_1] (in negative ion mode of the MCC) for MA and TMA. Overall, the NLD is within 20% of the measured [B] except for [MA]=7 pptv where NLD is a factor of 2 lower than measured. This could be due to MA sticking to the walls of the base injection system and raising the amount of [MA] added to the flow reactor. This would only affect the concentrations for the lowest [B]. Also from the graph, it can be seen that [B] remains constant for increasing [A_1].

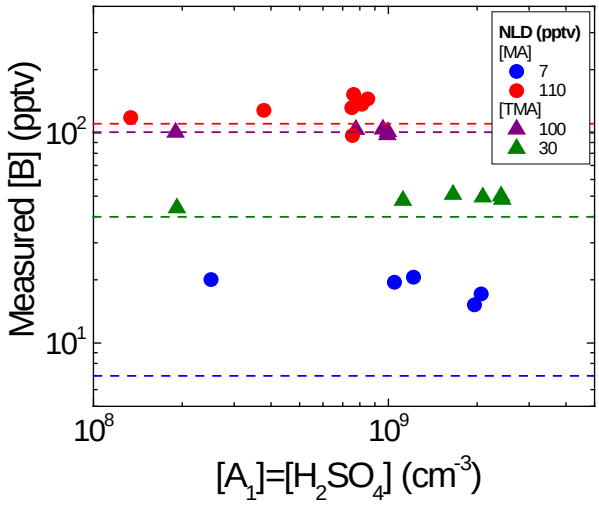

Figure S1 Measured [B] as a function of [A_1]. The different symbol types signify the base type and the colors (as defined in the legend to the right) indicate the predicted NLD. The dashed lines are NLD concentrations.

2.7.2 Ion-Induced Clustering (IIC) of the MCC

The MCC dimer signal (195 m/z) is composed of both pre-existing neutral dimers that are charged with nitric ion and charged monomers that go on to charge neutral A_1 to form dimers. The latter process is IIC, and its contribution to dimer signal is a source of

[b] This supporting information is reproduced with permission from Jen, C. N., McMurry, P. H., and Hanson, D. R.: Stabilization of sulfuric acid dimers by ammonia, methylamine, dimethylamine, and trimethylamine, Journal of Geophysical Research: Atmospheres, 119, 2014JD021592, 10.1002/2014JD021592, 2014.

uncertainty. Chen et al. [2012] (SI) lists a series of possible IIC reactions, with the pertinent reactions given below.

$$A_1 + HNO_3 \bullet NO_3^- \xrightarrow{k_1} A_1^-$$

$$A_1 + A_1^- \xrightarrow{k_{21}} A_2^-$$

$$A_2 + HNO_3 \bullet NO_3^- \xrightarrow{k_2} A_2^-$$

$$A_2 + A_1^- \xrightarrow{k_{31}} A_3^-$$

$$A_1 + A_2^- \xrightarrow{k_{32}} A_3^-$$

$$A_3 + HNO_3 \bullet NO_3^- \xrightarrow{k_3} A_3^-$$

where
A_1 = neutral monomer
A_1^- = charged monomer
A_2 = neutral dimer
A_2^- = charged dimer
k_i = nitrate ionization rate constant
k_{ij} = IIC rate constant

Chen et al. [2012] provides two sets of rate constants: one set contains the collision rate constants [*Hanson et al.*, 2011; *Su and Bowers*, 1973] and the second are rate constants fitted from ambient data [*Zhao et al.*, 2010]. To determine which set of IIC rate constants to use for this study, the chemical ionization (CI) reaction time of the MCC was varied by manipulating the electric field in the sampling region (see Figure 1) with constant [A_1]. Changing the CI reaction time does not change the amount of pre-existing neutral dimer but does affect the amount produced by IIC.

Consider first the ionization of A_1. Integrating the ionization rate equation and assuming the nitrate source ion (125 m/z) remains constant at short CI time scales, the ratio between signal 160 m/z and 125 m/z (S_{160}/S_{125}) can be used to calculate [A_1]:

$$\frac{S_{160}}{S_{125}} = k_1 [A_1] t \qquad \textbf{Equation S1}$$

where k_1 has been experimentally measured [*Viggiano et al.*, 1997] and is the collision rate constant. Equation S1 matches that given in Berresheim et al. [2000] with the implicit assumption that the MCC is able to transport and detect ions at 160 m/z and 125 m/z equally efficiently. However as is shown in Zhao et al. [2010], lighter ions are transported and detected less efficiently than heavier ions. The difference in efficiencies between these masses can be taken into account by dividing by the ratio of sensitivities for the different masses (see equation S11 in Chen et al. [2012] as an example). For the MCC between the masses of 125-195, the ratio of sensitivities is ~1.1-1.3, depending on the specific masses in the ratio; therefore, we have left out this sensitivity ratio to simplify the equation but have taken it into account in the MCC signal to concentration conversion. Figure S2 (left) shows S_{160}/S_{125} vs. time at varying [MA]. The linear fits of S_{160}/S_{125} vs. time gives a slope of $k_1[A_1]$ with non-zero y-intercepts for all [MA]. Two possible sources of uncertainty could cause this non-zero y-intercept. Other uncharacterized, ionizing species (x-ray or electrons) may escape from the source holder and ionize clusters in the flow reactor. Furthermore, the Po-210 lies inside an uncovered cavity within the source holder. Since the source holder sits in the flow reactor (see Figure 1), small amounts of sulfuric acid flow can enter into the cavity and mix with the nitrate ions. This would lead to longer than predicted CI reaction for some fraction of the sulfuric acid clusters.

Now consider both the nitrate ionization of A_2 and the IIC formation of A_2^-. Integrating these reaction equations at short time scales shows that the ratio of S_{195}/S_{160} is composed of neutral A_2 and A_2^- formed by IIC.

$$\frac{S_{195}}{S_{160}} = \frac{k_2}{k_1}\frac{[A_2]}{[A_1]} + \frac{1}{2}k_{21}[A_1]t \qquad \textbf{Equation S2}$$

A comparison between the slopes from Equation S1and Equation S2 provides evidence if k_{21} is the collision rate constant or not. A factor of 2 between the two slopes implies that $k_{21}=k_1$=collision rate constant. From comparing the two graphs in Figure S2 at [MA]=0 and 10 pptv, k_{21}=collision rate constant; however at [MA]=150 pptv, the ratio of the slopes is 2.5 (see Table S1). Although we suspect high uncertainty with these ratios, the trend still indicates that base effects IIC. Based upon conclusions from the main paper, we hypothesize that the concentration and identity of B will affect IIC. For the purpose of this paper, we assumed IIC proceeded at the faster collision rate. Thus, $[A_2]$ shown in Figure 2 is the lower limit. The actual $[A_2]$ will be higher (up to a factor of 4) than reported here but the fitted evaporation rates will still fall in the range reported in Table 2 and 2.

The y-intercepts from the linear fits of Figure S2 (right) show that for $[A_1]=4\text{x}10^9$ cm^{-3} and [MA]=0 pptv, the pre-existing $[A_2]=6\text{x}10^7$ cm^{-3}. The baseline measurements detailed in the main paper produced a fitted relationship for non-IIC corrected $[A_2]$ vs. $[A_1]$ of

$$[A_2] = 1.32\times10^{-10}[A_1]^{1.91} \qquad \textbf{Equation S3}$$

Therefore, at $[A_1]=4\text{x}10^9$ cm^{-3}, about 20% of the total 195 m/z signal is neutral dimer not produced via IIC.

Table S1 Comparison between slopes of S160/S125 and S195/S160 vs. time

[MA] (pptv)	Slope S_{160}/S_{125}	Slope S_{195}/S_{160}	Ratio of slopes S_{160}/S_{125} to S_{195}/S_{160}
0	7.0	3.4	2.0
10	4.5	2.2	2.0
150	1.6	0.64	2.5

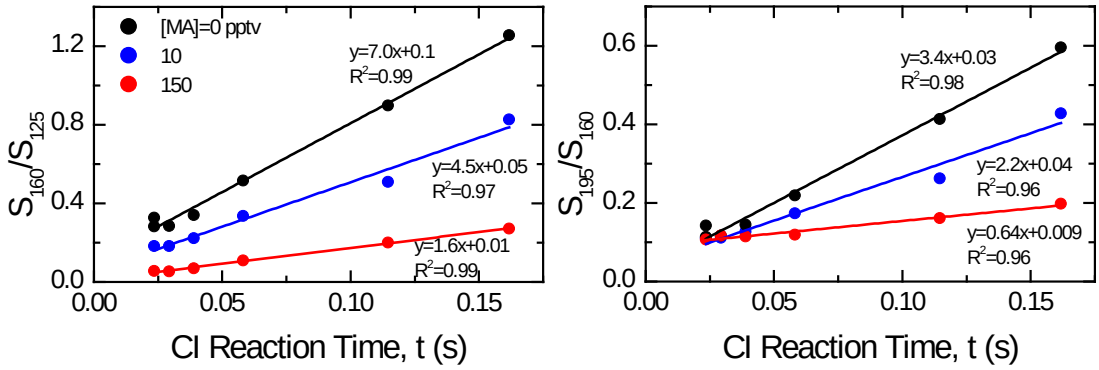

Figure S2 Left: Ratio of signals of 160 m/z and 125 m/z as a function of CI reaction time. Right: Ratio of signals of 195 m/z and 160 m/z as a function of CI reaction time. Each color represents a different [MA], and the lines are linear fits.

2.7.3 Repeatability of Flow Reactor Experiments and Uncertainty in Measurement

Several experiments were done at constant [B] on different times and days to study daily repeatability of measurements carried out in the flow reactor system. Figure S3 shows measurements of [A_1] and [A_2] made [MA]=80 pptv on three different days. Between these three days, 12 experiments of MA were conducted at [MA] from 10-260 pptv. The good daily repeatability (~10%) suggests that the flow reactor is able to quickly adapt to new [B] without significant “memory" of contamination from experiments carried out in the intervening period. Figure S3 also suggests that the base dilution/injection system developed in Zollner et al. [2012] and MCC have minimal daily variation. In addition to day-to-day variability, the total uncertainty also includes the systematic error of the MCC. The box on the bottom right of Figure S3 illustrates the systematic error of the MCC measurement. The systematic error in [A_2] could lower the predicted E_{2mv} and E_1 values, but they will fall in the range given in Tables 1 and 2. [A_2] error of 70% was determined from varying chemical ionization times and comparing the measured [A_2]. [A_1] error of 50% was calculated from error propagation [*Chen et al.*, 2012].

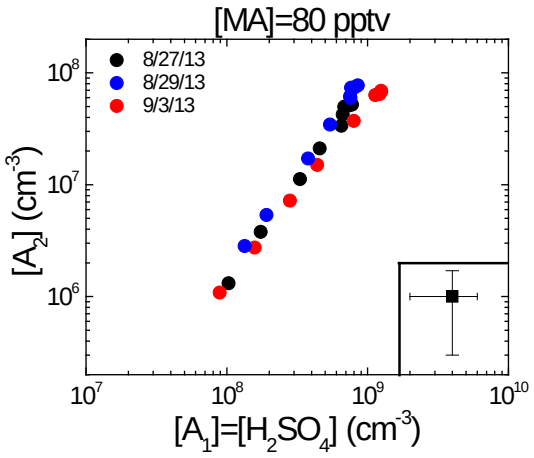

Figure S3 Measured $[A_2]$ vs. $[A_1]$ values for [MA]=80 pptv on three different days (black for 8/27/13, blue for 8/29/13, and red for 9/3/13). The box on the bottom right shows the systematic error of the MCC.

2.7.4 Collision-Controlled Limit at Steady State

The collision-controlled limit (CCL) is where every collision of A_1 with another A_1 or cluster forms a larger cluster that does not evaporate (no backward reaction). However, clusters are still lost via collisions with other particles (including monomer, clusters, or larger particles) and the wall of the Augsburg flow reactor. The CCL is important because it corresponds to the highest concentration of clusters that could be formed for a given $[A_1]$ [*McMurry*, 1983]. Observed cluster concentrations must be equal or less than the cluster-controlled limit. If less, then the difference must be related to the extent to which cluster concentrations are depleted by sulfuric acid evaporation. Figure S4 plots the measured $[A_2]$ vs. $[A_1]$ with the solid black line showing the CCL calculated from measured $[A_1]$. For all the bases except TMA, the measured $[A_2]$ falls on or below the CCL curve. This implies that either the monomer or dimer must be evaporating to depress the $[A_2]$ from the CCL concentration. Measured $[A_2]$ for TMA appears to exceed the CCL, possibly due to fault in the steady state assumption where long lifetime clusters would artificially raise the measured $[A_2]$. If this were true, then DMA would also suffer from inflated measured $[A_2]$. This does not change the conclusion that the series of conditions examined here predominately take place below CCL.

Figure S4 also shows that the measured $[A_2]$ approaches CCL curve for the highest $[A_1]$ and [B]. In this region, the production of A_2 (A_{2mv} and A_{2LV} from scheme 1

and A_2 from 2) will dominate the cluster balance equations due to high concentrations of reactants (e.g. $[A_1]$ and [B]). The rate of cluster evaporation is overwhelmed by the production rates because the evaporation rates depend on cluster composition and temperature but not on $[A_1]$ and [B].

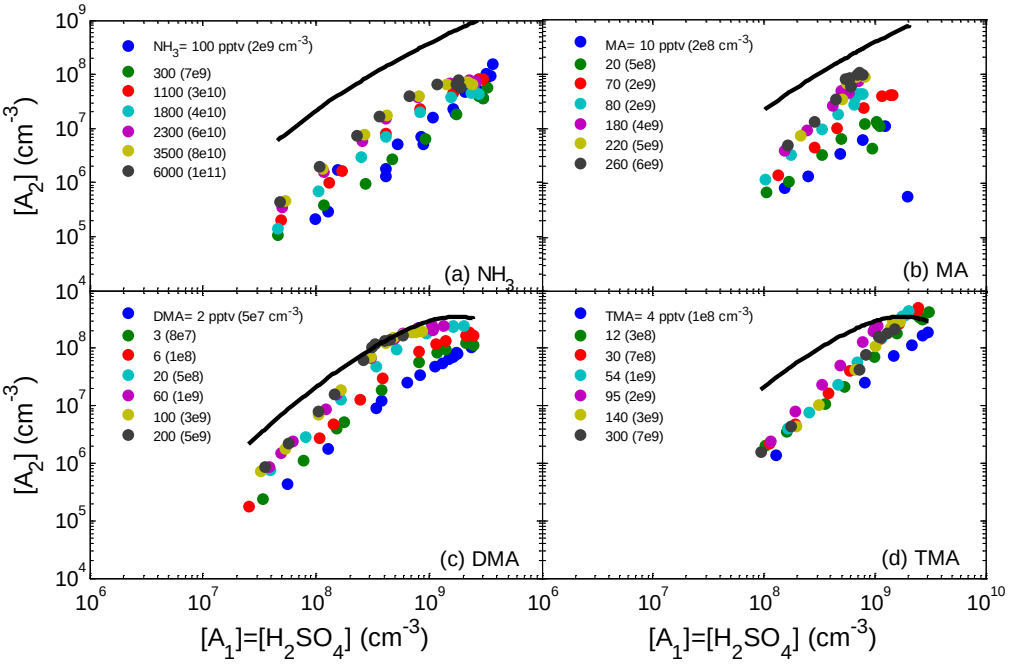

Figure S4 Measured $[A_2]$ vs. $[A_1]$ with the calculated collision controlled limit drawn as a black line. The collision-controlled $[A_2]$ was determined from measured $[A_1]$ and includes particle coagulation and wall losses. No cluster evaporation or base reaction is present at this limit. Most [B] and $[A_1]$ conditions produced measured $[A_2]$ below this limit. (a) NH_3, (b) MA, (c) DMA, and (d) TMA

2.7.5 Scheme 1 Acid-Base Reaction Model for Nucleation

Scheme 1 acid-base reaction model for nucleation is pictorially described on the left in Figure 4. The resulting rate equations for each species are given below.

Equation S4

$$\frac{d[A_1]}{dt} = -k_{11}[A_1]^2 + 2E_{2mv}[A_{2mv}] - k_{21}[A_{2LV}][A_1] - k_{31}[A_3][A_1] + E_3[A_3] - \kappa[A_1] - \eta[A_1]$$

$$\frac{d[B]}{dt} = -k_{21}^{'}[A_{2mv}][B] + E_{2Blv}[A_{2lv}] - \mu[B]$$ **Equation S5**

$$\frac{d[A_{2mv}]}{dt} = \frac{1}{2}k_{11}[A_1]^2 - E_{2mv}[A_{2mv}] - k_{21}^{'}[A_{2mv}][B] + E_{2BLV}[A_{2LV}] - k_{22}[A_{2LV}][A_{2mv}] - k_{21}^{"}[A_{2mv}]^2 - \kappa[A_{2mv}] - \eta[A_{2mv}]$$ **Equation S6**

$$\frac{d[A_{2LV}]}{dt} = k_{21}^{'}[A_{2mv}][B] - E_{2BLV}[A_{2LV}] - k_{21}[A_{2LV}][A_1] + E_3[A_3] - k_{22}[A_{2LV}][A_{2mv}] - k_{22}^{'}[A_{2LV}]^2 - \kappa[A_{2LV}] - \eta[A_{2LV}]$$ **Equation S7**

$$\frac{d[A_3]}{dt} = k_{21}[A_{2LV}][A_1] - E_3[A_3] - k_{31}[A_3][A_1] - \kappa_3[A_3] - \eta[A_3]$$ **Equation S8**

where
$[A_1]$ = monomer concentration
$[A_{2mv}]$ = more volatile dimer concentration
$[A_{2LV}]$ = less volatile dimer concentration
$[A_3]$ = trimer concentration
[B] = base concentration
E_{2mv} = evaporation rate constant for sulfuric acid from A_{2mv}
E_{2BLV} = evaporation rate constant for base from A_{2LV}
E_3 = evaporation rate constant of sulfuric acid from A_3
κ_i =first order coagulation rate to particles
η = wall loss rate
μ = base dilution coefficient

As an approximation, the forward rate constants, k_{ii}, are taken to be hard sphere collision rate for a sulfuric monomer using its bulk liquid density ($4x10^{-10}$ cm^3 s^{-1}) [*McMurry*, 1983; *Ortega et al.*, 2012]. For the transient solution, differential equations were solved numerically using Matlab's ode45 with an input of an initial $[A_1]$ and [B]. Initial $[A_1]$ was based upon the baseline concentration for a given sulfuric acid flow rate, and [B] was

taken to be 10 times the NLD. The other cluster concentrations were assumed to be zero at t=0 s.

2.7.6 Scheme 2 Acid-Base Reaction Model for Nucleation

Scheme 2 acid-base reaction model is pictorially described on the right in Figure 4. The resulting rate equations for each species are given below.

$$\frac{d[A_1]}{dt} = -k_{11}'[A_1][B] + E_1[A_1B] - k_{11}[A_1][A_1B] - k_{21}[A_1][A_2] + E_3[A_3] - \eta[A_1] - \kappa_1[A_1] \quad \textbf{Equation S9}$$

$$\frac{d[B]}{dt} = -k_{11}'[A_1][B] + E_1[A_1B] - k_2'[A_2][B] - k_3'[A_3][B] - \mu[B] \quad \textbf{Equation S10}$$

$$\frac{d[A_1B]}{dt} = k_{11}'[A_1][B] - E_1[A_1B] - k_{11}[A_1][A_1B] - k_{11}[A_1B]^2 - k_{21}[A_1B][A_2] + E_3[A_3] - \eta[A_1] - \kappa_1[A_1B] \quad \textbf{Equation S11}$$

$$\frac{d[A_2]}{dt} = k_{11}[A_1][A_1B] + \frac{1}{2}k_{11}[A_1B]^2 - k_{21}[A_1][A_2] - k_{21}[A_1B][A_2] - k_{22}[A_2]^2 + E_3[A_3] - \eta[A_2] - \kappa_2[A_2] \quad \textbf{Equation S12}$$

$$\frac{d[A_3]}{dt} = k_{21}[A_1][A_2] + k_{21}[A_1B][A_2] - E_3[A_3] - \eta[A_3] - \kappa_3[A_3] \quad \textbf{Equation S13}$$

where
$[A_1]$ = monomer concentration
$[A_1B]$ = more neutralized monomer concentration
$[A_2]$ = dimer concentration
$[A_3]$ = trimer concentration
[B] = base concentration
E_1 = evaporation rate constant of A_1B
E_3 = evaporation rate constant of sulfuric acid from A_3
κ_i =first order coagulation rate to particles
η = wall loss rate
μ = base dilution coefficient

2.7.7 Scheme 2 at Steady State and Applied to the Atmosphere

We assume all collision rate constants, k, are equal and clusters are only lost to larger clusters and not to the wall. The total signal at 160 m/z =[A_{1tot}] where

$$[A_{1tot}] = [A_1] + [A_1B] \qquad \textbf{Equation S14}$$

The monomer concentrations are assumed to be at equilibrium with [B] such that

$$\frac{k}{E_1} = \frac{[A_1B]}{[A_1][B]} \qquad \textbf{Equation S15}$$

Combining Equations S14 with S15 gives an expression for [A_1B].

$$[A_1B] = \frac{k[B]}{E_1 + k[B]}[A_{1tot}] \qquad \textbf{Equation S16}$$

The steady state balance from Equation S13 gives

$$[A_3] = \frac{k[A_{1tot}][A_2]}{E_3 + \kappa_3 + \eta} \qquad \textbf{Equation S17}$$

Combining the steady state balance from Equation S12 with Equations S14, S15, and S17 gives the steady state concentration of [A_2].

$$[A_2] = -\frac{1}{2k}\left(k[A_{1tot}]\left(1 - \frac{E_3}{E_3 + \kappa_3 + \eta}\right) + \kappa_2 + \eta\right) + \frac{1}{2k}\sqrt{\left(k[A_{1tot}]\left(1 - \frac{E_3}{E_3 + \kappa_3 + \eta}\right) + \kappa_2 + \eta\right)^2 + 4k[A_1B]^2\left(\frac{E_1}{[B]} + \frac{k}{2}\right)} \qquad \textbf{Equation S18}$$

From Chen et al. [2012], the nucleation rate is the formation of A_4 (i.e., J=J_4) and equals

$$J_4 = k[A_{1tot}][A_3] \qquad \textbf{Equation S19}$$

Substituting Equation S18 into S17 then S19 produces

$$J_4 = P' \bullet \frac{1}{2} k \left[A_{1tot} \right]^2$$ **Equation S20**

where P' is a prefactor. P' is always less than 1 and is defined as

$$P = -\frac{1}{E_3 + \kappa_3 + \eta} \left(k \left[A_{1tot} \right] \left(1 - \frac{E_3}{E_3 + \kappa_3 + \eta} \right) + \kappa_2 + \eta \right) + \frac{1}{E_3 + \kappa_3 + \eta} \sqrt{\left(k \left[A_{1tot} \right] \left(1 - \frac{E_3}{E_3 + \kappa_3 + \eta} \right) + \kappa_2 + \eta \right)^2 + 4k \left[AB \right]^2 \left(\frac{E_1}{[B]} + \frac{k}{2} \right)}$$ **Equation S21**

$[A_1B]$ is defined in Equation S19, leaving Equation S20 in terms of measurable concentrations.

2.7.8 $[A_2] / [A_1]$ vs. [B] for Constant $[A_1]$

The dependence of $[A_2]$ on [B] is better illustrated by taking a vertical slice of Figure 2. This creates the graphs in Figure S5 through Figure S8 where the measured $[A_2] / [A_1]$ ratio is a function of [B]. The lines on Figure S5 represent the steady state model of scheme 1 for the given fitted evaporation rates. This model and solution method does well in capturing the trend of increasing then plateauing trend of $[A_2] / [A_1]$ with increasing [B]. The leveling off is the saturation point. The model also captures decently well the dependence of the ratio on $[A_1]$. The model does not capture the peaking behavior of TMA curves. The steady state solution for scheme 2 is shown in Figure S6 and more accurately describes the observations seen in the DMA graph. However, this model underpredicts the ratio at low $[A_1]$.

Using the transient solution for scheme 1, given in Figure S7, to predict the ratios produces worse agreement with NH_3 and MA but better for DMA and TMA. This is consistent with our hypothesis that long-life time clusters are unsuited to be modeled via steady state. The transient solution for scheme 2 is given in Figure S8. This model most accurately reproduces the shape of DMA out of the four solution methods/schemes.

Overall, both schemes capture the correct trends of the ratio vs. [B] and the spread of the curves.

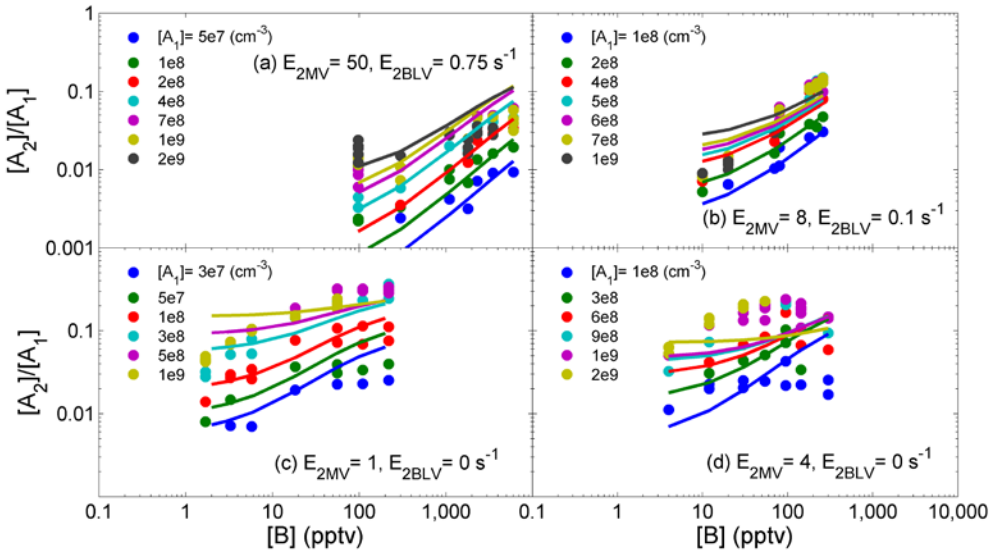

Figure S5 The ratio $[A_2]$ /$[A_1]$ vs. [B] better illustrates the dimer dependence on [B]. Each color is at a constant $[A_1]$ and the lines are the predicted steady state ratios from scheme 1. (a) NH_3, (b) MA, (c) DMA, and (d) TMA

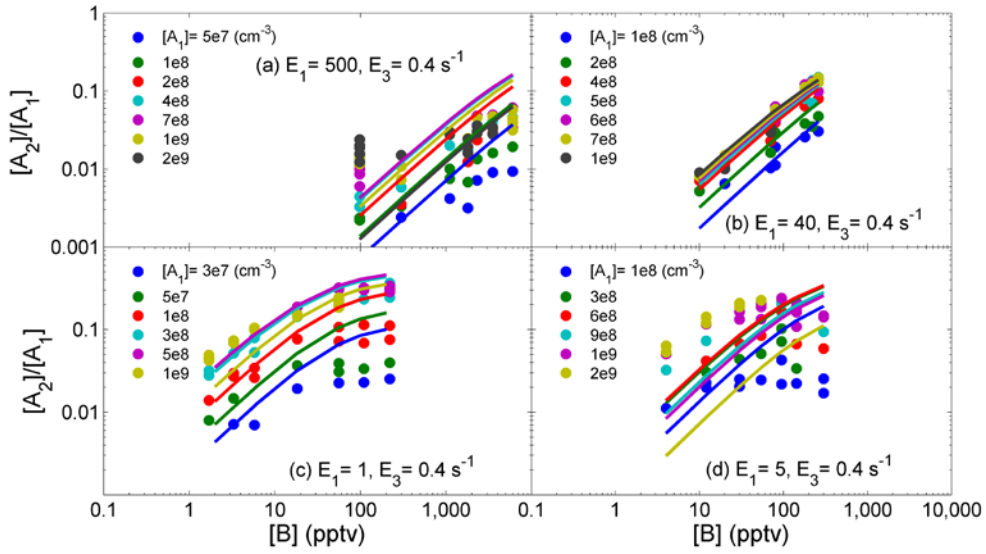

Figure S6 Ratio of $[A_2]$ /$[A_1]$ vs. [B] solved at steady state for scheme 2 (lines). (a) NH_3, (b) MA, (c) DMA, and (d) TMA

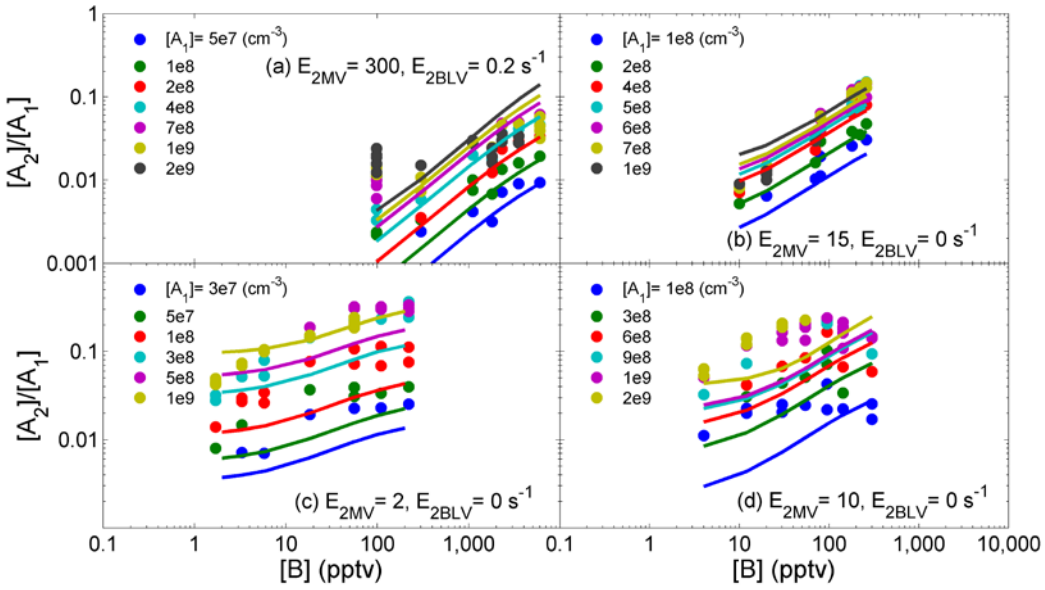

Figure S7 [A_2] / [A_1] vs. [B] at constant [A_1]. The lines were calculated from the transient solution of scheme 1. (a) NH_3, (b) MA, (c) DMA, and (d) TMA

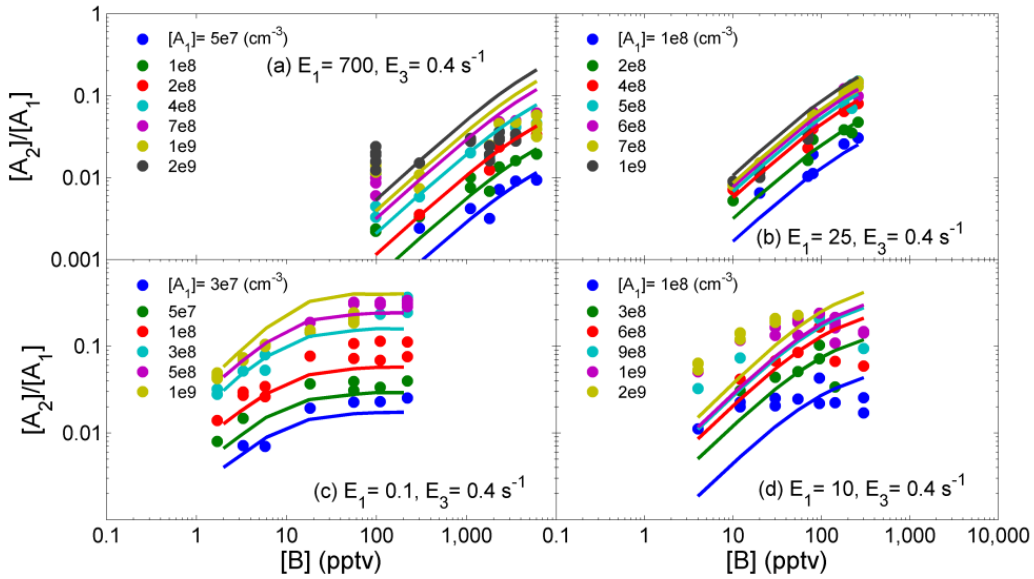

Figure S8 [A_2] / [A_1] vs. [B] at constant [A_1]. The lines were calculated from the transient solution of scheme 2. (a) NH_3, (b) MA, (c) DMA, and (d) TMA

2.7.9 Time Dependent Behavior of Particle Coagulation Loss

For this study, particle coagulation loss rate is calculated from the particle size distributions measured by the DEG SMPS [*Iida et al.*, 2009; *Jiang et al.*, 2011b] for particles >1.3 nm (geometric diameter). The instrument sampled from a 1/8 inch stainless steel tube inserted into the center of the flow reactor. The sampling point was ~2 cm above the MCC sampling region. The size distribution and thus loss rate to larger particles, κ, are functions of $[A_1]$, [B], and time. Figure S9 depicts κ as a function of $[A_1]$ for varying [DMA]. From this figure, κ was described as a power law extrapolation as a function of measured $[A_1]$. For conditions investigated in this study, κ is smaller than the wall loss rate of $\eta=0.05\ s^{-1}$ for almost all $[A_1]$. At high $[A_1]$, however, κ is large and plays a much larger role in the cluster balance equations. This helps to explain the downturn of $[A_2]$ at high $[A_1]$.

κ plays a much more complicated role in the transient solution method due to the evolving particle distribution with respect to time. The total number of particles at the point of injection is less than at the 3 sec sampling point. This is due to base reacting with the clusters and forming stable clusters. Therefore, κ will increase as time progresses. The maximum κ for the transient model can be approximated from the 3 sec particle distribution and held constant from t=0 to 3 sec. This high κ changes the model lines to those shown in Figure S10 and Figure S11 (*cf.* Figure 6 where total loss rate equals η). The increase of loss prevents the calculated $[A_1]$ and $[A_2]$ from reaching the full range seen in the measured data. However, increasing the loss rate does not alter the fitted evaporation rates.

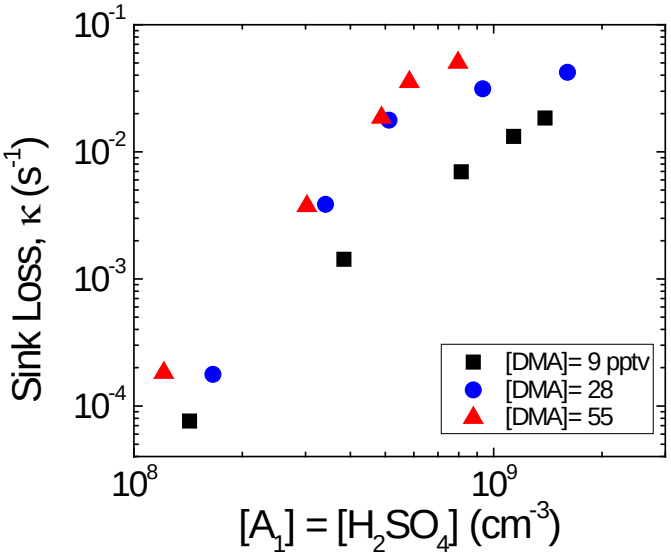

Figure S9 Particle sink loss rate vs. MCC measured [A_1]. Sink loss rate was determined from the A_{fuchs} of the DEG SMPS measured size distribution for particles >1.3 nm in this study.

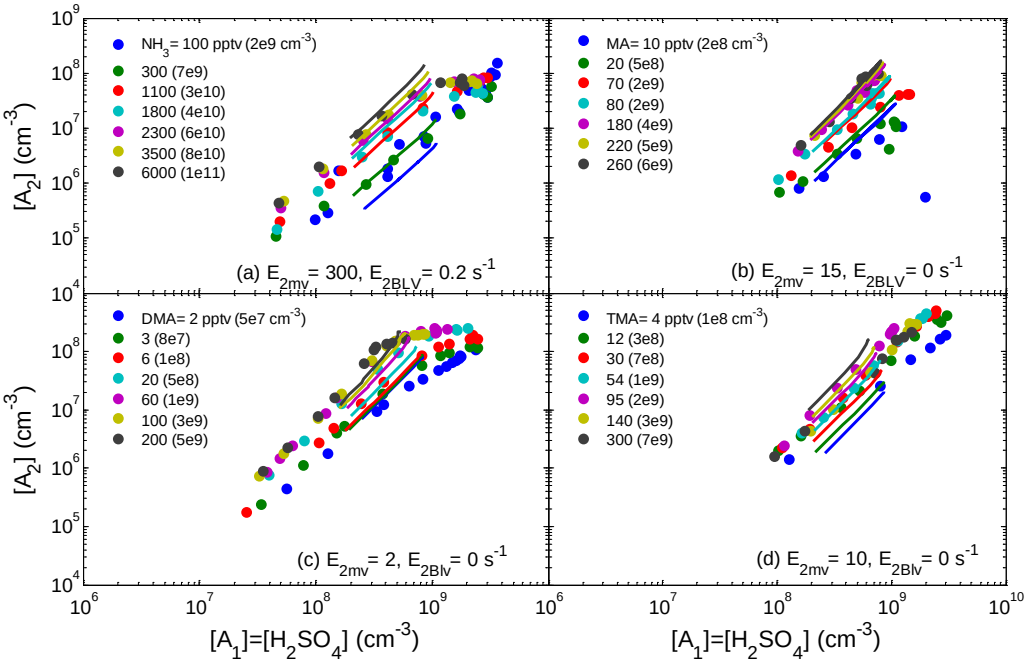

Figure S10 Transient solution to scheme 1 with maximum amount of particle coagulation loss. The lines are the model predictions and points are measured concentrations. The fitted evaporation rates remain unchanged. (a) NH_3, (b) MA, (c) DMA, and (d) TMA

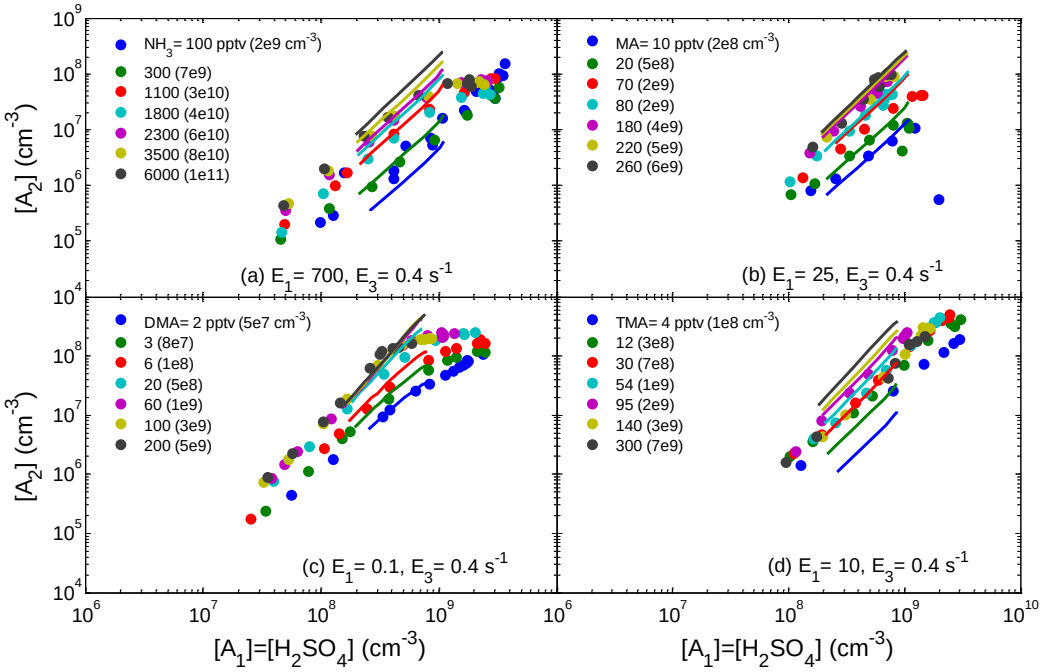

Figure S11 Transient solution of scheme 2 (lines) with maximum amount of particle coagulation loss. (a) NH_3, (b) MA, (c) DMA, and (d) TMA

Chapter 3. Towards Reconciling Measurements of Atmospherically Relevant Clusters by Chemical Ionization Mass Spectrometry and Mobility Classification/Vapor Condensation[c]

3.1 Overview

This chapter presents a method to compare number concentrations of cluster composed of sulfuric acid and dimethylamine measured by two fundamentally different instruments: a chemical ionization mass spectrometer (Cluster CIMS) and a mobility classification/vapor condensation particle counter (DEG SMPS). Both instruments have large uncertainties in their overlapping size range of ~1 nm geometric diameter. This size represents larger clusters between 3-5 sulfuric acid molecules. Comparison between the two instruments provides insights into which uncertainties affect the measured concentrations the most. The results indicate that inefficient nitrate chemical ionization limits the number of clusters the Cluster CIMS is able to detect. By changing the chemical ionization reagent ion to a stronger base (e.g. acetate ion), the Cluster CIMS is able to detect more cluster types and at higher concentrations. This leads to better agreement between the two instruments. Furthermore, a comparison at high sulfuric acid concentration (10^9 cm^{-3}) reveals that ion-induced clustering in the charger of the DEG SMPS may artificially produce particles large enough to be detected, resulting in higher than expected number concentrations at 1 nm.

3.2 Introduction

We have previously reported measurements of the complete particle number distribution down to one molecule made during atmospheric nucleation events [*Jiang et al.*, 2011c]. The Cluster Chemical Ionization Mass Spectrometer (Cluster CIMS) [*Zhao et al.*, 2010] measured concentrations of sulfuric acid vapor and sulfuric acid-containing

[c] This chapter except for the overview is reproduced with permission from Jen, C. N., Hanson, D. R., and McMurry, P. H.: Towards Reconciling Measurements of Atmospherically Relevant Clusters by Chemical Ionization Mass Spectrometry and Mobility Classification/Vapor Condensation, Aerosol Science and Technology, ARL, 49, i-iii, 10.1080/02786826.2014.1002602, 2015.

clusters, while a scanning mobility particle spectrometer equipped with a diethylene glycol condensation particle counter (DEG SMPS) measured number distributions down to ~1 nm. Cluster CIMS and DEG SMPS measurements typically agreed to within an order of magnitude in the overlap ~1 nm range and showed similar trends with size.

Jiang et al. [2011c] discussed sources of measurement error. For the Cluster CIMS, errors include interferences from high molecular weight gas molecules, and uncertainties in chemical ionization efficiencies, ion-induced clustering (IIC), and mass discrimination [*Chen et al.*, 2012; *Zhao et al.*, 2010]. For the DEG SMPS, uncertainties include material-dependent charging and DEG CPC activation efficiencies [*Iida et al.*, 2009], as well as possible IIC in the bipolar charger.

In this study, we carried out laboratory experiments aimed at exploring these uncertainties for clusters formed from sulfuric acid and dimethylamine (DMA). Trace gas interferences have been eliminated from the clean flow reactor used here [*Jen et al.*, 2014]. Cluster CIMS measurements were done using both nitrate ($HNO_3 \bullet NO_3^-$) and acetate ($H_2O \bullet CH_3CO_2^-$) to test the hypothesis that chemical ionization efficiencies depend on the proton affinity of the reagent ions and composition of neutral clusters. The transfer function for the DEG SMPS mobility classifier is sufficiently broad to allow more than one cluster type to simultaneously reach the DEG CPC, and this was explicitly taken into account when comparing data from the two instruments. The DEG SMPS measurements were done at three fixed classifying voltages corresponding to centroid mobility diameters of 1.23 nm, 1.34 nm, and 1.55 nm. Mass (geometric) diameters are 0.3 nm smaller than mobility diameters [*Larriba et al.*, 2011]. As voltages were not scanned, we refer to these as DEG MPS measurements.

The 5 cm diameter flow reactor has been described previously [*Jen et al.*, 2014]. In brief, sulfuric acid vapor ($[A_1]=10^7$-10^9 cm^{-3}) was introduced near the entrance, and DMA ([DMA]=2-110 ppt) was injected at a point to allow the sulfuric acid and DMA to react for 3 s before measurement. Further experimental details are described in Supplemental Information (SI).

3.3 Ion Mobilities and Mobility Classifier Transfer Function

Ion cluster mobilities were calculated using a particle dynamics program [*Larriba and Hogan*, 2013a; b]. The modeled ion compositions include dimer (A_2^-), trimer (A_3^-), and tetramer (A_4^-), as well as clusters with DMA molecules (see Table S1). The structures of these ion clusters are from Ortega et al. [2014]. The simulations ran at experimental conditions of T=300 K and P=1 atm. The reemission velocity was set to 92% of Maxwell distribution. Water is not included in these structures but is likely present in the ions. We assume that water does not significantly affect the cluster's mobility diameter.

The TSI 3085 transfer function, Ω, has been measured previously and interpolated to the conditions of this study [*Jiang et al.*, 2011a]. Figure 10 shows Ω for a classifying voltage of 4.5 V, sheath flow of 13 LPM, and aerosol flow of 2.0 LPM. The points signify clusters that would penetrate through the mobility classifier at these operating conditions. The Ω value for each cluster represents the fraction of clusters that will be delivered to the DEG CPC. The clusters highlighted in red are detected by nitrate whereas acetate detects all clusters.

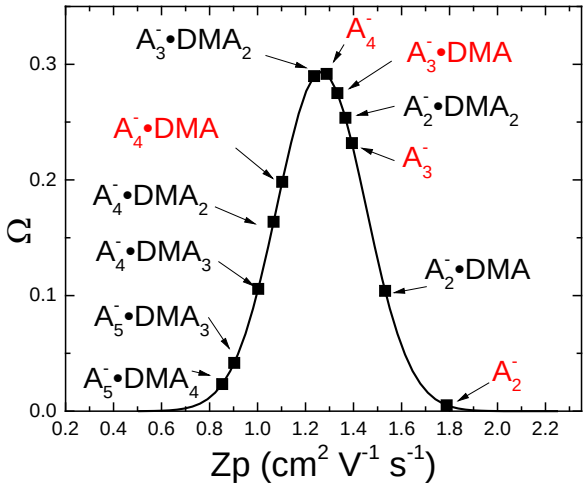

Figure 10 TSI 3085 transfer function at the classifying voltage and flow rate used in this study. Clusters that fall within the mobility window are also shown. Those in red were detected by the Cluster CIMS using nitrate.

3.4 Cluster CIMS vs. DEG MPS at 1.34 nm Centroid Mobility Diameter

The value of Ω was multiplied by the measured Cluster CIMS concentration for each cluster type. The resulting concentrations were summed over all Cluster CIMS

detected cluster types to give the predicted DEG MPS. The measured DEG MPS concentrations were inverted following Jiang et al. [2011b], taking into account transport losses in the mobility classifier at 2 LPM and size-dependent charging and activation efficiencies.

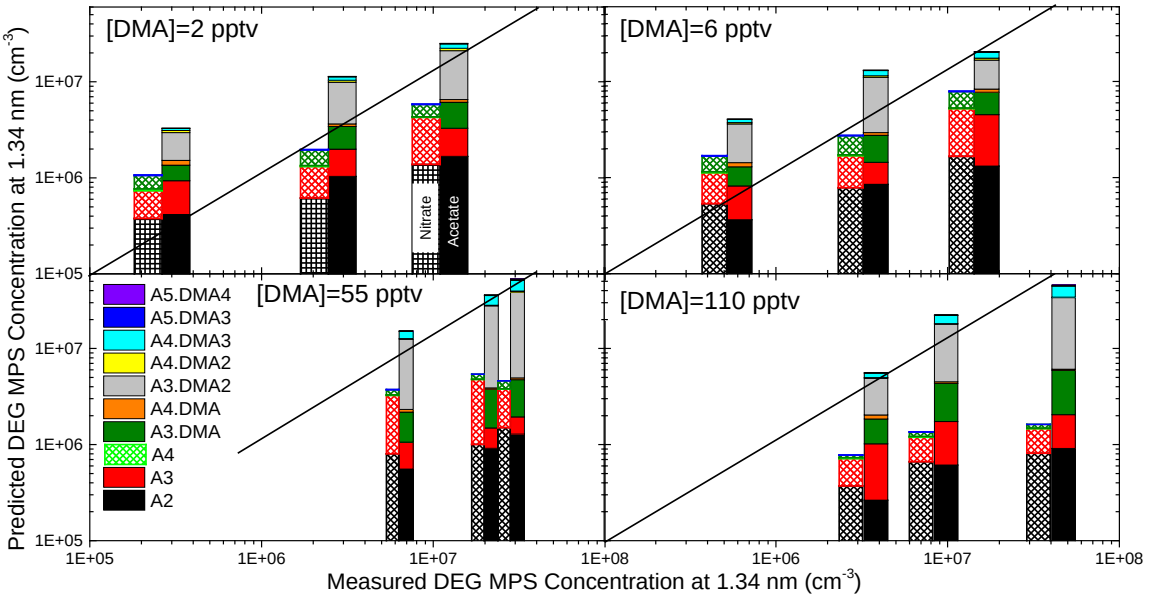

Figure 11 Comparison of predicted DEG MPS concentration at 1.34 nm centroid mobility diameter to measured DEG MPS concentration at various [DMA]. The colors in the bar represent each cluster type and its contribution to the total number concentration. Cluster CIMS measurements were done using acetate (solid bars) and nitrate (hash-marked bars). The lines show 1:1 comparisons. This method was applied to two other centroid mobility diameters: 1.23 (3.8 V) and 1.55 nm (6.0 V). These results are given in the SI and show good agreement.

Figure 11 compares these predicted DEG MPS concentrations to values measured by DEG MPS. Results are shown for four [DMA] using both nitrate (hashed bars) and acetate (solid bars). Cluster CIMS concentrations were not corrected for IIC as IIC contributions were deemed negligible (see SI). The various colors in the bar represent the various clusters detected by the Cluster CIMS. The height of each color segment represents the concentration of a specific cluster that would penetrate the mobility classifier (note log scale). For measurements carried out using nitrate, the agreement between the two instruments worsens as [DMA] increases. Acetate detects many more

clusters types than nitrate and also leads to better agreement between instruments. This suggests that acetate is more efficient at chemically ionizing more neutralized clusters. DEG MPS are below those measured by the Cluster CIMS at low [A_1]. Under these conditions, most of the clusters that penetrate through the mobility classifier are dimers. It is possible that the DEG CPC does not detect dimers efficiently.

3.5 Conclusion

This study demonstrates substantial progress towards reconciling measurements of ~1 nm cluster number concentrations in a sulfuric acid/DMA system by two independent measurement methods: chemical ionization mass spectrometry and mobility classification coupled to a vapor condensation particle counter. Chemical ionization measurements carried out with acetate ions led to significantly better agreement than those done with nitrate, especially at high [DMA]. This suggests that ion proton affinity plays an important role in the chemical ionization process. For the DEG MPS, the uncertainty in charging and activation efficiency increases as cluster size decreases. Thus, the largest uncertainty of the DEG MPS measured concentration is at low [A_1] where the size distribution is dominated by the smallest clusters.

3.6 Supporting Information[d]

3.6.1 Experimental Setup

The Cluster CIMS and DEG MPS data were taken in the extraordinarily clean and highly repeatable Augsburg flow reactor. The flow reactor setup and procedure have been described previously [*Jen et al.*, 2014]. The nitrogen flow rate in the reactor was 4 (STP) LPM with trace amounts of sulfuric acid, water vapor, and injected basic gases. The base injection point to the Cluster CIMS sampling region results in a ~3 s reaction time between the basic gas and the sulfuric acid vapor and clusters. Since the DEG MPS samples gas 10 cm above the Cluster CIMS sampling region, a higher base injection port was used to preserve the ~3 s reaction time. The basic gas studied here is dimethylamine (DMA) and its concentrations ([DMA]) were measured by the Cluster CIMS in positive ion mode (see Jen et al. [2014]) and calculated *a priori*. The Cluster CIMS separately used nitrate ion (with a ligand, $HNO_3 \bullet NO_3^-$) and acetate (with a water ligand, $H_2O \bullet CH_3CO_2^-$) to chemically ionize sulfuric acid clusters. Acetate was produced by passing nitrogen above a reservoir of acetic anhydride and then over a radioactive charger (Po-210). The cluster signals from the Cluster CIMS were converted to concentrations using a chemical ionization reaction time of 15 ms for nitrate and 18 ms for acetate and following the inversion detailed below and in Jen et al. [2014].

The DEG MPS also used a Po-210 strip to charge clusters and particles before they entered the TSI 3085 mobility classifier. From Jiang et al. (2011), we assume that theoretically predicted bipolar steady-state charging efficiencies can be extrapolated to the 1 nm size range. Premnath et al. [2011] showed that chemical ionization is important up to a critical size of ~0.5 nm for amino acids and trimethylamine, above which charging is controlled by ion transport. This critical size is dependent on the chemical

[d] Supporting information is reproduced with permission from Jen, C. N., Hanson, D. R., and McMurry, P. H.: Towards Reconciling Measurements of Atmospherically Relevant Clusters by Chemical Ionization Mass Spectrometry and Mobility Classification/Vapor Condensation, Aerosol Science and Technology, ARL, 49, i-iii, 10.1080/02786826.2014.1002602, 2015.

system involved and must differ from the system studied here as nitrate and acetate clearly chemically ionize different clusters at a much larger size of 1.34 nm. The Po-210 charger used with the DEG MPS produces numerous types of ionizing ions, many of which have not been characterized, that go on to charge the neutral sulfuric acid+DMA clusters. Further refinements in the bipolar charging of the smallest clusters require a better understanding of the chemical system.

The mobility classifier operated in positive polarity (negative ions) with 13.0±0.5 LPM sheath flow rate and a 2.2±0.2 LPM sample flow rate. Operating conditions of the DEG CPC followed that of Jiang et al. [2011b], with the saturator and condenser temperatures at 59 and 20˚C, respectively. The capillary and condenser flow rates were 0.03 and 0.3 LPM respectively.

3.6.2 Clusters and their Mobilities

Mobilities of various sulfuric acid and DMA ion clusters were calculated using a particle dynamics simulation [*Larriba and Hogan*, 2013a; b]. Table S2 lists the ion cluster compositions and their calculated mobilities. Ion structures were taken from the SI of Ortega et al. [2014] and computed via density functional theory. These structures represent the minimum energy at zero K. At room temperature, these clusters can access many lower energy structures and thus could alter the calculated mobility. Furthermore, under ambient conditions, clusters likely include water, and this is probably a larger source of uncertainty in the ion mobilities. The following shorthand notation is used: A_1^- is HSO_4^-, A_2^- is $H_2SO_4 \bullet HSO_4^-$, etc.

Table S2 Mobilities of sulfuric acid clusters with DMA in N_2 carrier gas

Cluster	Mobility ($cm^2\ V^{-1}\ s^{-1}$)
A_1^-	2.21
A_2^-	1.79
A_3^-	1.39
A_4^-	1.29
A_2^-•DMA	1.53
A_3^-•DMA	1.33
A_4^-•DMA	1.10
A_2^-•DMA_2	1.37
A_3^-•DMA_2	1.24
A_4^-•DMA_2	1.07
A_4^-•DMA_3	1.00
A_5^-•DMA_3 *	0.90
A_5^-•DMA_4 *	0.85

*Extrapolated mobility as no ion coordinates have been published.

3.6.3 Ion-Induced Clustering (IIC) in Sulfuric Acid/Dimethylamine Environment

IIC has been modeled for the pure sulfuric acid environment where the list of reactions is given in Chen et al. [2012]. The amount of IIC produced clusters depends primarily on the chemical ionization (CI) reaction time, t, and $[A_1]$. The relationship between the dimer signal (S_{195},for nitrate-detected A_2) to monomer signal (S_{160}, HNO_3•HSO_4^-, for nitrate-detected A_1) that takes into account direct ionization of A_2 and IIC-produced A_2^- can be obtained by integrating the rate equations with respect to time (see Hanson and Lovejoy [2006] and Chen et al. [2012]) and assuming no change in reagent ion concentration as a function of time.

$$\frac{S_{195}}{S_{160}} = \frac{k_2}{k_1}\frac{[A_2]}{[A_1]} + \frac{1}{2}k_{21}[A_1]t \qquad \textbf{Equation S22}$$

where
A_1 = neutral monomer
A_2 = neutral dimer
k_i = nitrate ionization rate constant
k_{ij} = IIC rate constant

This relationship implies that as time goes to 0 s, the amount of IIC-produced A_2^- reduces to zero. As a result, applying a linear fit to measurements of S_{195}/S_{160} as a function of t gives a y-intercept that describes the amount of neutral $[A_2]$ compared to $[A_1]$. For nitrate reagent ion, measured k_1 is 1.9×10^{-9} cm^3 s^{-1} [*Viggiano et al.*, 1997] and k_2 is taken to be the ion-molecule collisional rate constant of 1.9×10^{-9} cm^3 s^{-1} [*Su and Bowers*, 1973]. Therefore, with these values of $k_1$and k_2 and assuming negligible background signal, the y-intercept gives the amount of neutral $[A_2]$ for a measured $[A_1]$.

Figure S12 depicts how nitrate measured S_{195}/S_{160} changes with CI reaction time at four different [DMA] and equivalent initial concentrations of A_1, $[A_1]_o$. The dotted line illustrates the S_{195}/S_{160} at the CI reaction time used in this study of 0.018 s. A linear fit was applied to the data (solid line) and extrapolated to t=0 s (dashed line). At [DMA]=0 pptv, the S_{195}/S_{160} at t=0 s is significantly different than at t=0.018 s (0.004 compared to 0.05 respectively). This signifies that IIC produced dimers account for the vast majority of detected dimer ions and must be subtracted from the apparent $[A_2]$ to obtain true $[A_2]$. However, in the presence of DMA, S_{195}/S_{160} at t=0 s closely matches the ratio values at t=0.018 s. This suggests that IIC produces a negligible amount of dimer ions at t=0.018 s in the sulfuric acid+DMA system for conditions pertinent to this study.

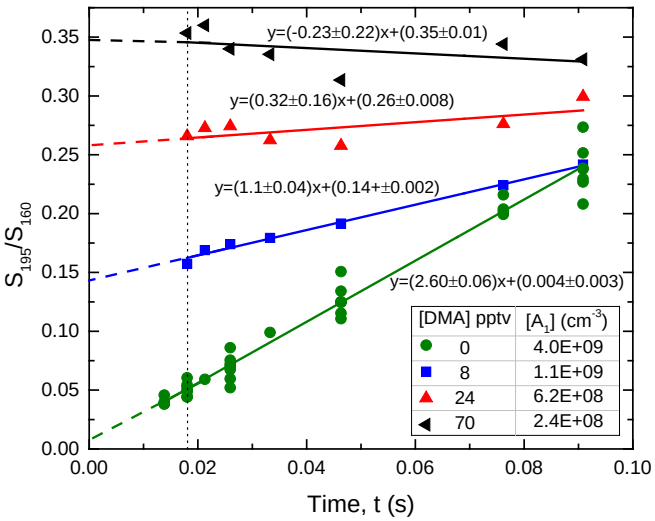

Figure S12 Nitrate measured ratios of S_{195}/S_{160} as a function of CI reaction time at the same $[A_1]_o$ and four [DMA]. Measured $[A_1]$ at each [DMA] is given in the legend. Dashed line extrapolates the linear fit to t=0 s, where the y-intercept gives the fraction of neutral $[A_2]$ to the neutral $[A_1]$. The dotted line indicates the CI reaction time used in this study with nitrate of 0.018 s.

3.6.4 Nitrate vs. Acetate Sulfuric acid/DMA Spectra Comparison

Figure S13 compares the mass spectra between nitrate (black) and acetate (red) at [DMA]=110 pptv and $[A_1]_o=4x10^9$ cm^{-3}. Note that higher cluster concentrations were found with acetate than nitrate. For example, $A_3^-•DMA_2$ measured using acetate is about a factor of 10 higher than with nitrate. Also, acetate allowed more types of cluster to be detected. As the only variation between these experiments is the chemical ionization ion, we infer that the difference in cluster signals is due to the higher proton affinity (gas phase basicity) of acetate relative to nitrate. These results would appear to be at variance with recent results of Kürten et al. [2014], who reported the efficient detection of clusters such as $A_3•DMA_2$ using nitrate. More work is needed to reconcile these results.

Figure S2 also shows that the nitrate spectrum is very clean with almost no background peaks obscuring the important sulfuric acid peaks. This is to be expected as nitrate is a very selective ion, i.e. it can only chemically ionize very acidic clusters. The acetate spectrum has a high background which can artificially increase the signals at the key masses. The background is due to trace impurities in the acetic anhydride reservoir or their evaporation from surfaces; we believe these impurities get ionized by Po-210 but do not affect the chemical ionization of sulfuric acid clusters by acetate or the formation of neutral clusters in the flow reactor. This assumption is based upon very good agreement for both total $[A_1]$ and $[A_2]$ as measured by either nitrate or acetate. In addition, the acetate spectrum shows a nitrate peak (125 m/z) at ~15% of the value in the nitrate spectrum. Nitrate in the acetate system is probably due to adsorbed nitric acid on the surfaces outside the source holder from when the Cluster CIMS used nitrate as its source ion. We believe that such a small amount of nitrate will not alter the amount of sulfuric acid clusters detected by acetate.

Since there is high background using acetate, we took the signals at low $[A_1]_o \approx 10^7$ cm^{-3} (DMA=0 pptv) as the background concentration level for all pure sulfuric acid cluster concentrations (e.g., $[A_2]$ at 195 m/z, $[A_3]$ at 293 m/z, etc.). The backgrounds for the aminated clusters was taken to be the concentration at those specific masses without

DMA added but at the equivalent $[A_1]_o$, though changes in $[A_1]_o$ had no effect on these background concentrations.

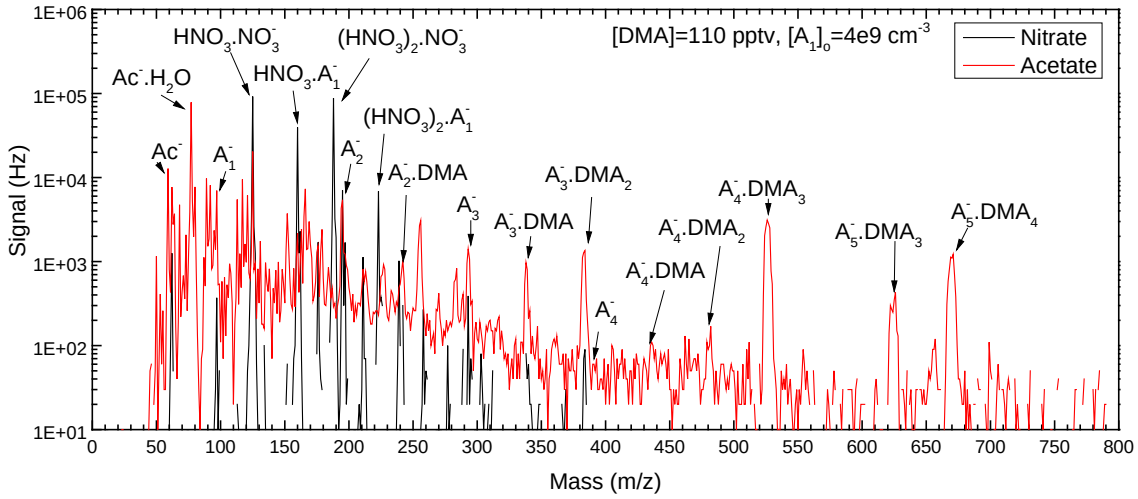

Figure S13 Mass spectra comparison between nitrate (black) and acetate (red) chemical ionization ions. These spectra were measured at [DMA]=110 pptv and $[A_1]_o$=4x10^9 cm^{-3}. Key peaks are identified with acetate abbreviated as Ac$^-$.

3.6.5 Cluster CIMS vs. DEG MPS at 1.34 nm Centroid Mobility Diameter without DMA

The comparison detailed in the main body of the paper was also done for a pure sulfuric acid environment ([DMA]=0 pptv). Figure S14 shows the comparison between predicted DEG MPS concentration and measured concentrations at 1.34 nm centroid mobility diameter. Cluster concentrations measured by acetate and nitrate were nearly equal, thus only measurements using nitrate are shown. While concentrations measured by the DEG MPS are correlated with those predicted from Cluster CIMS measurements, the DEG MPS concentrations are about 100 times higher.

Two possibilities exist: either the Cluster CIMS is under-measuring the cluster concentrations or the DEG MPS is over-measuring. We believe that in the pure sulfuric acid/water environment, the Cluster CIMS accurately measures the cluster concentrations. The chemical ionization of sulfuric acid by nitrate is fairly well understood and occurs at the collision rate. In addition, the formation of A_2^- via IIC from

sulfuric acid vapor and bisulfate ion can be modeled accurately and subtracted from the measured [A_2] (see section above). Both processes depend on the chemical ionization reaction time which can be calculated from the electric field and gap distance between the ion source and the Cluster CIMS inlet. Overall, the uncertainties from these processes are estimated to be no greater than 50% and they cannot not account for a factor of 100 difference.

Therefore, we conclude the DEG MPS over measures the cluster concentrations under these conditions. One reason is that IIC can occur after the sample flow is ionized. The residence time of the ionized sample flow is ~1 s (from the charger to the point the sample enters the mobility classifier), resulting in the formation of ionic clusters large enough to penetrate the mobility classifier. Unlike the Cluster CIMS, a straightforward method does not exist to take account for IIC in the DEG MPS.

Another possibility is that sulfuric acid vapor or clusters reacts with the diethylene glycol condensation vapors in the DEG CPC. Hanson et al. [2002] showed that sulfuric acid reacts with n-butanol to form particles. Dehydration of ethylene glycol by sulfuric acid is a well-known reaction [*McMurry*, 2008], so it is possible that diethylene glycol may also undergo a similar dehydration reaction. This process could produce particles inside the DEG CPC in a pure sulfuric acid environment or could alter the activation efficiency of the smallest clusters.. In the presence of a base such as DMA, a large fraction of the sulfuric acid vapor is bound to one or two DMA molecules. Sulfuric acid+DMA clusters may not interact with DEG in the same manner as pure sulfuric acid. Regardless, more studies need to be done to understand the activation efficiency of DEG in the presence of atmospherically relevant small clusters.

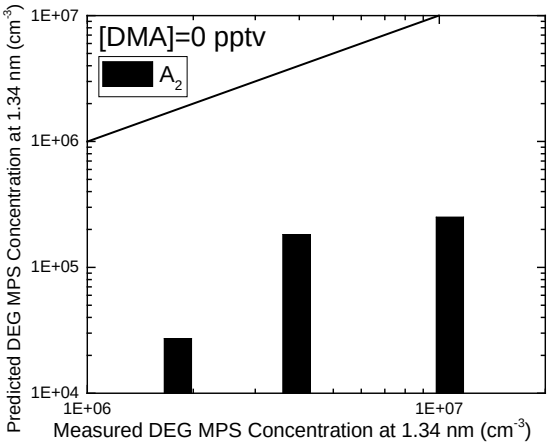

Figure S14 Comparison between predicted DEG MPS concentration from Cluster CIMS (nitrate) to the measured DEG MPS concentration at a classifying voltage of 4.50 V (1.34 nm centroid mobility diameter) and [DMA]=0pptv. The black line is the 1:1 comparison. Only one type of cluster was detected. The other clusters were below detection limit.

3.6.6 Predicted DEG MPS Comparisons at 1.23 and 1.55 nm Mobility Diameter

Figure S15 shows the transfer functions of the TSI 3085 mobility classifier at three different voltages: 3.80, 4.50, and 6.00 V. This corresponds to the centroid sizes of 1.23, 1.34, and 1.55 nm mobility diameter and mobilities of 1.47, 1.27, and 0.92 $cm^2\ V^{-1}\ s^{-1}$ respectively. Following the procedure detailed in the main paper, Figure S16 and Figure S17 compare predicted DEG MPS concentrations measured using acetate as the reagent ion with the Cluster CIMS to measured DEG MPS concentration at 1.23 and 1.55 nm. For all three sizes, the predicted concentrations agree well with the measured concentrations to within an average factor of 3. However, we observe two systematic trends: 1) the ratio between predicted concentrations to those measured decrease with increasing [DMA] and 2) the ratio between predicted and measured concentrations increase as the measured concentration (or $[A_1]$) decreases. For the latter at low $[A_1]$, the cluster distribution is primarily composed of dimers. The DEG MPS calibration curves have not been measured down to this size and could explain the poorer agreement.

The [DMA] dependence indicates a systematic uncertainty with one of the instruments. We believe this may be due to very small clusters/vapors that are unobserved by the Cluster CIMS but still penetrate the mobility classifier. Consider at 1.23 nm where this trend is most pronounced (Figure S16). The transfer function for 1.23 nm displayed on the left of Figure S15 suggests that clusters smaller than the dimer can

penetrate through the mobility classifier but are not observed by the Cluster CIMS. For example, A_1•DMA_x, where x≥1 and is number of DMA molecules, is not seen by the Cluster CIMS with either nitrate or acetate but would penetrate the mobility classifier and might be measured by the DEG MPS. Also sulfuric acid vapor can pass through the mobility classifier, which could mean that other vapor molecules, such as amines, might also be measured by the DEG CPC. Both possibilities might explain why at high [DMA], the agreement worsens.

However in the presence of DMA, the overall agreement is reasonable (on average a factor of 5 difference) which gives us confidence that our method for comparing the two types of instruments is valid. Also, this agreement supports our conclusions drawn from the IIC study detailed above. If IIC played a role in the sulfuric acid+DMA system, then we would expect the DEG MPS measured number concentration at 1.23 nm to be biased much higher because even in a short reaction time IIC would still produce a considerable amount of A_2^-. These would penetrate the mobility classifier and may be counted by the DEG CPC in the 1.23 nm size bin. Our measurements suggest this does not occur.

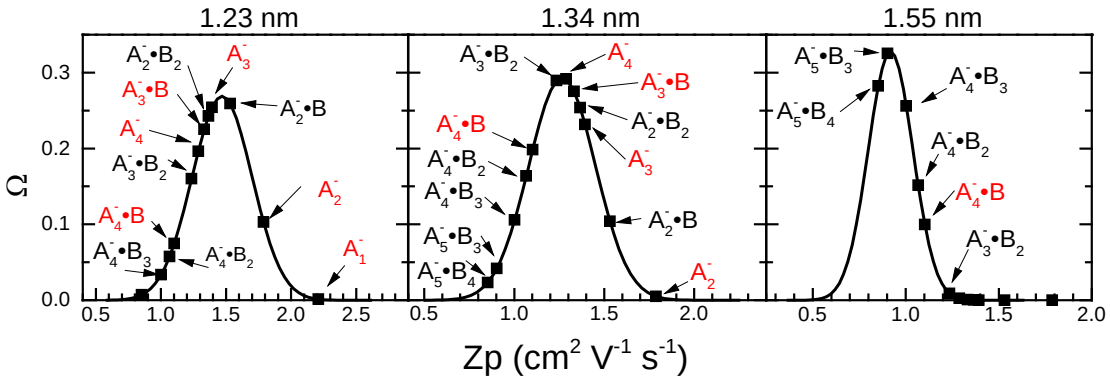

Figure S15 Transfer function (lines) of the TSI 3085 mobility classifier at three different voltages (3.80, 4.50, 6.00 V), corresponding to centroid mobility diameters of 1.23, 1.34, and 1.55 nm and centriod geometric (mass) diameters of 0.83, 1.04, and 1.25 nm. The points represent the clusters' mobilities and their tranfer function value at each size bin. Red clusters are detected by the Cluster CIMS using nitrate and red+black detected using acetate.

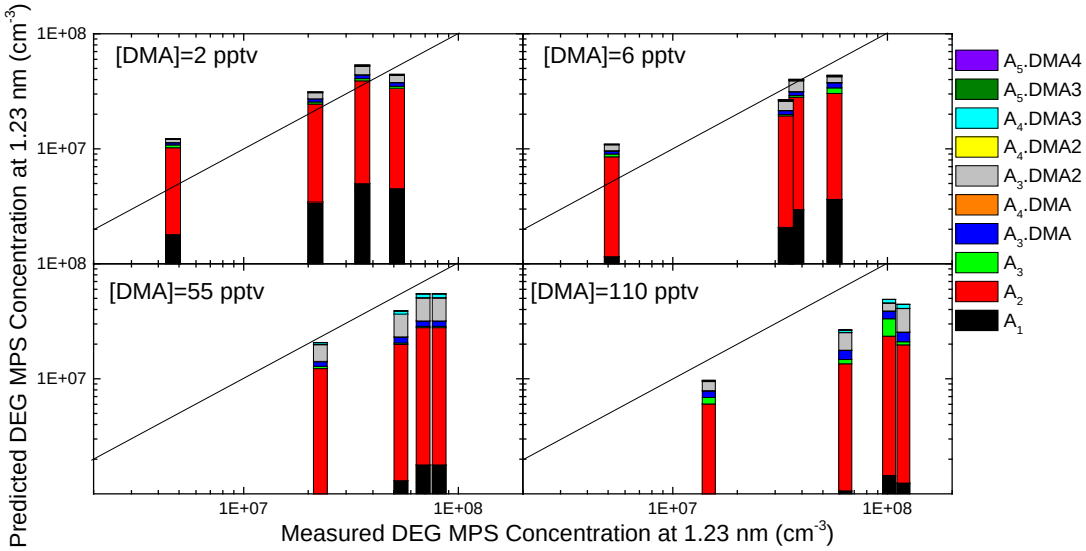

Figure S16 Comparison between predicted DEG MPS concentration from Cluster CIMS measured concentration (using acetate) to the measured DEG MPS concentration at a classifying voltage of 3.80 V (1.23 nm centroid mobility diameter) at four different [DMA]. The different color types in the bar represent the different types of clusters measured by the Cluster CIMS and their contribution to the predicted total number concentration.

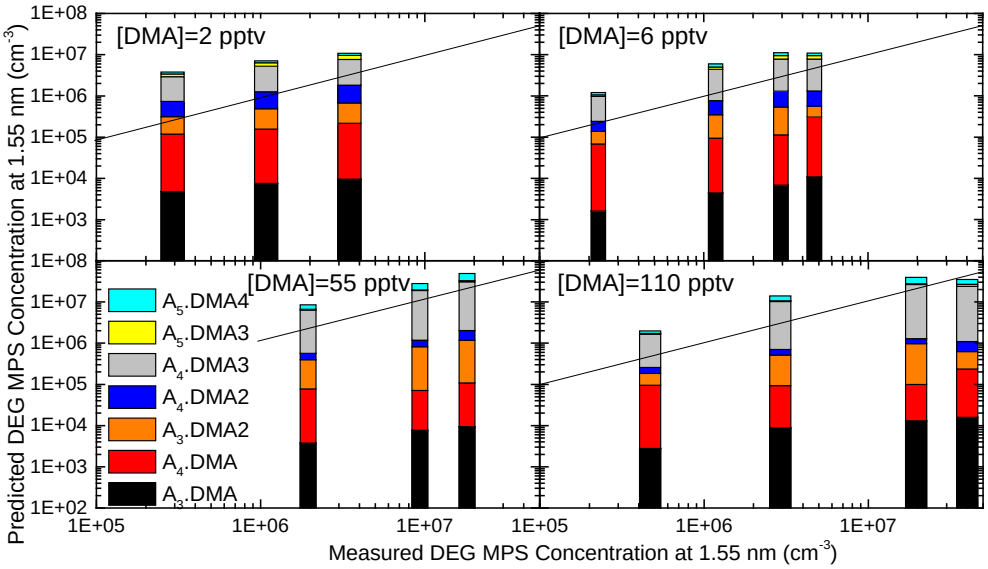

Figure S17 Comparison between predicted DEG MPS concentration from Cluster CIMS measured concentration (acetate) to the measured DEG MPS concentration at a classifying voltage of 6.00 V (1.55 nm centroid mobility diameter) at four different [DMA].

Chapter 4. Diamine-Sulfuric Acid Reactions are a Potent Source of Atmospheric Particle Formation[e]

4.1 Overview

With potential sources of uncertainty identified for the DEG MPS measurements in the 1 nm geometric size range, the DEG MPS was used to show how reactions of sulfuric acid and diamines produce more particles than dimethylamine, a monoamine. Particle concentrations 1.77 nm (centroid mobility diameter) and larger were examined to avoid interferences with potential ion-induced particles formed charger before the DEG MPS mobility classifier, as explained in Chapter 3. This chapter presents the first evidence from laboratory and field measurements that diamines are more powerful nucleating agents than monoamines. Diamines, a previously unstudied group of compounds, likely originate from both natural and man-made sources, and can facilitate particle nucleation in both clean and polluted environments. Under controlled flow reactor conditions, diamines were observed to react with sulfuric acid and its clusters to produce 10-100 times more particles than monoamines, including dimethylamine which is currently the basic compound considered to enhance nucleation rates the most. We also measured putrescine and cadaverine, both diamines, concentrations in rural Oklahoma during spring, 2013. Their concentrations ranged from 10-100 pptv during nucleation events and were equal to or greater than concentrations of dimethylamine. We conclude from our observations that diamines are potent nucleating agents and contribute significantly towards atmospheric nucleation.

[e] This chapter except for the overview is reproduced from Jen, C. N., Bachman, R., Zhao, J., McMurry, P. H., and Hanson, D. R.,: Diamine-sulfuric acid reactions are a potent source of atmospheric particle formation, *Nature Geoscience*, under review, 2015.

4.2 Introduction

Atmospheric nucleation is the formation of stable aerosol particles from trace precursor gases and accounts for up to half the global cloud condensation nuclei [*IPCC*, 2014]. Thus, accurate predictions of global climatic cooling by aerosols and clouds require understanding the chemical processes that lead to nucleation [*Kuang et al.*, 2009]. Atmospheric nucleation typically correlates with sulfuric acid concentrations [*Kuang et al.*, 2008], but clusters formed from water and sulfuric acid alone are unstable and require stabilizing compounds to reduce cluster evaporation rates and form stable particles. Here, we examine how diamines, a previously unstudied class of compounds, affect sulfuric acid nucleation in both a controlled flow reactor and in the atmosphere. We found that the number of particles formed from sulfuric acid and diamines was equal to or greater than the number formed from monoamines, implying that the diamines are more effective nucleating agents. Sulfuric acid and diamine concentrations were also monitored using chemical ionization mass spectrometers during spring, 2013 at the Southern Great Plains (SGP) site in Lamont, OK. Field measurements suggest that high concentrations of diamines significantly contribute to the number of freshly nucleated particles. We conclude that diamines are an important class of compounds that participate in atmospheric nucleation and warrant consideration in nucleation measurements and models.

Ammonia and monoamines (i.e., organic compounds with a single amine group) have been researched extensively in chamber and flow reactor studies. Amines are much more effective than ammonia at enhancing nucleation, with dimethylamine (DMA) and trimethylamine observed to stabilize sulfuric acid clusters the most [*Almeida et al.*, 2013; *Jen et al.*, 2014; *Kürten et al.*, 2014; *Yu et al.*, 2012] In the complete absence of cluster evaporation, nucleation rates reach a maximum, referred to as the collision-controlled limit (CCL) [*McMurry*, 1980; *McMurry*, 1983]. Our previous flow reactor results suggest that sulfuric acid concentrations of 10^8-10^9 cm^{-3} with either DMA≥20 pptv ($5x10^8$ cm^{-3}) or trimethylamine≥ 30 pptv ($7x10^8$ cm^{-3}) form clusters at the CCL [*Jen et al.*, 2014]. Kürten et al. studied DMA at 5-32 pptv ($1x10^8$ - $8x10^8$ cm^{-3}) and sulfuric acid at 10^5-10^7

cm^{-3} in the CLOUD chamber and also concluded that clusters form at the CCL [*Kürten et al.*, 2014].

Nonetheless, the atmospheric boundary layer contains numerous compounds in addition to DMA that can stabilize sulfuric acid clusters. Current research is focused on (1) linking highly oxidized, high molecular weight organics to nucleation events in pristine environments such as boreal forests [*Schobesberger et al.*, 2013] and (2) amines in industrial and agricultural/livestock regions [*Chen et al.*, 2012; *Freshour et al.*, 2014; *Zhao et al.*, 2011]. Diamines have been largely neglected in atmospheric studies, even though some limited measurements suggest that diamines have similar sources as monoamines (e.g. sewage, livestock, industrial operations, tobacco smoke) [*Ge et al.*, 2011]. Additional sources are likely but have not been characterized. With two basic amine groups, diamines can oligomerize with atmospherically relevant dicarboxylic acids, such as malonic and oxalic acid, and esters to form low volatility and high molecular weight products [*Hiemenz and Lodge*, 2007]. With no previous computational chemistry studies, we hypothesize that the two amine groups of diamines form more stable clusters with sulfuric acid than monoamines.

4.3 Flow Reactor Results

Three diamines and two monoamines were separately injected into a flow reactor containing sulfuric acid vapor: ethylene diamine (EDA), tetramethylethylene diamine (TMEDA), and butanediamine (or putrescine, Put), DMA, and methylamine (MA). All three diamines are used in industrial processes like polymer and food production, with Put also produced during biological processes and the decomposition of large amino acids [*Slocum and Flores*, 1991]. Figure 12 shows the dependencies of total particle number concentrations larger than 1.77 nm mobility diameter (1.47 nm geometric diameter [*Larriba et al.*, 2011]), N_{tot}, on base concentration,[B], and at constant initial sulfuric acid concentration of $[A_1]_o=2x10^9$ cm^{-3} (for dependence of N_{tot} on $[A_1]_o$, see supporting information). Both vapor phase concentrations correspond to the amount of reactants at the entrance to the flow reactor and prior to the acid-base reaction (see

Methods section). The top axis of Figure 13 provides $[B]/[A_1]_o$, a ratio that illustrates the relative importance of base and acid uptake during particle formation. N_{tot} for all bases increases with [B], reaching a maximum value of $2x10^7$ cm^{-3} at [B]~10 pptv for DMA and diamines and [B]~100 for MA. N_{tot} is likely limited by particle coagulation and wall losses in the flow reactor. Higher [MA] is required to reach the maximum N_{tot}, indicating that sulfuric acid with MA clusters evaporate more than clusters with DMA or diamines. Differences between particle formation with DMA or the diamines can be seen at low [B]~1 pptv where diamines produce ~10 times more particles than DMA and 100 times more than MA. In this environment where base molecules are scarce compared to acid (i.e., low $[B]/[A_1]_o$), nucleation rates are controlled by the ability of a base molecule to stabilize sulfuric acid clusters and reduce cluster evaporate rates. Therefore, these results demonstrate that diamines stabilize sulfuric acid more effectively than monoamines.

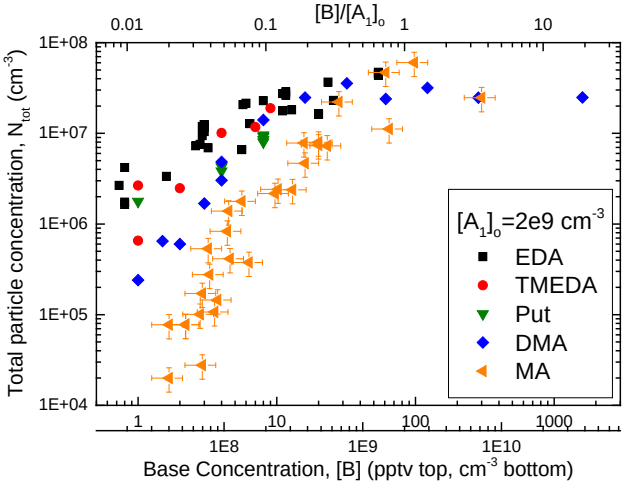

Figure 12 [N_{tot}] as a function of [B] (bottom two axes show [B] and top provides the equivalent $[B]/[A_1]_o$). Each color represents a different base compound with $[A_1]_o = 2x10^9$ cm^{-3}. The estimated random uncertainties for [B] and N_{tot} are depicted with the MA points and apply to all measurements.

Figure 13 provides further insights regarding nucleation process for these reactants. The solid and open symbols show the ratios of base and sulfuric acid molecules introduced into the reactor to the total number of particles formed, $[B]/N_{tot}$ and $[A_1]_o/N_{tot}$, for a diamine (EDA) and two monoamines (DMA and MA). Put and TMEDA show similar trends as EDA and are provided in supplementary section S2. These ratios provide an upper limit to the number of base and acid molecules per particle since not all reactants are incorporated into particles; some deposit on the reactor walls and others remain in the gas phase. Also shown in Figure 13 is the approximate total number of acid

and base molecules per particle, n_p, calculated from the mean of the measured particle volumes. Note, mobility diameters were converted to geometric diameters prior to calculating n_p [*Larriba et al.*, 2011]. The increase in n_p with [B] reflects the observed larger volumes as [B] increased. Also n_p values vary slightly between bases (see supporting information). The range shown for n_p was obtained by assuming that particles were composed of a combination of acid and base molecules (including water) determined from (1) aqueous sulfuric acid solutions in equilibrium at 30% relative humidity (uncorrected for curvature) and (2) dry <8.5 nm particles formed from DMA and sulfuric acid [*Ouyang et al.*, 2015]. Since diamines are larger than DMA, a particle composed of diamine and sulfuric acid would have slightly fewer molecules than the value shown for sulfuric acid and DMA.

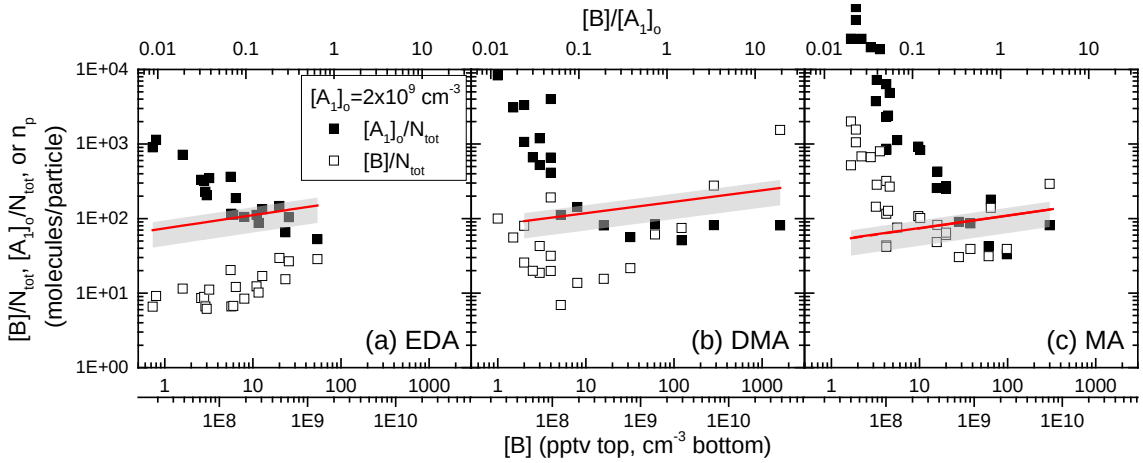

Figure 13 $[A_1]_o$ /N_{tot} (filled symbol) and $[B]/N_{tot}$ (open symbol) as a function of [B] (bottom x-axis, given as pptv and cm^{-3}). $[A_1]_o$ was held constant at $2x10^9$ cm^{-3}. $[B]/[A_1]_o$ is shown on the top x-axis. Three bases are shown: (a) EDA, (b) DMA, and (c) MA. Red lines illustrate the estimated number of molecules per particle, n_p, with the gray region showing a range of values corresponding to aqueous sulfuric acid (higher) or solid DMA+sulfuric acid (lower).

Taken together, the results for $[B]/N_{tot}$, $[A_1]_o/N_{tot}$, and n_p in Figure 13 illustrate nucleation processes and the differences between diamines and monoamines. For all these compounds, $[B]/N_{tot}+[A_1]_o/N_{tot}$ is close to n_p for $[B]/[A_1]_o$ about unity ($0.5<[B]/[A_1]_o<2.5$), where base and acid collision rates are similar. This indicates that under these conditions, near equal amounts of basic and acidic reactants were taken up,

leading to particles with basic or acidic vapor pressures well below [B] and $[A_1]_o$, respectively. This could only occur if acid and base evaporation from the clusters were negligible and if most of the gases were immediately consumed during particle formation thereby preventing loss to the reactor walls. However as observed from Figure 12, cluster evaporation plays a larger role in limiting particle formation at low values of $[B]/[A_1]_o$ when the acid collision rate is higher than that of base. In this low $[B]/[A_1]_o$ regime for EDA, a comparison of $[B]/N_{tot}$ and n_p reveals that base accounts for at most 10% of the molecules in nucleated particles, with sulfuric acid presumably accounting for the balance. Thus, these particles are very acidic. In contrast, the $[B]/N_{tot}$ for monoamines equals or exceeds n_p, suggesting that some base molecules must remain in the gas phase. The higher values of $[B]/N_{tot}$ for monoamines at low $[B]/[A_1]_o$ confirms that monoamines are not as effective as diamines at stabilizing clusters.

Furthermore, trends of $[B]/N_{tot}$ for EDA and the monoamines contrast at low $[B]/[A_1]_o$. Values of $[B]/N_{tot}$ for EDA are nearly independent of [EDA], i.e. N_{tot} is linearly proportional to [diamine] (see supporting information for power dependencies of N_{tot} on [B] and $[A_1]_o$). This would occur if one diamine molecule forms a stable cluster, and subsequently a particle, before it was lost to the walls. Thus, the crucial first step for nucleation of diamines with sulfuric acid may be the initial encounter of acid and base vapors. For monoamines, however, $[B]/N_{tot}$ decreases with increasing [monoamine], i.e. N_{tot} is proportional to $[\text{monoamine}]^2$ [*Glasoe et al.*, 2015]. This entails that one monoamine forms an unstable cluster which will evaporate unless another monoamine reacts to stabilize the cluster. As base collision rates increase with [B], the likelihood that more than one monoamine collides with and stabilizes a cluster to ultimately form a particle also increases. Combined, lower values of $[B]/N_{tot}$ and the independence of $[B]/N_{tot}$ on [diamine] at low $[B]/[A_1]_o$ clearly show that diamines are superior to monoamines in stabilizing sulfuric acid clusters and therefore are more potent nucleating agents.

In the terrestrial atmospheric boundary layer, $[B]/[A_1]$ is typically much greater than unity, indicating that nucleation rates are limited by sulfuric acid uptake. In this regime, a basic molecule would be taken up immediately following the uptake of a sulfuric acid molecule. This corresponds to $[B]/[A_1]_o > 1$ in Figure 13, where $[B]/N_{tot}$ for DMA greatly exceeds n_p, indicating that some of this excess base likely remained in the gas phase. (Measurements were not carried out for $[B]/[A_1]_o > 1$ for the other bases, but we expect they would exhibit the same trend.) Under these high base:acid conditions and neglecting possible synergistic effects, diamines will contribute more to nucleation rates than DMA if [diamine] exceed [DMA].

4.4 Field Measurements

The Ambient pressure Proton transfer Mass Spectrometer (AmPMS) [*Hanson et al.*, 2011] and Cluster Chemical Ionization Mass Spectrometer (Cluster CIMS) [*Zhao et al.*, 2010] measured the basic gases and sulfuric acid concentrations, respectively, at the Southern Great Plains (SGP) site in Lamont, OK during spring of 2013. The air mass around SGP is affected by industrial agriculture (wheat fields and cow pastures) and oil extraction/refinement. Figure 14 shows the measured DMA, Put, cadaverine (Cad), and sulfuric acid concentrations ($[A_1]$) throughout the SGP campaign. The diamine concentrations were corrected posteriori for interferences by isobaric compounds using a measured constant that represents the diamine fraction of signal (see supplementary section S5 for discussion on detection of diamines with AmPMS). The vertical lines in Figure 14 indicate the start of nucleation events (labeled with number).

Measured $[A_1]$ ranged from 10^6-10^7 cm^{-3} during nucleation events, and average [total diamine]/$[A_1]$ was 10^2-10^3. Events 8, 9, and 10 show clear spikes in either Put or Cad at the start of nucleation such that [Put]+[Cad] exceeded [DMA]. Here, $[A_1]$ ranged from $5x10^6$-$1x10^7$ cm^{-3} and more closely match $[A_1]$ in cleaner environments [*Chen et al.*, 2012]. Diamines and monoamines (and other compounds) may act synergistically to stabilize sulfuric acid clusters, as was observed for ammonia and monoamines [*Glasoe et al.*, 2015; *Yu et al.*, 2012], making it difficult to isolate the contribution of a single basic

gas to atmospheric nucleation. Nevertheless, for most of the events at SGP, [DMA]~[Put] or [Cad] with the [total diamine] always greater than [DMA]. Because total diamines were more abundant than DMA and because they are more effective stabilizing agents, diamines likely contributed significantly, perhaps predominantly, to nucleation.

Particle formation from a single acid and single base depends on the relative uptake rates of acid and base, which varies in proportion to $[B]/[A_1]_o$. The ability of base molecules to stabilize sulfuric acid clusters and reduce evaporation rates plays a dominant role for nucleation in acid-rich environments, where particle formation is limited by base uptake. Here we observed that diamines react with sulfuric acid to produce 10 times more particles than DMA and 100 times more than MA, clearly signifying that diamines are more potent nucleating agents. In addition, our results indicate that under the conditions investigated, just one diamine molecules is needed to form a stable particle while more than one monoamine molecule is required. Field measurements in rural Oklahoma reveal that concentrations of total diamines typically exceeded those of DMA. We conclude that diamines likely contribute significantly towards atmospheric nucleation and warrant consideration in future nucleation research.

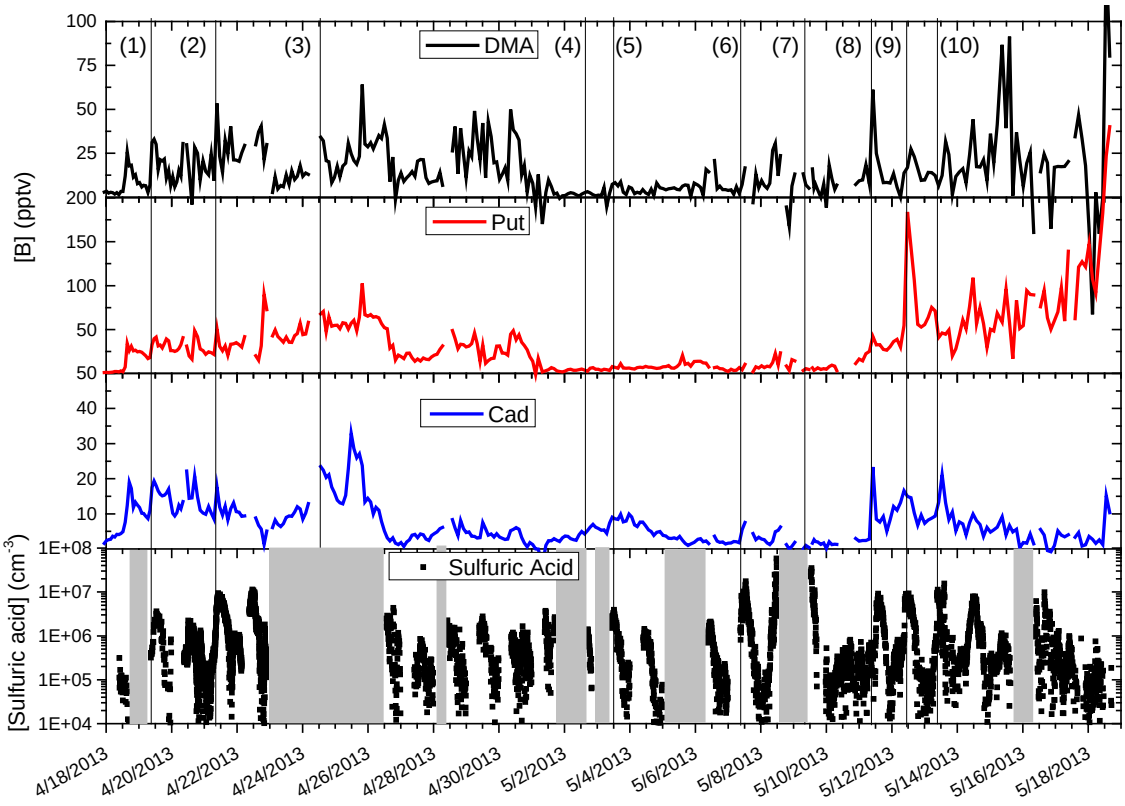

Figure 14 Measured amine and sulfuric acid concentration during the SGP field campaign of spring, 2013. The vertical lines indicate the start of a nucleation event. The gray box indicates when the Cluster CIMS was not operating. The numbers at the top identify specific events.

4.5 Methods

Laboratory experiments were conducted in a well-characterized, extraordinarily clean, and highly repeatable flow reactor [*Jen et al.*, 2014; *Zollner et al.*, 2012] that was operated at 296 K and 28% relative humidity. Sulfuric acid vapor was produced by passing clean nitrogen over a sulfuric acid reservoir and injected at the top of the reactor. Each basic gas was injected into the centerline of the sulfuric acid flow. The basic gas mixed and reacted with the sulfuric acid vapors, and the particle size distributions along the centerline of the flow reactor were measured with a diethylene glycol mobility

particle sizer (DEG SMPS) after ~40 s[f]. The operating parameters and sources of uncertainties of the DEG SMPS have been described previously [*Glasoe et al.*, 2015; *Jen et al.*, 2015; *Jiang et al.*, 2011b]. The region where basic gas initially encounters and mixes with the sulfuric acid flow is known as the nucleation zone (NZ); the initial sulfuric acid concentration in the NZ, $[A_1]_o$, is set by the flow rate over the sulfuric acid reservoir. The value of $[A_1]_o$ has been estimated by computational fluid dynamics [*Panta et al.*, 2012] and compared to the measured value at the exit of the flow reactor [*Panta et al.*, 2012; *Zollner et al.*, 2012]. We estimate the systematic uncertainty of $[A_1]_o$ to be a factor of two[*Glasoe et al.*, 2015]. This uncertainty would affect all of our measurements equally and therefore would not change the conclusions presented in this study. Small random variations contribute additional estimated uncertainties in $[A_1]_o$ of 20%. TMEDA and Put vapor were taken from diffusion tubes where clean nitrogen was passed over a tee connected, via a ~10 cm length of a ~1.5 mm ID tube, to a temperature controlled liquid reservoir of the compound. EDA, DMA, and MA were produced by flowing clean nitrogen over permeation tubes [*Freshour et al.*, 2014]. The dilution and measurement of basic gas concentrations have been described previously [*Freshour et al.*, 2014; *Jen et al.*, 2014; *Zollner et al.*, 2012]. Estimated uncertainties of ~25% on reported [B] are shown in Figure 1 and were based upon comparing measured [B] via chemical ionization mass spectrometry with measured base permeation/diffusion rates [*Jen et al.*, 2014]. During the SGP campaign, amines were measured using the AmPMS [*Freshour et al.*, 2014; *Hanson et al.*, 2011] (see supplementary section S5). Sulfuric acid concentration was monitored with the Cluster CIMS using nitrate as the chemical ionization ion [*Chen et al.*, 2012]. The nucleation events were measured by scanning mobility particle sizers.

[f] Jen et al. (2014) reported Cluster CIMS measurements of clusters formed from sulfuric acid and various bases following a 3 s reaction time. In the current study, 40 s was used to allow particles to grow to well into the size range accessible to the DEG SMPS.

4.6 Supporting Information[g]

4.6.1 Effects of $[A_1]_o$ on N_{tot} at Fixed [B]

Figure S18 shows N_{tot} as a function of $[A_1]_o$, with [B] held constant at 4 pptv. Higher $[A_1]_o$ leads to more particles produced for all bases, with N_{tot} reaching a limit at high $[A_1]_o$ due to particle coagulation losses. Specifically at low $[A_1]_o$=1.5x10^9 cm^{-3}, the three diamines produce ~10 times more particles than DMA. As $[A_1]_o$ increases, the differences between the diamines and monoamines lessen.

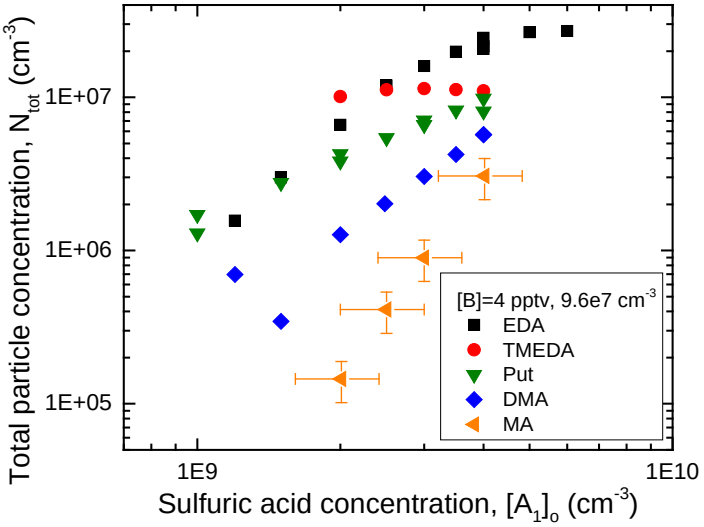

Figure S18 Total particle number concentration as a function of $[A_1]_o$. Each color/symbol represents a different base compound at 4 pptv. The estimated random uncertainties are given for MA but represent all measurements.

4.6.2 $[B]/N_{tot}$, $[A_1]_o/N_{tot}$, and n_p for TMEDA and Put

Figure S19 provides TMEDA and Put versions Figure 13 from the main text. These two diamines exhibit the same $[B]/N_{tot}$ and $[A_1]_o/N_{tot}$ trends as EDA whereby the particles are very acidic at low $[B]/[A_1]_o$ and require one diamine to form a stable particle. From this graph and Figure 13, we conclude that diamines are capable of stabilizing more sulfuric acid molecules than monoamines and are thus more potent nucleating agents.

---

[g] This supporting information is reproduced from Jen, C. N., Bachman, R., Zhao, J., McMurry, P. H., and Hanson, D. R..: Diamine-sulfuric acid reactions are a potent source of atmospheric particle formation, *Nature Geoscience*, under review. 2015

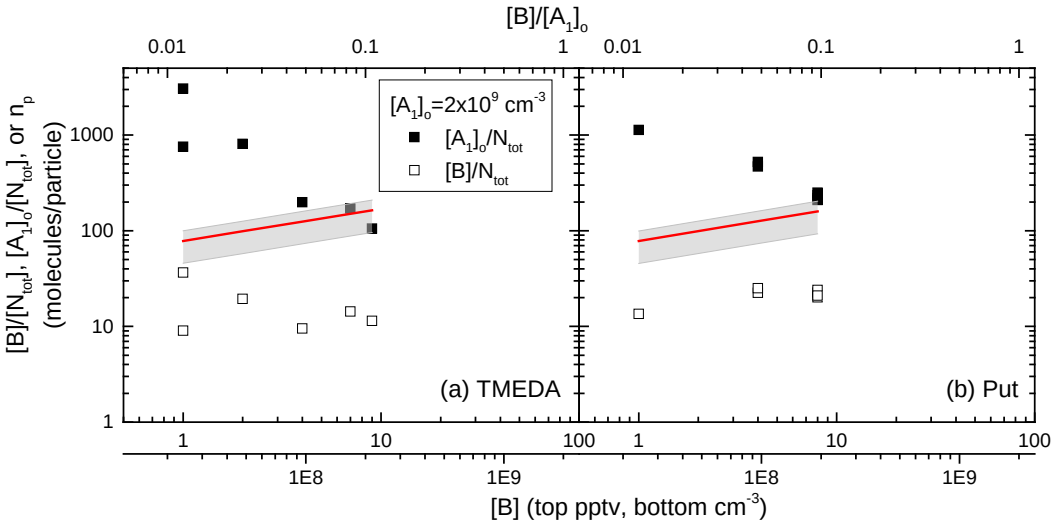

Figure S19 $[A_1]_o$ /N_{tot} (filled symbol) and $[B]/N_{tot}$ (open symbol) as a function of [B] (bottom x-axis, given as pptv and cm^{-3}). $[A_1]_o$ was held constant at $2x10^9$ cm^{-3}. $[B]/[A_1]_o$ is shown on the top x-axis. Two diamines are shown: (a) TMEDA and (b) Put. Red lines illustrate the estimated number of molecules per particle, n_p, with the gray region showing the range of values corresponding to aqueous sulfuric acid (higher) or solid DMA+sulfuric acid (lower).

4.6.3 Size Distributions for Particles Formed from Sulfuric + Mono or Diamines

Figure S20 illustrates how $[A_1]_o$ alters the measured size distribution with [B] held constant at 4 pptv (±1 pptv) for the three diamines and two monoamines. Particle size distributions were measured using a diethylene glycol SMPS with operating parameters described previously [*Glasoe et al.*, 2015; *Jiang et al.*, 2011b]. The graph on the left is at $[A_1]_o=2x10^9$ cm^{-3} and the right at $4x10^9$ cm^{-3}. The number mean diameter increases from 2-3 nm to 4-5 nm at double the $[A_1]_o$ for all bases. Specifically, sulfuric acid+diamine particles exhibit slightly larger mean volumetric diameters (3.0 and 5.2 nm) compared to DMA (2.8 nm and 5.1 nm) at both $[A_1]_o$. For both graphs, $[B]/[A_1]_o<1$ and particles grow primarily by sulfuric acid uptake. Figure S20 also depicts the higher number concentrations produced from sulfuric acid+diamines than monoamines.

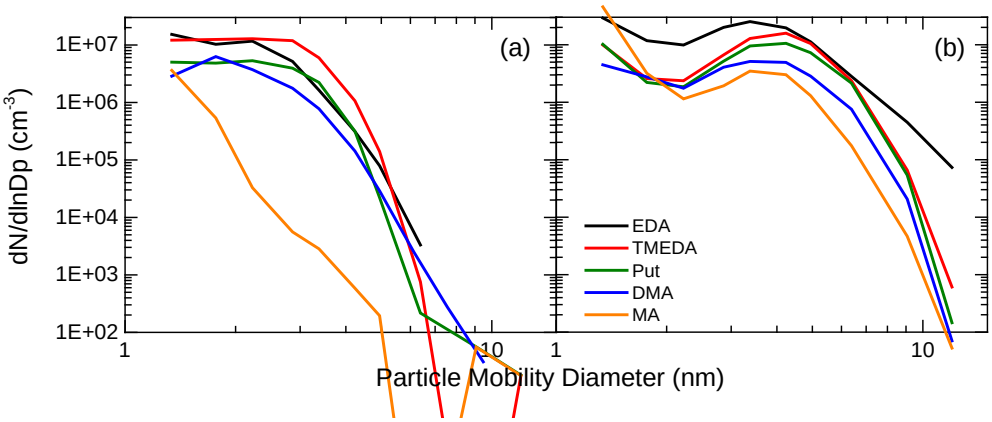

Figure S20 Particle size distribution for [B]=4 pptv (9.6×10^7 cm^{-3}) at two different $[A_1]_o$: (a) 2×10^9 cm^{-3} and (b) 4×10^9 cm^{-3}.

4.6.4 Power Dependencies of N_{tot} on $[A_1]_o$ and [B]

Figure S21 illustrates how N_{tot} increases with [diamine] at various constant $[A_1]_o$. The slopes of the linear regressions are given in the legends. At low $[A_1]_o$ for all three diamines, the slopes are approximately 1. As $[A_1]_o$ increases, these slopes decrease due to increasing particle coagulation losses. Figure S22 shows N_{tot} as a function of $[A_1]_o$ at various but constant [B] for the three diamines. The slopes of the linear regression are given in the legends and ~2 at low [B]. Similar to high $[A_1]_o$, slope values tend to be lower at high [B]. We also attribute this to high particle coagulation losses that limit N_{tot}. These two figures taken together suggest

$$N_{tot} \sim [A_1]_o^2 \times [\text{diamine}]^1 . \qquad \textbf{Equation S23}$$

This contrasts with the power dependencies described in Glasoe et al. [2015] where

$$N_{tot} \sim [A_1]_o^{2.5} \times [\text{DMA}]^2 . \qquad \textbf{Equation S24}$$

They hypothesized that the formation of a stable particle requires 2-3 sulfuric acids and 2 DMA molecules. The power dependencies for diamines suggest 2 sulfuric acids and 1 diamine molecule. This supports our conclusion from the main paper where $[B]/N_{tot}$ for diamines are independent of [B] at low $[B]/[A_1]_o$ because only one diamine molecule is needed to form a stable particle. We hypothesize that both amine groups in a diamine react with sulfuric acid, leading to more stable clusters than are formed from equal amounts monoamines.

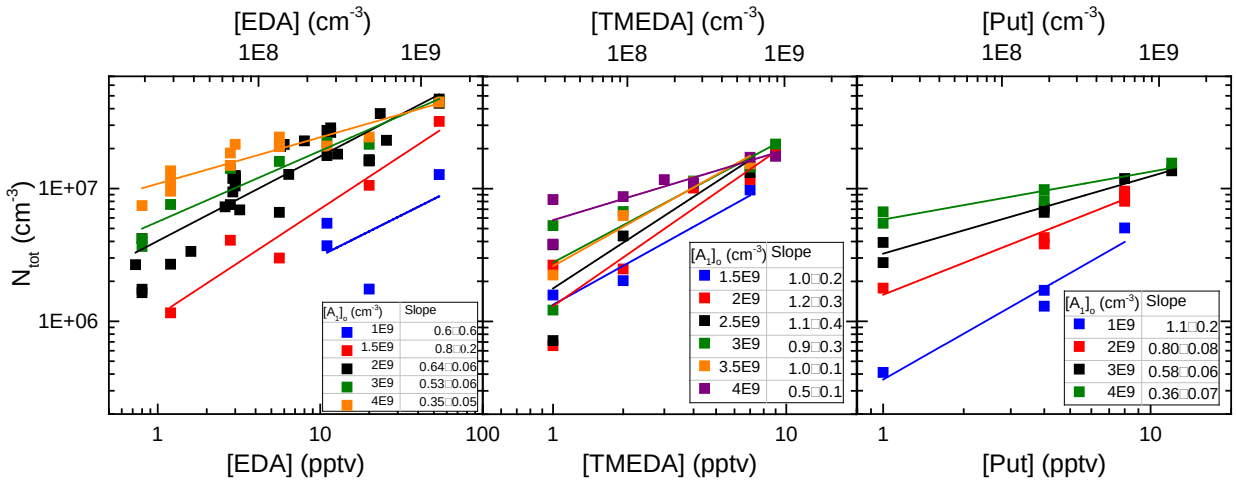

Figure S21 N_{tot} as a function of [diamine] for EDA (left), TMEDA (center), and Put (right). Each color in a panel represents a constant $[A_1]_o$, and its corresponding line represents a linear regression at a constant $[A_1]_o$. The slopes and their standard errors are given in the legends.

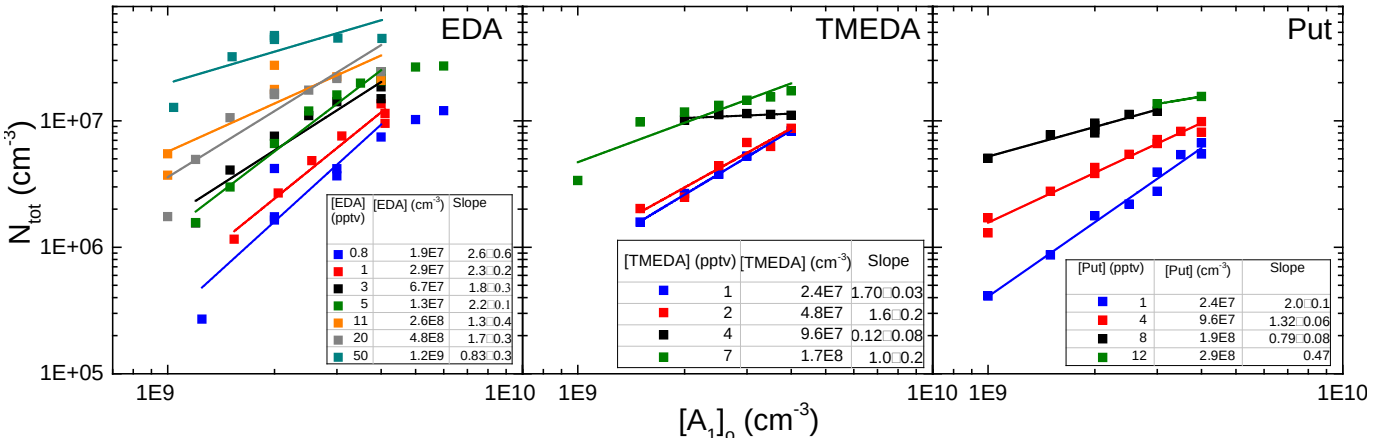

Figure S22 N_{tot} as a function of $[A_1]_o$ for EDA (left), TMEDA (center), and Put (right). Each color in a panel represents a constant [B], and its corresponding line represents a linear regression at a constant [B]. The [B] are given in both pptv and cm^{-3}. The slopes of the regressions are given in the legends.

4.6.5 Measurement of Diamines in the Atmosphere

The operation and 2-hour signal averaging technique used for the AmPMS have been described previously [*Freshour et al.*, 2014]. In addition, the diamine concentrations displayed in Figure 14 of the main paper have been corrected for possible interference from other isobaric compounds. These compounds are likely organic and not basic. We measured the fraction of the protonated diamine signal due to a diamine by adding an acid scrubber onto the inlet of the AmPMS. The acid scrubber consists of a tube coated with either liquid phosphoric or sulfuric acid. The scrubber efficiently removed diamines from the sample flow, leaving only non-basic compounds to be detected by the AmPMS. The acid scrubber was added onto the inlet after the SGP field campaign where we sampled outdoor air during spring, 2014 in Minneapolis, MN. Its efficiency for removal of basic gases was high based on the behavior observed for ammonia and amines.

Table S3 lists the average fractional amounts of various diamine signals that were removed by the acid scrubber, i.e. fraction of signal due to a diamine. The values of Put and Cad concentrations shown in Figure 14 were obtained by multiplying measured signals by their corresponding fractions. As the acid scrubber was not added until after the SGP campaign, it is possible this correction method does not accurately account for the mixture of compounds that may have existed at SGP and their temporal dependence, so the diamine concentrations in Figure 14 should be regarded as our best estimate.

Table S3 Summary of diamine signal from a dozen acid scrubber experiments in Minneapolis, spring 2014

Diamine, abbrev.	Mass, amu	Diamine fraction of signal	Average abundance (pptv)
Ethylenediamine, EDA	60	0.45	1.0
Propanediamine, PDA	74	No signal	0
Putrescine, Put	88	0.75	1.3
Cadaverine, Cad	102	0.75	5.9
Hexanediamine, HDA	116	0.34	3.9

Chapter 5. Cluster Formation of Sulfuric Acid with Dimethylamine or Diamines and Detection with Chemical Ionization

5.1 Overview

Chemical ionization (CI) mass spectrometers are used to study atmospheric nucleation by detecting clusters produced in the reactions of sulfuric acid and various basic gases. These instruments typically used nitrate to chemically ionize clusters for detection. In this study, we compare measured cluster concentrations formed by reacting sulfuric acid vapor with either dimethylamine, ethylene diamine, tetramethylethylene diamine, or butanediamine (also known as putrescine) using nitrate and acetate ions. We show from flow reactor measurements that nitrate is unable to chemically ionize clusters with weak acidities. We then model the neutral and ion cluster formation pathways, including chemical ionization, ion-induced clustering, and ion decomposition, to better identify which cluster types cannot be chemically ionized by nitrate. Our results show that sulfuric acid monomer containing one diamine, sulfuric acid dimer with two diamines, and sulfuric acid trimer with 2 or more base molecules cannot be chemical ionized by nitrate. We conclude that cluster concentrations measured with acetate CI gives a better representation of both cluster abundancies and their base content than nitrate CI.

5.2 Introduction

Atmospheric nucleation is an important source of global atmospheric particles [*IPCC*, 2014]. In the atmospheric boundary layer, most nucleation occurs when sulfuric acid [*Kuang et al.*, 2008; *Kulmala et al.*, 2004; *Riipinen et al.*, 2007; *Weber et al.*, 1996] and its clusters react with other trace compounds to produce stable, electrically neutral molecular clusters; these compounds include ammonia [*Ball et al.*, 1999; *Coffman and Hegg*, 1995; *Kirkby et al.*, 2011], amines [*Almeida et al.*, 2013; *Glasoe et al.*, 2015; *Zhao et al.*, 2011], water [*Leopold*, 2011], and oxidized organics [*Schobesberger et al.*, 2013]. Stable clusters subsequently grow and can serve as cloud condensation nuclei. The primary instruments used for detecting freshly nucleated, sulfuric acid-containing clusters

are atmospheric pressure chemical ionization mass spectrometers (CIMS) such as the Cluster CIMS [*Chen et al.*, 2012; *Zhao et al.*, 2010] and the CI atmospheric pressure interface-time of flight mass spectrometer (CI-APi-ToF) [*Jokinen et al.*, 2012]. Both mass spectrometers use nitrate (NO_3^- with ligands) to chemically ionize neutral sulfuric acid clusters. The detected ion clusters are then assumed to represent the neutral cluster composition, and the signal ratio of the ion cluster to the reagent ion translates to the neutral cluster concentration [*Berresheim et al.*, 2000; *Eisele and Hanson*, 2000; *Hanson and Eisele*, 2002].

The amounts and types of ions detected by the mass spectrometer are determined by four key processes: neutral cluster formation, chemical ionization, ion-induced clustering, and ion decomposition. The first process, neutral cluster formation, follows a sequence of acid-base reactions [*Almeida et al.*, 2013; *Chen et al.*, 2012; *Jen et al.*, 2014] whereby sulfuric acid vapor and its clusters react with basic molecules to produce more stable clusters than sulfuric acid alone. The concentration of a specific cluster type depends on its stability (i.e. evaporation rates of the neutral cluster) and on concentrations of the precursor vapors (i.e. the formation rate).

Neutral clusters then need to be ionized to be detect by a mass spectrometer. In most prior work, this has been accomplished by chemical ionization with the nitrate ion whereby the neutral clusters are exposed to nitrate ions for a set amount of time known as the chemical ionization reaction time. Chemical ionization (CI) can be conceptualized as another acid-base reaction where an acid (sulfuric acid) donates a proton to the basic reagent ion (nitrate, the conjugate base of nitric acid). To illustrate, the CI reaction of a sulfuric acid dimer, $(H_2SO_4)_2$, is shown in Reaction 4.

$$\left(H_2SO_4\right)_2 \bullet DMA \bullet \left(H_2O\right)_x + HNO_3 \bullet NO_3^- \xrightarrow{k_2} HSO_4^- \bullet H_2SO_4 \bullet DMA + 2HNO_3 + x\left(H_2O\right)$$

Reaction 4

This dimer of sulfuric acid contains a dimethylamine (DMA) molecule and an unknown number of *x* water molecules. Water molecules evaporate upon ionization or entering the vacuum region of the CIMS and are not detected unless temperatures are low (see Figure

3 in Hanson and Eisele [2002]). The forward rate constant, k_2, is assumed equal to the collision rate of 1.9×10^{-9} cm^3 s^{-1} [*Su and Bowers*, 1973], while the reverse rate constant is zero. Other ligands may attach to the reagent ion and decrease the collision rate, but nitrate is assumed to be the major reagent ion. Reaction 4 can be extended to CI reactions for larger neutral clusters of sulfuric acid and implicitly assumes that every collision between nitrate and sulfuric acid cluster results in an ionized cluster. However Jen et al. [2015] showed that nitrate CI, with the stated assumptions, leads to significantly lower concentrations of clusters that contain 3-5 sulfuric acid molecules and DMA compared to results using acetate reagent ions. Furthermore, the concentrations of clusters detected using acetate are in overall better agreement with values measured using a diethylene glycol mobility particle sizer (DEG MPS). As no other experimental conditions changed except the CI reagent ion, we hypothesize that nitrate has a lower proton affinity and is less able to chemically ionize clusters (i.e., a non-zero reverse rate constant) with near equal amounts of sulfuric acid and base than acetate CI. Poor CI efficiency reduces the amount and types of ions detected by the mass spectrometer.

After neutral clusters are ionized, the resulting ion may be unstable and quickly decompose. Experimental studies have shown ion decomposition in the ammonia-sulfuric acid system at 275 K [*Hanson and Eisele*, 2002], with computational chemistry studies showing that ion decomposition may occur during the CI reaction time scales [*Kurtén et al.*, 2011; *Lovejoy and Curtius*, 2001; *Ortega et al.*, 2014]. These studies demonstrate that base molecules often evaporate from sulfuric acid+base ion clusters. After the CI reaction given above, the sulfuric acid dimer ion with 1 DMA molecule will likely decompose into the bare sulfuric acid dimer ion.

$$HSO_4^- \bullet H_2SO_4 \bullet DMA \xrightarrow{E_d} HSO_4^- \bullet H_2SO_4 + DMA \qquad \textbf{Reaction 5}$$

The decomposition rate, E_d, for Reaction 5 is fast at ~100 s^{-1} at 298 K [*Ortega et al.*, 2014]. Therefore, the mass spectrometer will detect the neutral sulfuric acid dimer with 1 DMA as the bare dimer ion at room temperature.

The bare sulfuric acid dimer ion can also be produced by ion-induced clustering (IIC). In general, IIC occurs when the sulfuric acid ion (HSO_4^-), formed by CI of sulfuric acid monomer (with ligands), reacts with H_2SO_4 or its clusters. The signal due to these IIC products must be subtracted from signals measured by mass spectrometry to determine neutral cluster concentrations. Specifically, the sulfuric dimer ion can be formed via the IIC pathway given in Reaction 6.

$$HSO_4^- + H_2SO_4 \xrightarrow{k_c} HSO_4^- \bullet H_2SO_4 \qquad \textbf{Reaction 6}$$

The forward rate constant, k_c, is the collision rate constant of $2x10^{-9}$ cm^3 s^{-1}. IIC produced dimer ion is identical to a dimer ion formed by CI of the neutral dimer. A method has been developed to correct for IIC based upon measured sulfuric acid vapor concentrations and CI reaction time [*Chen et al.*, 2012; *Hanson and Eisele*, 2002]. However, the bisulfate ion may not cluster with and charge all neutral clusters formed by reactions of sulfuric acid and basic compounds, as the proton affinity of the neutralized sulfate salts may be too high to form a bisulfate-ligand bond. If so, assuming the collision rate for reactions such as Reaction 6 would lead to an over-correction of the neutral cluster concentrations. As the thermodynamic properties of all cluster types composed of sulfuric acid and various bases are virtually unknown, evaluating the propensity of these IIC reactions is difficult and cannot be modeled with certainty.

Measured CIMS signals reflect the combined influences of all these processes, with each occurring on time scales that depend on the chemistry, experiment, and measurement technique. Assuming one process is dominant for all processes can lead to large errors in reported neutral cluster composition and concentrations. Here we examine all four processes, neutral cluster formation, chemical ionization, IIC, and ion decomposition that influence the abundance of ion clusters composed of sulfuric acid and various bases. These bases include DMA, ethylene diamine (EDA), tetramethylethylene diamine (TMEDA), and butanediamine (also known as putrescine, Put). The diamines, a previously unstudied class of basic compounds, react with sulfuric acid vapors to produce higher particle concentrations than monoamines (Chapter 4). We present observations that 1) show a clear difference between acetate and nitrate CI for the larger cluster sizes

and 2) provide evidence of ion decomposition. Also presented are modeling results in order to identify possible neutral cluster formation pathways, those cluster types that do not undergo nitrate CI, and clusters that are formed by IIC.

5.3 Method

Sulfuric acid clusters containing either DMA, EDA, TMEDA, or Put were produced in an extremely clean and repeatable flow reactor as detailed in Jen et al. [2014]. Each basic gas was injected into the flow reactor at a point to yield ~3 sec reaction time between the basic gas and sulfuric acid vapor (see Jen et al. [2014] for a schematic). The initial sulfuric acid concentration ($[A_1]_o$) before basic gas reaction was set at specified concentrations. The basic gas concentration ([B]) was measured by the Cluster CIMS in positive ion mode (see SI of Jen et al. [2014] for further details) and confirmed with calculated concentrations [*Zollner et al.*, 2012]. The basic vapors were produced by passing clean nitrogen gas over either a permeation tube (for DMA and EDA) or liquid reservoir of a diamine. The basic gas was then diluted in a process described in Zollner et al. [2012]. The temperature of the flow reactor was held constant throughout an experiment but varied day-to-day from 295-305 K to minimize natural convection swirls near the Cluster CIMS sampling region. The relative humidity was maintained at ~30%.

Two types of experiments were conducted. The first set followed closely to those detailed in Jen et al. [2014] where the base, base concentration ([B]), and $[A_1]_o$ were varied. The resulting concentrations were measured with the Cluster CIMS using either nitrate or acetate as the CI reagent ion. Nitrate and acetate were respectively produced by passing nitric acid vapor and acetic anhydride vapors over Po-210 sources. Different Po-210 sources were used for the acetate and nitrate to avoid cross-contamination. The cluster concentrations were calculated by using calculated CI reaction time based upon inlet dimensions and electric field strength, measured and extrapolated mass-dependent sensitivity (see Supporting Information), and the collision rate constant between CI ion

and sulfuric acid clusters (see Jen et al. [2014] and [2015] for a discussion on the data inversion process). The CI reaction time was 18 ms for nitrate and 15 ms for acetate.

The second set of experiments focused on varying the CI reaction time at fixed [B] and $[A_1]_o$. CI reaction time was increased by decreasing the electric field used to draw ions across the sample flow into the inlet. Similar experiments have been previously performed on other atmospheric pressure mass spectrometers [*Hanson and Eisele*, 2002; *Jen et al.*, 2014; *Zhao et al.*, 2010].

5.4 Acetate vs. Nitrate Comparison

Figure 15 shows the comparison between cluster concentrations measured by acetate (solid bars) and nitrate (hashed bars) at a constant $[A_1]_o=4x10^9$ cm^{-3} for four different [DMA]. Bars are shown for clusters that contain a given number of sulfuric acid molecules in a cluster (N_1 is the monomer, N_2 is the dimer, etc.), while the number of DMA molecules per cluster is indicated by color (e.g., $A_4^-•DMA_{0–3}$). The notation used here differs slightly from [*Jen et al.*, 2014] such that $[N_m]$ denotes the total concentration for clusters that contain *m* sulfuric acids molecules (i.e., $[N_m]=[A_m]+[A_m•B_1]+A_m•B_2]…$) and $A_m•B_j$ represents a specific sulfuric acid (A) cluster type with *m* sulfuric acid molecules and *j* basic molecules (B). A logarithmic axis is used for $[N_1]$ and $[N_2]$, while the larger cluster concentrations are given on a linear scale. The measured $[N_1]$ and $[N_2]$ obtained using nitrate and acetate are in good agreement for DMA. As DMA is a strong base in comparison to ammonia, methylamine (MA), DMA, or trimethylamine, these results gives us confidence in the accuracy of previously reported values of $[N_1]$ and $[N_2]$ in [*Jen et al.*, 2014] at high $[A_1]_o$.

Figure 16, 17, and 18 show the acetate and nitrate comparison for EDA, TMEDA, and Put, respectively. Nitrate always detects lower $[N_1]$ and $[N_2]$ than acetate by up to a factor of 4. These comparisons strongly suggest that nitrate does not detect all N_1 and N_2 in the presence of diamines. As only bare sulfuric acid cluster type was detected for both sizes, we cannot determine which neutral clusters types cannot be CI by nitrate. Thus more sensitive experiments that help separate out each formation pathway (i.e. variations

in CI reaction time detailed below) will allow us to examine the CI efficiency of N_1 and N_2.

Figure 15 through 18 clearly show that more of the larger clusters (N_3 and higher) were detected by acetate CI than nitrate. For all bases, the measured [N_3] by acetate is up to a factor of 10 higher than concentrations measured by nitrate CI. Nitrate did not detect any types of N_4 or N_5, probably because the ionized [N_4] and [N_5] fell below detection limits ($<10^5$ cm^{-3}). In addition as [B] increases, the differences between acetate and nitrate cluster concentrations become more pronounced. This likely occurs because sulfuric acid clusters become more chemically neutral as [B] increases, thereby decreasing their tendencies to donate protons to nitrate ions. We conclude that acetate more efficiently chemically ionizes the larger cluster population than nitrate.

The large difference between nitrate and acetate measured [N_3] and [N_4] provide a better understanding of previous atmospheric measurements. Chen et al. [2012] and Jiang et al. [2011c] published [N_3] and [N_4] measured by a larger version of the Cluster CIMS [*Zhao et al.*, 2010]. For both studies, the measurements were conducted using nitrate CI and only at the clusters' bare masses (A_3 and A_4). These measurements may have under-detected the amount of trimer and tetramer in the atmosphere, though this is uncertain because the atmosphere contains numerous compounds that may behave differently than DMA and diamines. If the actual concentrations of trimer and tetramer were higher than those reported by Zhao et al. [2010], then the fitted evaporation rate of E_3=0.4 s^{-1} from Chen et al. [2012] would be lower and be closer to 0 s^{-1} reported by Kürten et al. [2014].

Comparing these results to the CLOUD experiments, the clusters detected via nitrate CI using the Cluster CIMS differ from those detected by nitrate using the CI-APi-ToF [*Kürten et al.*, 2014]. They observed clusters that contained near equal number of sulfuric acid and DMA molecules (e.g., A_3•DMA_2). Our experiments suggest that such highly neutralized clusters are not ionized by nitrate. We do not yet understand why we were unable to detect highly neutralized large clusters by nitrate chemical ionization while Kürten et al. [2014] were. The Cluster CIMS and CI-APi-ToF use different

approaches to produce the reagent ions, and this could be one reason for the differences. Kürten et al. [2014] use corona discharge to ionize nitric acid to produce nitrate whereas the Cluster CIMS uses a Po-210 source. The corona discharge may produce ions in addition to nitrate that ionize neutral sulfuric acid clusters. Also, their experiments were conducted at a lower temperature of 278 K which may lead to more stable ions than at 300 K.

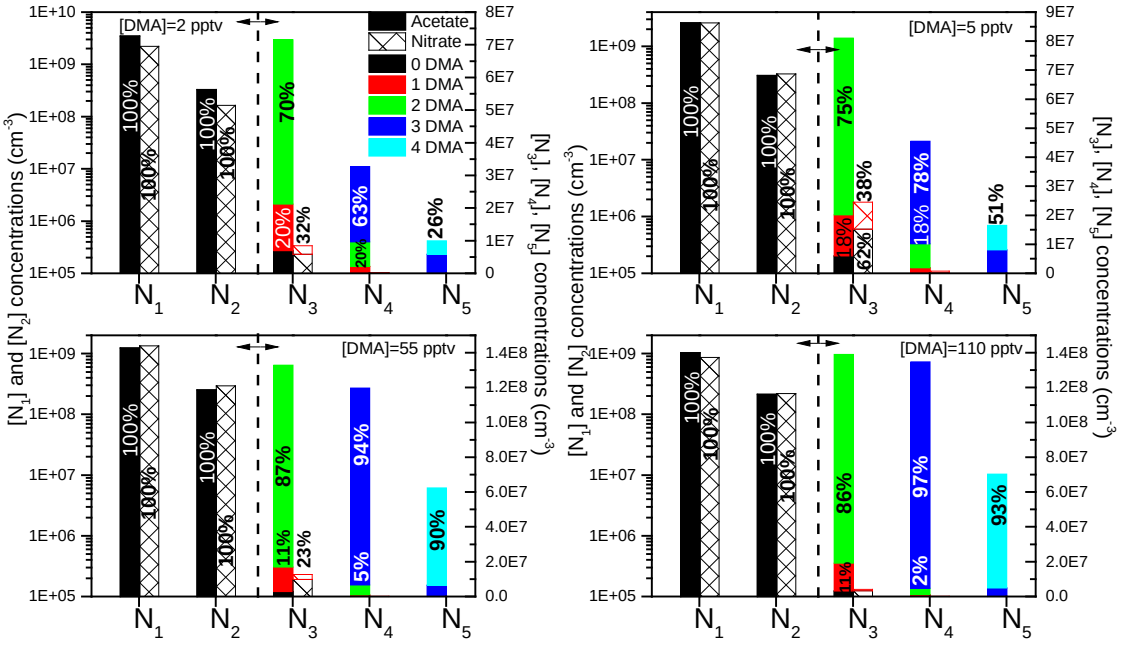

Figure 15 Comparison of cluster concentrations measured using acetate (solid bars) and nitrate (hashed bars) reagent ions at four different [DMA] and constant intial $[A_1]_o=4x10^9$ cm^{-3}. $[N_1]$ and $[N_2]$ are on a log scale (left y-axis), while the larger clusters are on a linear scale (right y-axis). Each color in the bar represent the measured number of DMA molecules in the cluster. The percentages indicate the fraction of each cluster type compared to the total concentration of a cluster of a specified size.

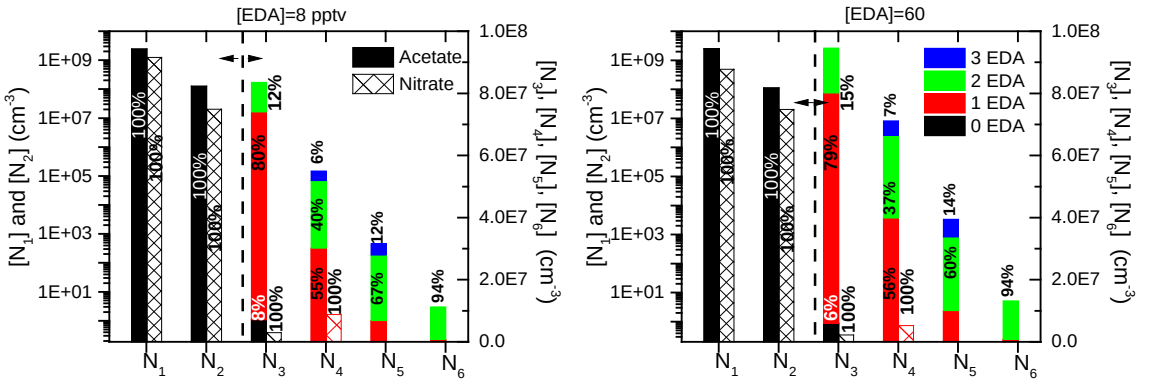

Figure 16 Comparison of cluster concentrations measured using acetate (solid bars) and nitrate (hashed bars) reagent ions at two different [EDA] and constant intial $[A_1]=4x10^9$ cm^{-3}. $[A_1]$ and $[A_2]$ are on a log scale (left y-axis), while the larger clusters are on a linear scale (right y-axis). Each color in the bar represent the number of EDA molecules in the cluster.

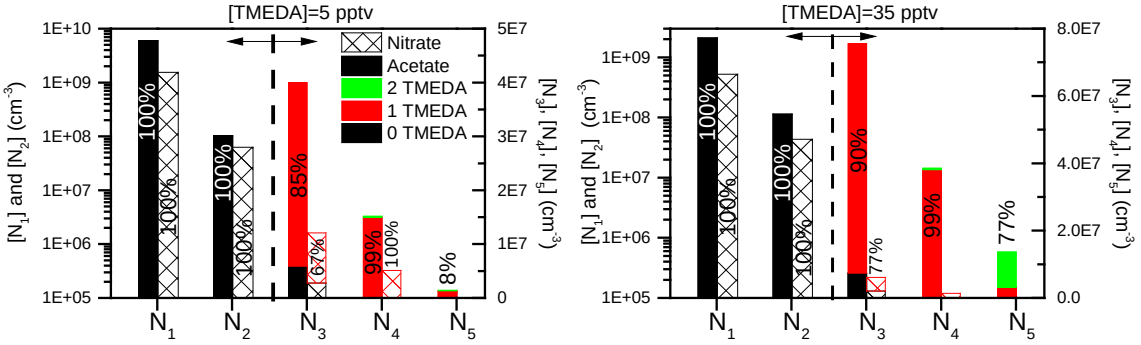

Figure 17 Comparision of cluster concentrations measured using acetate (solid bars) and nitrate (hashed bars) reagent ion at two different [TMEDA] and $[A_1]_o=4x10^9$ cm^{-3}. $[N_1]$ and $[N_2]$ are on a log scale (left y-axis) ,while the larger clusters are on a linear scale (right y-axis). Each color in the bar represent the number of DMA molecules in the cluster.

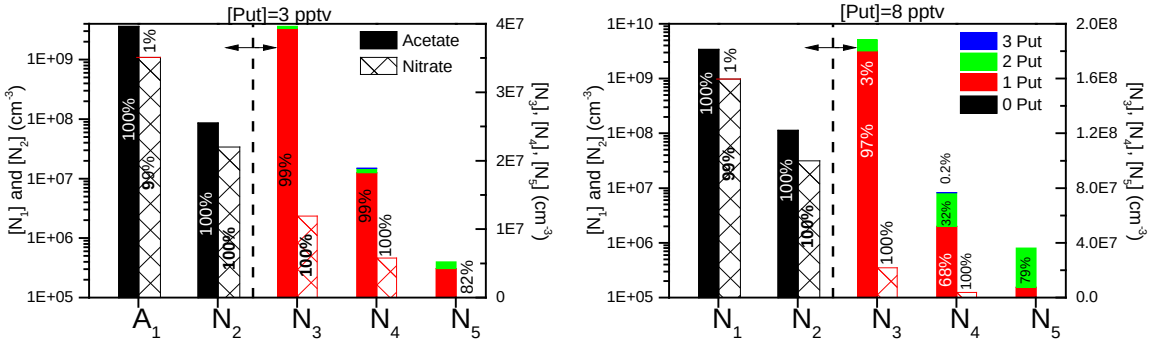

Figure 18 Comparison of cluster concentration mesaured using acetate (solid bars) and nitrate (hashed bars) reagent ions at two different [Put] and $[A_1]_o=4x10^9$ cm^{-3}. $[N_1]$ and $[N_2]$ are on a log scale (left y-axis), while the larger clusters are on a linear scale (right y-axis). Each color in the bar represent the number of DMA molecules in the cluster.

Chemical ionization efficiency clearly plays a role in both the types and amounts of clusters detected. However to obtain the concentrations in Figure 15 through 4, we assumed negligible contributions of IIC and ion decomposition. Testing the validity of these assumptions requires examining the ion behavior as a function CI reaction time and comparing the differences between bases. We attempt to model the complex series of reactions that govern neutral cluster formation, chemical ionization, IIC, and ion decomposition in order to explain observed phenomena. These models likely oversimplify all the chemical reactions occurring in the flow reactor, but they do provide valuable qualitative insights into the processes that may explain observed trends. In the following sections we use model simulations to interpret our experimental observations for each cluster size (N_1, N_2, etc.).

5.5 Monomer, N_1

Over the 3 s acid-base reaction time in this flow reactor, initial N_1 is depleted as it forms larger clusters/particles or is lost to walls; N_1 is formed only by evaporation of larger clusters. Thus, the change of [N_1] as a function of acid-base reaction time is straight forward (see Supporting Information, SI). Computational chemistry predicts only two types of monomer will form between sulfuric acid and DMA: A_1 and A_1•DMA. The latter has an evaporation rate of 10^{-2} s^{-1} and a long lifetime of ~100 s [*Ortega et al.*, 2012]. However the ion A_1^-•DMA is very unstable with an evaporation rate of 10^9 s^{-1} [*Ortega et al.*, 2014]. Therefore, even if A_1•DMA is a significant fraction of the total monomer concentration, the Cluster CIMS will only detect the monomer as A_1^- due to DMA evaporation from the ion. This agrees with our experimental observations (Figure 15) as A_1^-•DMA (142 m/z) was not detected with either acetate or nitrate CI and all monomer signals were detected at the bare sulfuric acid mass (with nitric acid ligand in the nitrate CI case). No computational studies exist for sulfuric acid+diamines but we assume that A_1 and A_1•diamine constitute the population of monomers.

The monomer ions are only formed by the CI of neutral N_1. If all types of N_1 instantly decompose into A_1^- upon ionization (i.e. [N_1^-]=[A_1^-]), then amount of neutral

$[N_1]$ is linearly proportional to the signal ratio of the sulfuric acid monomer (S_{160}) to the reagent ion (S_{125} for nitrate) [*Berresheim et al.*, 2000]. The signals represent the ion concentrations but take into account the mass-dependent sensitivity of the mass spectrometer. See SI for detailed derivation of Equation 7 and discussion on mass-dependent sensitivity. S_{160}/S_{125} as a function of CI reaction time, t, is given in in Equation 7, which is used to determine the neutral $[N_1]$.

$$\frac{S_{160}}{S_{125}} = k_1 [N_1] t \qquad \textbf{Equation 7}$$

For nitrate, $k_1=1.9\text{x}10^{-9}$ cm^3 s^{-1}[*Viggiano et al.*, 1997] and is assumed constant for all types of monomers. Equation 7 assumes negligible depletion of the reagent ion and neutral N_1. Figure 19 shows the signal ratios as a function of t for DMA and EDA as detected by nitrate CI at equivalent $[A_1]_o=4\text{x}10^9$ cm^{-3}. TMEDA and Put graphs look very similar to EDA (see SI). At long t, more of $[N_1]$ is chemically ionized, leading to higher S_{160}/S_{125}. As [B] increases, both the signal ratios and the slopes of the lines decrease. We interpret this to indicate that $[N_1]$ is depleted by the formation of more larger clusters as concentrations of the basic gas increase.

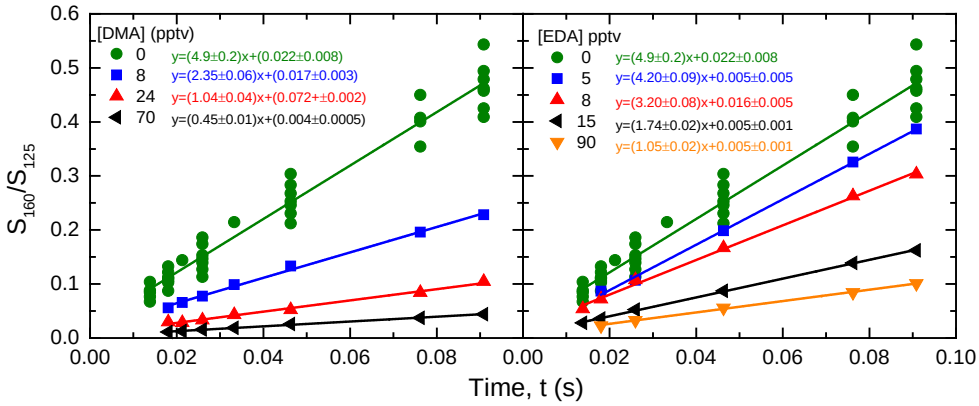

Figure 19 Measuerd S_{160}/S_{125} as a function of CI reaction time for DMA (left) and EDA (right) as measured by nitrate CI at $[A_1]_o=4\text{x}10^9$ cm^{-3}.

Combining the results from acetate vs. nitrate comparisons with Figure 19, we can outline a model that encompasses the depletion and CI of neutral monomer. We know

sulfuric acid+DMA produces monomers that are equally detected by nitrate and acetate. In contrast, sulfuric acid with diamines produces one or more types of monomer that cannot be detected by nitrate CI. Based upon the high computed evaporation rate of A_1•DMA_2, we hypothesize that the monomers are A_1 and A_1•diamine. Since diamines contain two amine groups, A_1•diamine is likely too basic to donate a proton to NO_3^-. The Cluster CIMS operating in positive ion mode, with protonated water clusters as the reagent ion ($(H_2O)_{1\text{-}3}$•H_3O), detects [A_1•diamine$^+$] at ~10% of the [A_1^-•diamine] and may help account for the invisible N_1 fraction with nitrate CI. Concentrations were calculated using similar logic as Equation 7 with further positive ion discussion provided in SI. Following scheme 2 of Jen et al. [2014], we posit the likely monomer pathways in Table 5.

Table 5 Summary of possible pathways for neutral monomer formation and chemical ionization

Neutral formation	Nitrate CI and ion decomposition
DMA and Diamines: $A_1 + B \underset{E_1}{\overset{k}{\rightleftarrows}} AB$	DMA: $A_1 + NO_3^- \xrightarrow{k_c} A_1^-$ $A_1 \bullet DMA + NO_3^- \xrightarrow{k_c} A_1^- \bullet DMA \xrightarrow{fast} A_1^-$ Diamines: $A_1 + NO_3^- \xrightarrow{k_c} A_1^-$ $A_1 \bullet \text{diamine} + NO_3^- \not\rightarrow A_1^- \bullet \text{diamine}$

The neutral cluster balance equations can be solved at the 3 s acid-base reaction time for [A_1] and [A_1•B], and the CI balance equations at the 18 ms CI reaction time to solve for the ion concentrations. Ion decomposition was implicitly taken into account by assuming the base molecule instantly evaporates upon ionization. The model also takes into account monomer depletion via wall deposition, particle coagulation, and IIC. Figure 20 displays the modeled results for DMA and EDA at the [B] an $[A_1]_o$ that were used for the measurements made for Figure 19. The modeled predicts a non-linear dependence of

S_{160}/S_{125} on time that differs from Equation 7 because this model takes into account [N_1] and [NO_3^-] depletion. In addition, the predicted values of S_{160}/S_{125} and their dependence on [B] are in good qualitative agreement with observations. However, the amount of N_1 that is not chemically ionized by nitrate depends heavily on evaporation rate of A_1•diamine and requires a better estimate of E_1 than is currently available.

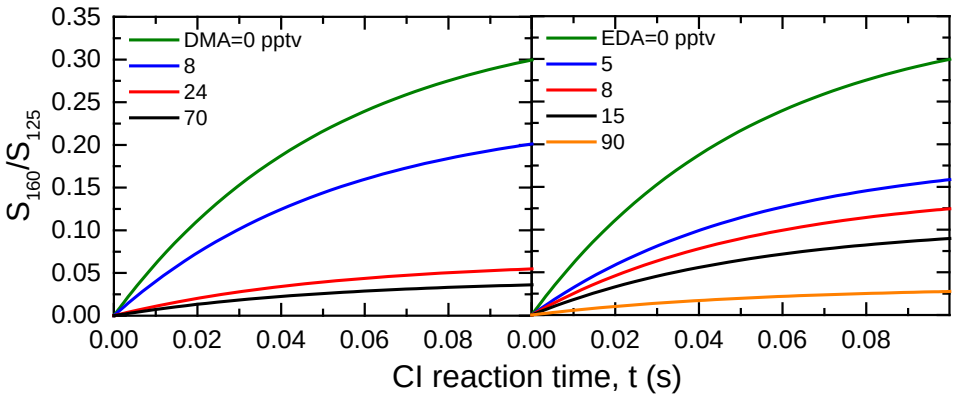

Figure 20 Modeled S_{160}/S_{125} as a function of CI reaction time at equivalent concentrations as Figure 19.

5.6 Dimer, N_2

Modeling neutral dimer concentrations is more complicated as it can be formed from two types of monomer and the dimer types may evaporate at different rates. For sulfuric acid+DMA, the N_2 likely exists as A_2•DMA or A_2•DMA_2 with both cluster types equally stable [*Ortega et al.*, 2012]. However, the DMA evaporation rate of A_2^-•DMA_2 and A_2^-•DMA are, respectively, 10^8 s^{-1} and 10^2 s^{-1} [*Ortega et al.*, 2014]. Therefore, all chemically ionized N_2 will be detected at A_2^-. This mirrors our experimental observations as all sulfuric+DMA dimers are detected at A_2^- mass (195 m/z). We suspect the diamine molecule also evaporates from A_2^-•diamine as we only measure dimers as A_2^-. This is supported by our positive ion data where we observe A_2•$diamine^+$ at approximately equal concentrations of A_2^- detected by nitrate CI (see SI for positive ion results). Also, the nitrate vs. acetate comparisons show that some fraction of [N_2] is not chemically ionized by nitrate. Following the same logic used for the monomer, we hypothesize that A_2•$diamine_2$ is too basic to undergo nitrate CI. We also detect A_2•$diamine_2^+$ at ~10% of nitrate detected [A_2^-].

A_2^- can also be created from IIC between A_1^- and N_1. Equation 8 shows the predicted ratio of sulfuric acid dimer (m/z=195) and monomer (m/z=160) signal intensities. This relationship includes a constant (the t=0 intercept), proportional to the neutral dimer to monomer ratio in the sampled gas, and a term due to IIC that increases linearly with time. The derivation is described in the SI.

$$\frac{S_{195}}{S_{160}} = \frac{k_2}{k_1}\frac{[N_2]}{[N_1]} + \frac{1}{2}k_{21}[N_1]t \qquad \textbf{Equation 8}$$

The rate constants, k_{ij}, are the collision rate constants. Figure 21 shows S_{195}/S_{160} as a function of t for DMA, EDA, and TMEDA as detected by nitrate CI at $[A_1]_o=4x10^9$ cm^{-3}. Put is similar to EDA and is shown in the SI. For all bases, increasing the CI reaction time will produce more IIC-dimer and reduce $[A_1^-]$. The observed linear increase in the S_{195}/S_{160} ratio for all bases provides evidence for the influence of IIC on dimer measurements (Equation 8). However, the y-intercepts for DMA exhibit a pattern that is distinctly different from that observed for the diamines. For DMA, the y-intercept increases with increasing [B]. This is consistent with our expectation, as higher concentrations of the base will both deplete monomer and enhance dimer concentrations. We would have expected a similar trend for the diamines, but a more complex result was observed with the intercept and shows no clear dependence on diamine concentration. As no computational studies have been done on diamines, we cannot conclude if the neutral cluster formation pathways are significantly different than that of sulfuric acid+DMA and would lead to this observed result.

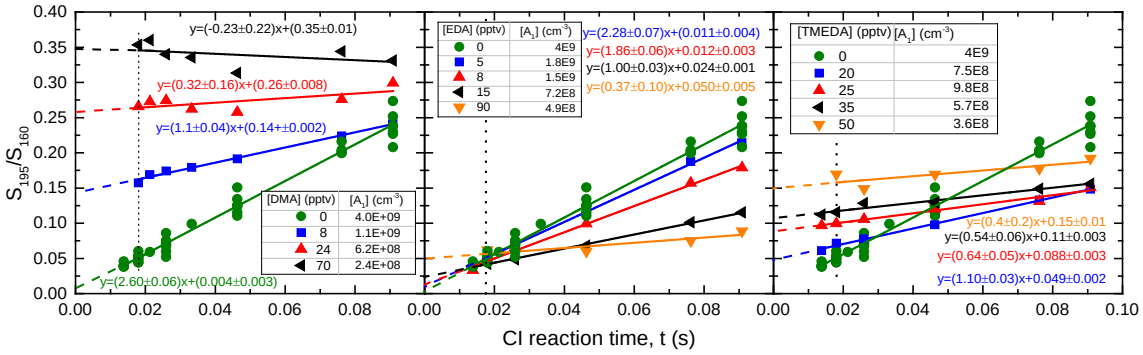

Figure 21 Measured S_{195}/S_{160} as a function of CI reaction time for DMA (left), EDA (center), and TMEDA (right) detected by nitrate CI at $[A_1]_o=4x10^9$ cm^{-3}. The table in each graph provides the measured $[A_1]$ at that [B]. The dotted vertical line is the CI reaction time of 18 ms used in Figure 15and Figure 16 for nitrate CI.

Identifying processes that may cause these differences requires modeling all the reactions that form A_2^-. Building upon the model for the monomer given in Table 5, we include additional dimer formation, CI, and IIC reactions. Ion decomposition was indirectly included for the dimer as it was assumed the base molecule instantly evaporates upon chemical ionization. However, our experimental results do not lend enough sensitivity to determine if dimer evaporation rates affect the trends observed in Figure 21. The dimer model is provided in Table 6.

Table 6 Summary of possible pathways for neutral and ion dimer formation

Neutral formation	**Nitrate CI and ion decomposition reactions**	**IIC reactions (only A_1^-)**
DMA, Put, EDA: $AB + A_1 \xrightarrow{k} A_2B$ $AB + AB \xrightarrow{k} A_2B_2$ $A_2B + B \xrightarrow{k} A_2B_2$ TMEDA: $AB + A_1 \xrightarrow{k} A_2B$ $AB + AB \not\rightarrow A_2B_2$ $A_2B + B \not\rightarrow A_2B_2$	DMA: $A_2B + NO_3^- \xrightarrow{k_c} A_2B^- \xrightarrow{fast} A_2^-$ $A_2B_2 + NO_3^- \xrightarrow{k_c} A_2B_2^- \xrightarrow{fast} A_2^-$ Diamines: $A_2B + NO_3^- \xrightarrow{k_c} A_2B^- \xrightarrow{fast} A_2^-$ $A_2B_2 + NO_3^- \not\rightarrow A_2B_2^-$	All bases: $A_1^- + A_1 \xrightarrow{k_c} A_2^-$ $A_1^- + AB \xrightarrow{k_c} A_2B^- \xrightarrow{fast} A_2^-$

Figure 22 shows modeling results for DMA, EDA, and TMEDA. The modeled curve for [B]=0 pptv is remarkably similar to what was measured, indicating that A_2^- is almost completely formed by $A_1^-+A_1$ and not by the CI of A_2. A_2 is too unstable and does not exist at 300 K [*Hanson and Lovejoy*, 2006]. The qualitative trends for each base match those from Figure 21 by varying several key reactions. For DMA, we assumed all clusters can undergo chemical ionization and can undergo IIC via A_1^- clustering. The primary difference between DMA and EDA is the assumption that A_2•EDA_2 cannot be chemically ionized. Higher [EDA] results in a larger fraction of the dimer population existing as A_2•EDA_2 which would result in a lower S_{195}/S_{160}. The key difference between the TMEDA and DMA model is A_2•$TMEDA_2$ does not form, probably due to one TMEDA molecule sterically hindering the uptake of another TMEDA molecule in the dimer. Preventing the neutral formation of A_2•$TMEDA_2$ is not equivalent to A_2•B_2 not undergoing CI because the former removes a neutral monomer depletion pathway, thereby leading to higher $[A_1^-]$ (i.e. higher S_{160}). We conclude from our modeling that the difference between sulfuric acid+DMA dimers and diamine dimers lies in either the formation or chemical ionization of A_2•B_2. Computational chemistry studies on diamines is required to better understand these processes.

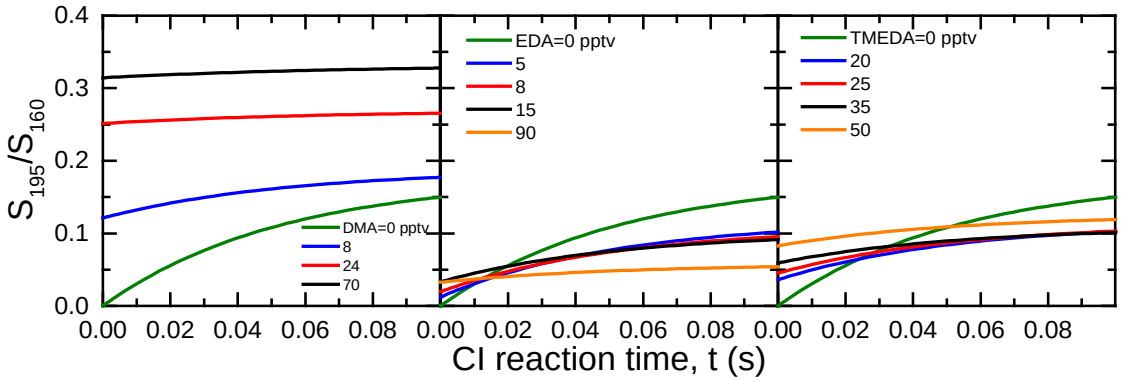

Figure 22 Modeled S_{195}/S_{160} as a function of CI reaction time for DMA (left), EDA (center), and TMEDA (right) at the same concentrations used for Figure 21.

The model also provides an estimate on the fraction of [A_2^-] formed by IIC at t=18 ms. For DMA, IIC dimers account for <1% (less for higher [DMA]) of the total dimer signal and agrees with the conclusions drawn in [*Jen et al.*, 2015]. In contrast, the IIC fraction of total dimer signal for EDA is ~50%, due to the large fraction of the dimer population that does not undergo chemically ionization. IIC produced dimers account for ~20% of the total dimer signal for TMEDA. However, these numbers are likely highly uncertain due to the limitations of the model. Our model is not sensitive enough to determine if A_1^- can cluster with A_1•B which will significantly influence the amount of IIC dimer without significantly affecting S_{195}/S_{160}. Since acetate CI detects more N_2 than nitrate for the diamines (up to a factor of ~10), we believe IIC produced A_2^- is negligible compared to the overall [N_2]. We provide similar graphs as Figure 21 for acetate detected N_2 with TMEDA and Put in the SI.

5.7 Trimer, N_3

The cluster balances describing the creation and destruction of neutral N_3 are much more complicated compared to N_2. In the sulfuric acid+DMA system, computational chemistry predicts A_3•DMA, A_3•DMA_2, and A_3•DMA_3 are present after a 3 s acid-base reaction time with A_3•DMA_3 the most stable [*Ortega et al.*, 2012]. For longer reaction times, the first two types of trimer would likely evaporate. Once ionized, A_3^-•DMA_3 evaporates at a rate of 10^4 s^{-1} into A_3^-•DMA_2. A_3^-•DMA_2 and A_3^-•DMA have lifetimes of ~1 and 100 s, respectively [*Ortega et al.*, 2014], leading to lifetimes comparable to the CI reaction time, given uncertainties from electronic structure calculations. From Figure 15, nitrate only detected A_3^-•DMA and A_3^-. We believe A_3^- is primarily from IIC and A_3^-•DMA is from the CI of A_3•DMA at the CI reaction time of 18 ms for Figure 15. The fact that nitrate CI did not detect A_3^-•DMA_2 with its semi-long lifetime of 1 s leads us to believe that nitrate cannot chemically ionize A_3•DMA_2 or A_3•DMA_3. (Positive ion data for sulfuric acid+DMA is discussed in the SI). Acetate detects a much higher [A_3^-•DMA] than nitrate, perhaps due to decomposition of a larger cluster or because A_3•DMA is not completely chemically ionized by nitrate. In addition,

acetate CI leads to A_3^-•DMA_2 at the highest concentration compared to the other trimer types because A_3^-•DMA_2 was originally A_3•DMA_3 before ionization.

Similar to DMA, nitrate CI only detects A_3^- and A_3^-•diamine, with the latter at a higher concentration. However, the types of trimer clusters detected via acetate CI have on average 1 diamine molecule compared to 2 DMA. This may reflect differences between DMA and diamine ion decomposition or neutral cluster formation pathway. Based upon particle measurements, we believe one diamine molecule is able to stabilize more sulfuric acid molecules than a DMA molecule (see Chapter 4) and would explain the lower number of diamines in a trimer cluster.

If we assume A_3^- is produced from IIC of A_1^-+A_2•DMA and A_2^-+A_1 (A_2 does not exist, see dimer discussion above), then signal ratio of trimer (S_{293}) to monomer as function of t can be written as Equation 9 (derived in the SI).

$$\frac{\left[A_3^-\right]}{\left[A_1^-\right]} = \frac{k_3}{k_1}\frac{\left[N_3\right]}{\left[N_1\right]} + \frac{1}{2}\left(k_{31} + \frac{k_2 k_{32}}{k_1}\right)\left[N_2\right]t + \frac{1}{6}k_{21}k_{31}\left[N_1\right]^2 t^2 \qquad \textbf{Equation 9}$$

Figure 23 shows the nitrate measured S_{293}/S_{160} as a function of CI reaction time for DMA, EDA, and TMEDA at $[A_1]_o$=4x10^9 cm^{-3}. S_{293}/S_{160} curves for all bases indicate minimal creation of A_3^-, likely due to IIC, in the presence of base.

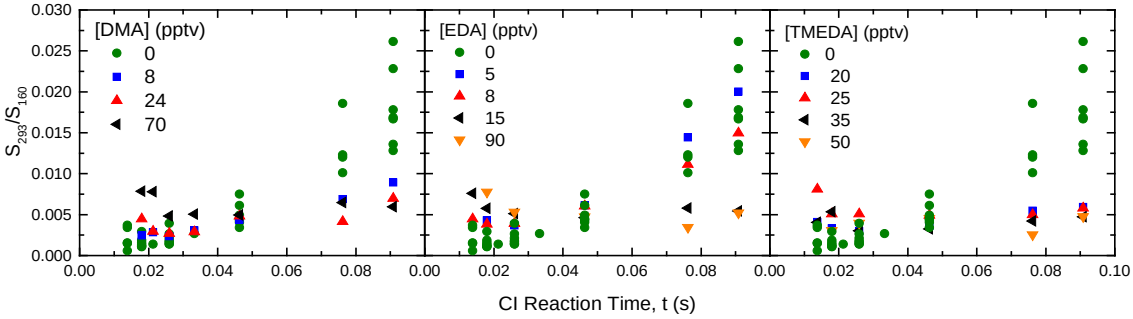

Figure 23 Measured S_{293}/S_{160} as a function of CI reaction time for DMA (left), EDA (center), and TMEDA (right) detected by nitrate CI at $[A_1]_o$=4x10^9 cm^{-3}.

A_3^- can also be formed by the decomposition of larger ions such as A_3^-•B which is not accounted for in Equation 9. Evidence of this decomposition can be seen in Figure 24, presenting the measured $S_{A3•B}/S_{160}$ relationship with t at $[A_1]_o=4x10^9$ cm^{-3}. Data for all three bases were obtained using nitrate CI. At very short time scales (t approaching 0 s), $S_{A3•B}/S_{160}$ increases due to the measurement capturing more A_3^-•B. It follows that at long t, more A_3^-•B will decompose to form A_3^-, thereby increasing S_{293}/S_{160}. We see a slight increase of S_{293}/S_{160} for DMA approximately proportional to the increase of $S_{A3•DMA}/S_{160}$ at short t. Our observations confirm the computational results that show A_3^-•DMA decomposes via DMA evaporation; however our results show A_3^-•DMA decomposes in ~0.01 s whereas Ortega et al. [2014] predicts ~100 s. A comparable trend is not observed for the diamines, indicating that A_3^-•diamine may decompose in a different fashion than A_3^-•DMA.

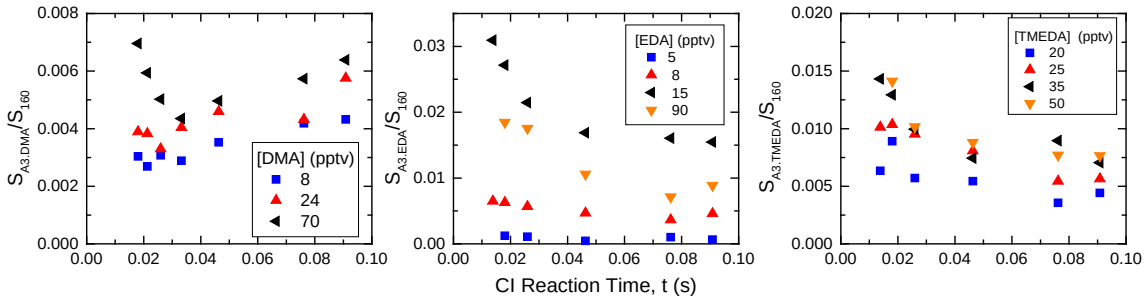

Figure 24 Nitrate measured $S_{A3•B}/S_{160}$ as a function of CI reaction time for DMA (left), EDA (center, and TMEDA (right) at $[A_1]_o=4x10^9$ cm^{-3}. Note the different y-axis scales between bases.

Figure 24 shows numerous other trends that hint towards more significant processes. $S_{A3•DMA}/S_{160}$ increases at long time for DMA but not for EDA or TMEDA. This could be due to IIC formation of A_3^-•DMA, perhaps from A_1^-+A_2•DMA, or decomposition of A_3^-•DMA_2. It is difficult to conclude which process explains this trend without accurate ion decomposition rates and modeling. These processes do not occur with TMEDA and EDA. Furthermore, the value of $S_{A3•DMA}/S_{160}$ is about a factor of 10 lower than the ratios for EDA and TMEDA. Any of the four processes could contribute to the differences between DMA and the other bases.

Table 7 lists the reactions deduced from our results and computational chemistry simulations for sulfuric acid and DMA. We attempt to model the neutral and ion cluster balance equations for these reactions by preventing ion decomposition. This simplifies the number of fitting parameters. As no studies have been conducted on diamines, we only attempt to model the sulfuric acid and DMA system.

Table 7 Summary of possible pathways for neutral and ion trimers formed from sulfuric acid+DMA

Neutral formation	**Chemical ionization and ion decomposition reactions**	**IIC reactions (only A_1^-)**
$A_2B + A_1 \xrightarrow{k} A_3B$	$A_3B + NO_3^- \xrightarrow{k_c} A_3B^-$	$A_2^- + A_1 \xrightarrow{k_c} A_3^-$
$A_3B + B \xrightarrow{k} A_3B_2$	$A_3B_3 + NO_3^- \not\rightarrow A_3B_3^-$	$A_1^- + A_2B \xrightarrow{k_c} A_3B^-$
$A_2B_2 + A_1 \xrightarrow{k} A_3B_2$	$A_3B_2 + NO_3^- \not\rightarrow A_3B_2^-$	
$A_2B + AB \xrightarrow{k} A_3B_2$		
$A_2B_2 + AB \xrightarrow{k} A_3B_3$		

Figure 25 shows the modeled results for S_{293}/S_{160} and $S_{A3.DMA}/S_{160}$ as a function of CI reaction time. At [DMA]=0 pptv, the model accurately predicts the value and trend of S_{293}/S_{160} versus CI reaction time, indicating that A_3^- is primarily from the IIC pathway of $A_2^-+A_1$. The model also predicts the observed decrease of S_{293}/S_{160} with increasing [DMA]. At short t, the model predicts S_{293}/S_{160} for [DMA]=8 pptv exceeds that of [DMA]=0 pptv and is not seen in the measured data. This difference suggests that model takes into account an IIC reaction that does not actually occur or that evaporation of base molecules from neutral trimers occurs. Our model is not sensitive enough to pinpoint the exact reason. The modeled $S_{A3.DMA}/S_{160}$ values agree with the observed values for high [DMA]. However at [DMA]=8 pptv, the model shows a much higher $S_{A3.DMA}/S_{160}$ than observed because the model predicts $[N_3]$ is composed primarily of A_3•DMA. The model likely does not predict the behavior of A_3•DMA correctly.

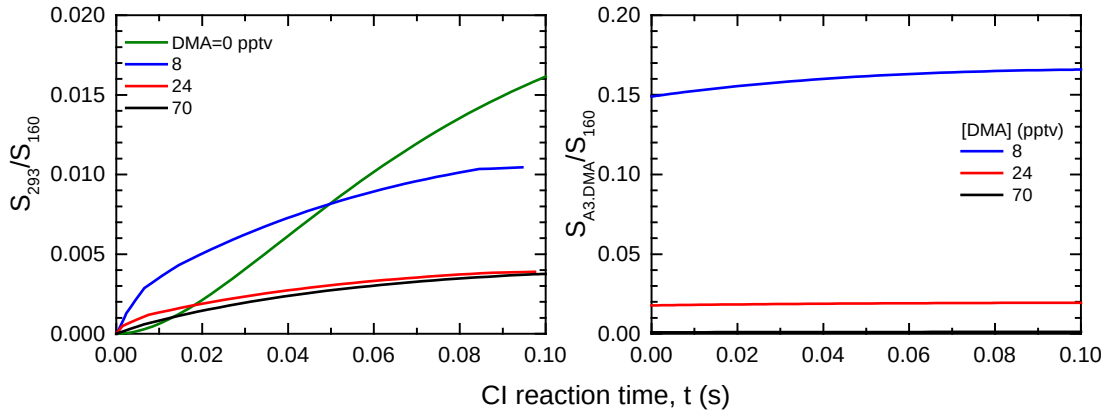

Figure 25 Modeled S_{293}/S_{160} (left) and $S_{A3.DMA}/S_{160}$ (right) as a function of CI reaction time for DMA at conditions used for Figure 23 and Figure 24.

5.8 Tetramer, N_4

Nitrate CI detected none of the larger clusters. The tetramer likely exists as A_4•DMA_{2-4} during the 3 s acid-base reaction time, with A_4•DMA_4 dominating the population [*Ortega et al.*, 2012]. The acetate data confirm the trends predicted by computational chemistry with acetate CI showing A_4^-•DMA_3 as the largest fraction which likely A_4•DMA_4 before ionization [*Ortega et al.*, 2014]. Nitrate may be able to CI A_4•DMA_{1-2}, however their concentrations are probably too low after the 3 s acid-base reaction time. Nitrate was able to detect A_4^-•diamine, suggesting that the most stable neutral tetramers contain less number of diamines than DMA. This is supported by the acetate data for the diamines which show the majority of N_4 containing 1 diamine.

The stability and behavior of A_4^-•diamine can be examined by looking at nitrate detected $S_{A4•diamine}/S_{160}$ as a function of t, given in Figure 26 for EDA and TMEDA. Similar to A_3^-•EDA, $S_{A4•EDA}/S_{160}$ increases at very short t, indicating that A_4^-•EDA likely decomposes in the 0.01 s time scale but A_4^-•TMEDA does not. Decomposition of A_4^-•EDA likely entails evaporation of A_1 instead of diamine from the cluster as nitrate CI did not detect any A_4^-. Furthermore, the lack of a rise in $S_{A4•diamine}/S_{160}$ at long t implies that A_4^-•diamine is not the product of IIC.

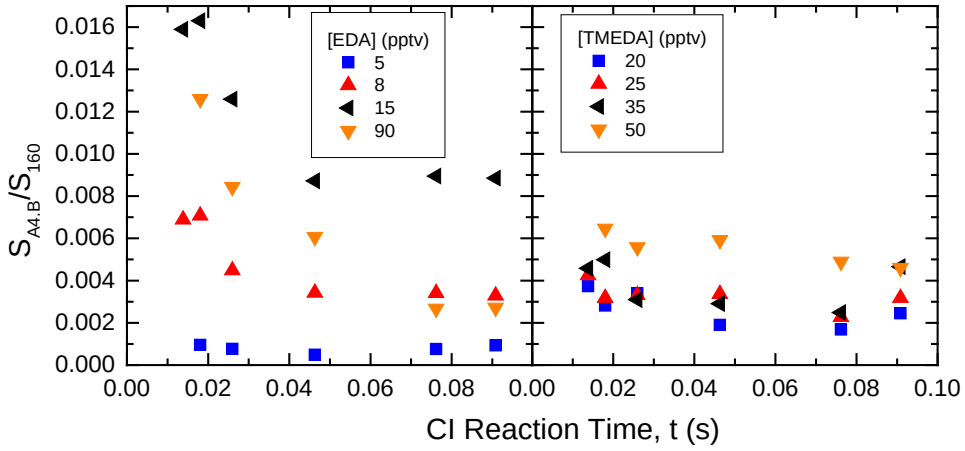

Figure 26 Nitrate measured $S_{A4.diamine}/S_{160}$ as a function of CI reaction time for EDA (left) and TMEDA (right).

5.9 Pentamer, N_5

The most abundant N_5 detected by acetate CI is A_5^-•DMA_4 (no N_5 was detected by nitrate CI). Following the logic for the other sulfuric acid+DMA clusters, we believe this cluster type was A_5•DMA_5 and was the most significant contributor to [N_5]. No computed evaporation rates have been published for N_5 with DMA molecules to confirm this hypothesis. Acetate detected A_5^-•EDA_2 but not A_5^-•EDA_3, suggesting that the latter cluster, in either neutral or ion form, might be unstable. A_5^-•$EDA_{>3}$, A_5^-•$TMEDA_{>1}$, and A_5^-•$Put_{>2}$ fall outside the Cluster CIMS mass range of 710 amu. Thus, we may not have measured the complete population of N_5.

We can draw several conclusions from our measurements and models for all cluster sizes. First, nitrate does not chemically ionize clusters of all sizes with attached diamines. Nitrate also cannot detect sulfuric acid trimer and larger clusters with near equal amounts of DMA. However by comparing sulfuric acid+DMA clusters via nitrate with acetate CI, we can confirm the qualitative trends of both neutral and ion clusters predicted from computational chemistry [*Ortega et al.*, 2012; *Ortega et al.*, 2014]. In addition, ion decomposition does occur for clusters containing DMA and diamines which will in turn affect the predicted composition and concentrations of neutral clusters. However, the extent to which decomposition affects the concentrations is difficult to determine without knowing the decomposition rates and products. Furthermore, our

modeling shows that A_2^- and A_3^- are primarily produced via IIC pathways. When a basic gas is present, the N_3^- population is dominated by aminated clusters, thus IIC is negligible in the total [N_3] at our 18 ms CI reaction time. In contrast, the aminated sulfuric acid dimers decompose almost instantly, resulting in N_2 detected almost completely as A_2^-. IIC contributes negligible amounts of A_2^- for nitrate detected sulfuric acid+DMA dimers, agreeing with our previous assessment of IIC in this system [*Jen et al.*, 2015]. IIC contributes up to 50% of nitrate detected [N_2] for sulfuric acid+diamines; however, acetate CI detects more [N_2] with diamines, suggesting that IIC is negligible for these [N_2].

5.10 Observed Cluster Concentrations Using Acetate CI

We have shown that acetate more accurately measures the cluster concentrations than nitrate in environments containing sulfuric acid and a strong base. Figure 27 shows [N_2], [N_3], [N_4], and [N_5] (abbreviated as [N_m]) as a function of measured [N_1] in the presence of DMA using acetate with the Cluster CIMS. At low [N_1]~2x10^8 cm^{-3}, the measured [N_2] is higher than the values reported in Jen et al. [2014] by a factor of ~5. Note, concentrations in [*Jen et al.*, 2014] have been corrected for IIC; we have removed the IIC correction to the sulfuric acid+DMA [N_2] of Jen et al. [2014] for this comparison. The differences between acetate [N_2] and nitrate [N_2] is likely due to acetate background signals obscuring the true [N_2] at low [N_1]. A higher mass resolution mass spectrometer would be able to separate out the background signals from dimer signal. Overall, the dimer concentrations for the monoamines reported in Jen et al. [2014] are more accurate due to lower background interferences of nitrate ionization.

Figure 27 also illustrates that all cluster concentrations reach a saturation limit where increasing [DMA] does not produce more clusters. The saturation point for DMA is between concentrations in the 5 to 55 pptv range, agreeing with the value of 20 pptv reported by Jen et al. [2014]. This saturation limit implies that at this [DMA] or higher, cluster formation is limited by sulfuric acid uptake. Figure 28 through Figure 30 show the cluster concentrations as a function of measured [N_1] for EDA, TMEDA, and Put

respectively. From these figures, the saturation points are [EDA]=6-9 pptv, [TMEDA]=4-35 pptv, and [Put]=2-14 pptv. These results are summarized in Table 8.

Following Jen et al. [2014], evaporation rates (e.g. E_1 and E_3) were fitted from the cluster concentration data by solving Scheme 2 of the acid-base reaction model (where A_1 reacts with B to form A_1•B) at 3 s. These evaporation rates represent an average for clusters that contain a given number of sulfuric acid molecules and do not account for the number of base molecules in a cluster. For example, a fitted E_3 from the data would combine the evaporation rates of A_3•B_{1-3}. This might be reasonable if most clusters of a given size consist of a single composition. However, if evaporation occurs for clusters of a given size consisting of at least two compositions, then this approach will require refinement in the future. In addition, fitted rates are interdependent since cluster concentrations are linked. E_3 was calculated by fixing E_1 and minimizing the least square residual for each type of cluster concentration. The range of fitted E_3 and E_1 values are summarized in Table 8 and are very similar between DMA and the diamines. In addition, their evaporation rates indicate the clusters have lifetimes on the order of acid-base reaction time of 3 s. Therefore, we cannot say with confidence that one of these four bases will stabilize clusters more than the others: they behave similarly during the 3 s reaction time. In a separate paper we report on measurements of particle concentrations after 40 s of reactions. Those measurements showed that, for given reactant concentrations, diamines consistently produce more particles than monoamines, indicating that they are more potent nucleating agents (i.e., that diamines produce clusters that are more stable and evaporate more slowly than clusters formed from monoamines).

Table 8 Observed saturation [B] and fitted evaporation rates for four different bases using acetate CI cluster concentrations.

Base	Saturation [B] pptv	E_1 (s^{-1})	E_3 (s^{-1})
DMA	5-55	<1	<1
EDA	6-9	<1	<2
Put	2-14	<1	<1
TMEDA	4-35	<1	<5

At short acid-base reaction times, the more accurate method for fitting evaporation rates is to model all four processes to compare measured ion ratios as a function of CI reaction time (Figure 21, Figure 23, Figure 24, and Figure 27). The number of chemical reactions and fitted parameters can be simplified by knowing the stability of neutral and ion clusters, as provide by computational chemistry, to lay out the most likely chemical reaction pathway clusters can form. However, the number of fitted parameters and their interdependencies are too high to allow for reliable determinations of rate constants by fitting a model to data, especially for clusters larger than N_2. In addition, some cluster lifetimes are on the order of the reaction time used in these experiments, which constrains the range of values that can be found. In this study we identify the challenges in using chemical ionization to study the formation of neutral clusters and propose a method to determine the effects of various ion processes on the measured cluster concentrations and compositions. Future computational chemistry studies on the sulfuric acid and diamine environment would allow us to further refine our interpretation of the observations and help model the complex system.

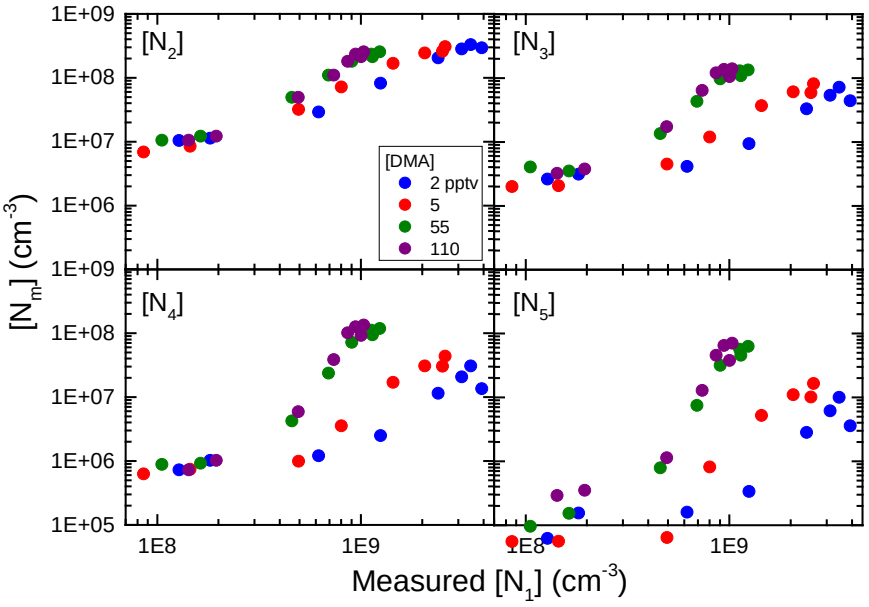

Figure 27 [N_m] vs. measured [N_1] for four different [DMA], as indicated by different color points.

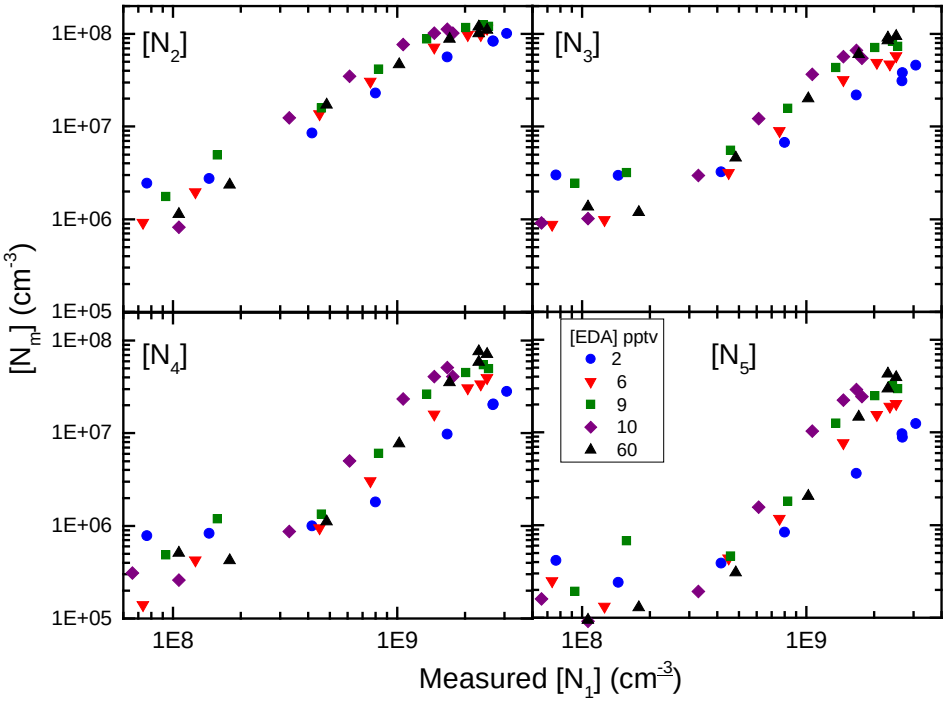

Figure 28 [N_m] vs. measured [N_1] for five different [EDA], as indicated by different color points.

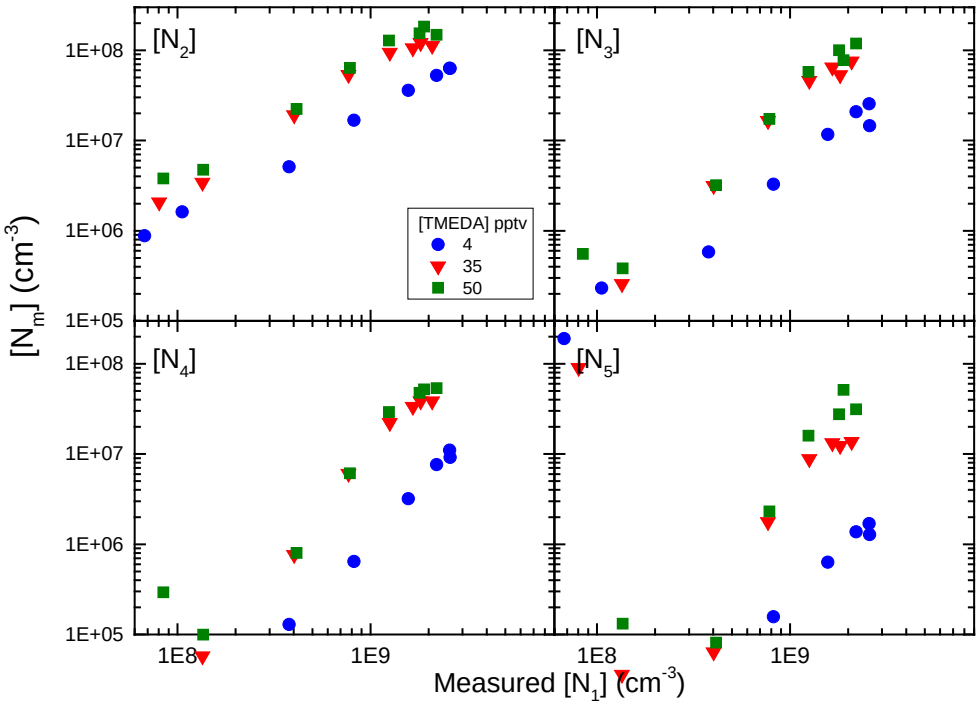

Figure 29 [N_m] vs. measured [N_1] for three different [TMEDA], as indicated by different color points

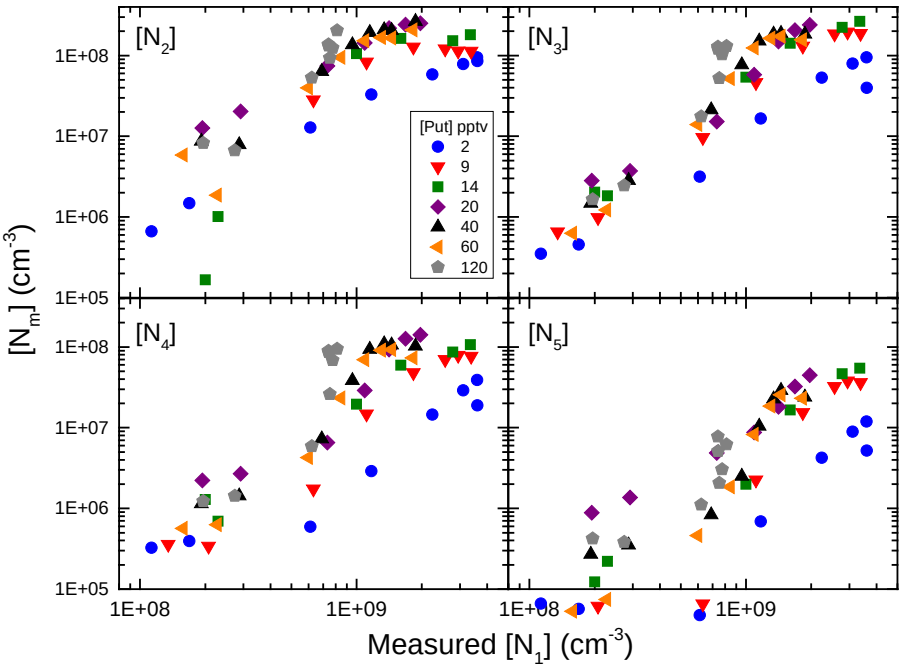

Figure 30 [N_m] vs. measured [N_1] for seven different [Put], as indicated by different color points

5.11 Conclusion

Measured cluster concentrations and compositions using chemical ionization mass spectrometry depends on four key processes: neutral cluster formation, chemical ionization, ion decomposition, and ion-induced clustering. Each of these processes must be examined to determine its effect on the observed clusters. We compared nitrate and acetate chemical ionization and determined that nitrate is unable to chemically ionize all types of aminated sulfuric acid clusters (including DMA and the diamines) and may lead to under-reported cluster concentrations. Acetate CI more accurately measures sulfuric acid cluster concentrations but also exhibits a higher background. In addition, we provide evidence that ions, such as A_3^-•B, decompose in the short CI reaction time scale and will alter the observed cluster composition. IIC primarily produces bare sulfuric acid clusters and mostly impacts measured [N_2]. The sulfuric acid reaction with a basic gas reduces the amount of ionizable monomer available for IIC and thus limits the contribution of IIC to [N_2]. Our results indicate that IIC contributes negligible amounts of A_2^- for nitrate detected sulfuric acid+DMA dimers and for acetate detected [N_2] for sulfuric acid and a diamine.

5.12 Supporting Information

5.12.1 Mass-Dependent Sensitivity of the Cluster CIMS

Mass-dependent sensitivity experiments were performed on the University of MN Cluster CIMS following a near identical procedure as detailed in Zhao et al. [2010], with pertinent details described here. Four tetra-alkyl ammonium halide salts were used in this experiment: tetramethyl ammonium iodide (TMAI at 74 and 275 m/z), tetrapropyl ammonium iodide (TPAI at 186 m/z), tetrabutyl ammonium iodide (TBAI at 242 m/z), and tetraheptyl ammonium bromide (THAB at 410 m/z). These salts were dissolved in methanol and electrosprayed in positive ion mode. Specific ion mobilities [*Ude and de la Mora*, 2005] were selected using a high resolution differential mobility analyzer (HDMA) [*Rosser and de la Mora*, 2005]. The flow containing mono-mobile ions was split into two equal streams with one measured by an electrometer and the other by the Cluster CIMS. The ions were directly delivered to the inlet of the Cluster CIMS where they first entered a conical octopole (1 MHz and 24 V pk-pk) then the quadrupole mass analyzer. The signals of the Cluster CIMS were divided by the electrometer concentrations to obtain the sensitivity. Since the ions were delivered directly to the Cluster CIMS inlet, these experiments only probe the mass-dependent sensitivity of the inlet, octopole, quadrupole, and detector.

Figure S23 shows measured sensitivity at specific masses corresponding to the alkyl halide positive ions. We assume the mass-dependent sensitivity for positive ions is the same for negative ions. The sensitivity at smaller masses is lower than at larger masses, indicating that the Cluster CIMS more efficiently measures larger ions. The black line in Figure S23 is the average sensitivity of the acetate ions (including $CH_3CO_2^-$, $CH_3CO_2^-{\bullet}H_2O$, and $CH_3CO_2^-{\bullet}CH_3CO_2H$). For masses between 450 to 710 m/z, we assume a sensitivity value of 0.037 Hz cm^3. Masses larger than 710 m/z are not detected (i.e. sensitivity of zero) due to limits of our quadrupole. A constant sensitivity assumes that all mass from ~200-710 m/z are measured equally efficient. This contrasts to Zhao et al. [2010] where they observed a steep decline in sensitivity at large masses. We base our assumption on the size and shape of largest mass peaks. Figure S24 shows a sample mass

scan of sulfuric acid with [EDA]=60 pptv. The largest ion detected is A_6^-•EDA_2 at 707 m/z. The peak is ~4 m/z wide and ~600 Hz tall. If the sensitivity for this large ion were low, then the resulting [A_6^-•EDA_2] would exceed that of [A_2^-], an unlikely scenario.

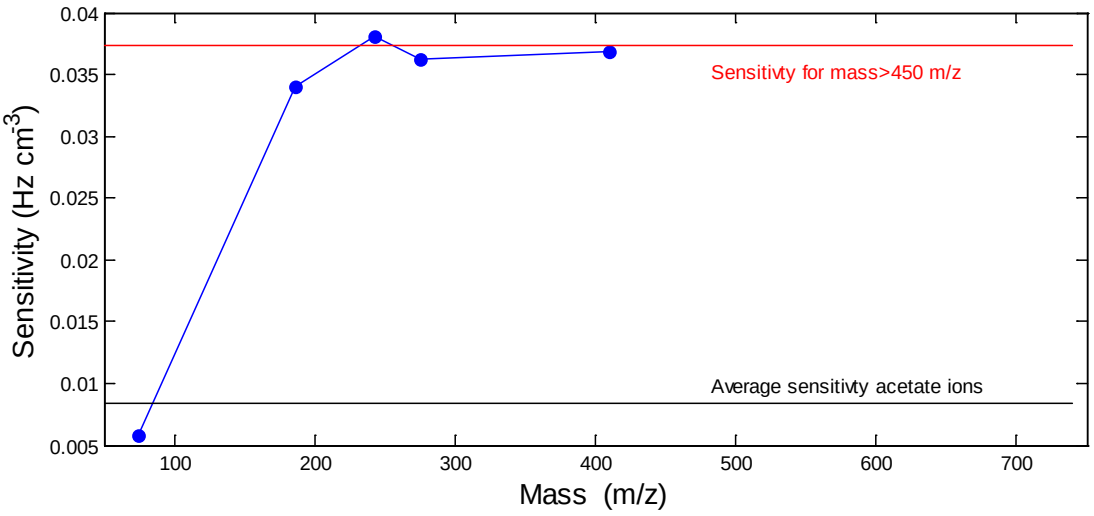

Figure S23 Sensitivity of the UMN Cluster CIMS as a function of mass. The points indicate the measured sensitivity of the positive alkyl halide ions and the red line is the extrapolated sensitivity for masses larger than 450 m/z. The black is the average sensitivity of the acetate ions.

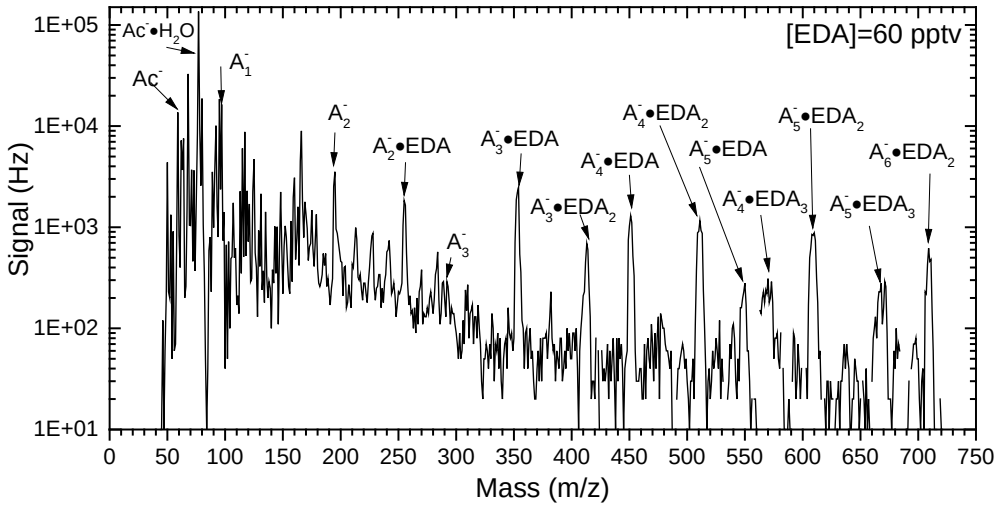

Figure S24 Mass scan of sulfuric acid at $[A_1]_o$=4x10^9 cm^{-3} and [EDA]=60 pptv measured using acetate. Identities of sulfuric acid+EDA peaks are labeled.

5.12.2 Chemical Ionization and IIC Reactions

Negative ion chemical ionization of any sulfuric acid cluster follows a similar reaction whereby the neutral entity donates a proton to the charged reagent ion (e.g. nitrate). For example, CI of neutral sulfuric acid monomer can be written as

$$H_2SO_4 + HNO_3 \bullet NO_3^- \xrightarrow{k_1} HSO_4^- \bullet HNO_3 + HNO_3$$

where k_1 is the collision rate measured at 1.9×10^{-9} cm^3 s^{-1} [*Viggiano et al.*, 1997]. For larger clusters, the resulting nitric acid evaporates from the ion cluster. IIC reactions up to the trimer are as follows.

$$N_1 + A_1^- \xrightarrow{k_{21}} N_2^-$$

$$N_2 + A_1^- \xrightarrow{k_{31}} N_3^-$$

$$N_1 + A_2^- \xrightarrow{k_{32}} N_3^-$$

The production of $\left[A_1^-\right]$ can be described by Equation S25 if we assume IIC depletion of $[A_1]$ is negligible compared to CI depletion. This is a good assumption because $\left[A_1^-\right] << \left[NO_3^-\right]$.

$$\frac{d\left[A_1^-\right]}{dt} = k_1\left[N_1\right]\left[NO_3^-\right] \qquad \textbf{Equation S25}$$

If $\left[NO_3^-\right]$ and $\left[N_1\right]$ are assumed to not change as a function of CI reaction time, t, then this equation can be integrated to give

$$\frac{\left[A_1^-\right]}{\left[NO_3^-\right]} = k_1 t\left[N_1\right] \qquad \textbf{Equation S26}$$

The left-hand side of the equation can be easily converted to measured signals by introducing the mass-dependent sensitivity factor for masses of A_1^- and NO_3^- (see above section). At long CI reaction times, $\left[N_1\right]$ will decrease significantly. $\left[N_1\right]$ can then be estimated by assuming

$$\left[NO_3^-\right]\Big|_{t=0s} = \left[A_1^-\right] + \left[NO_3^-\right] \qquad \textbf{Equation S27}$$

This leads to

$$\left[N_1\right] = \frac{1}{k_1 t}\ln\left(1 + \frac{\left[A_1^-\right]}{\left[NO_3^-\right]}\right) \qquad \textbf{Equation S28}$$

We used this equation for the N_1 data inversion of the main paper; however for simplicity, we will use Equation S26 for the remainder of this IIC model derivation. The formation of A_2^- is described by both CI of neutral N_2 and formation from IIC.

$$\frac{d\left[A_2^-\right]}{dt} = k_2\left[N_2\right]\left[NO_3^-\right] + k_{21}\left[N_1\right]\left[A_1^-\right] \qquad \textbf{Equation S29}$$

Equation S26 can be substituted into Equation S29 to give

$$\frac{d\left[A_2^-\right]}{dt} = k_2\left[N_2\right]\left[NO_3^-\right] + k_{21}k_1 t\left[N_1\right]^2\left[NO_3^-\right] \qquad \textbf{Equation S30}$$

Integrating and assuming $\left[NO_3^-\right]$, $\left[N_2\right]$, and $\left[N_1\right]$ remain constant with time results in

$$\left[A_2^-\right] = k_2\left[N_2\right]\left[NO_3^-\right]t + \frac{1}{2}k_{21}k_1 t^2\left[N_1\right]^2\left[NO_3^-\right] \qquad \textbf{Equation S31}$$

Dividing Equation S31 by Equation S26 gives

$$\frac{\left[A_2^-\right]}{\left[A_1^-\right]} = \frac{k_2}{k_1}\frac{\left[N_2\right]}{\left[N_1\right]} + \frac{1}{2}k_{21}t\left[N_1\right] \qquad \textbf{Equation S32}$$

The production of A_3^- is also a combination of CI of neutral N_3 and production from IIC.

$$\frac{d\left[A_3^-\right]}{dt} = k_c\left[NO_3^-\right]\left[N_3\right] + k_{21}\left[A_1^-\right]\left[N_2\right] + k_{32}\left[A_2^-\right]\left[N_1\right] \qquad \textbf{Equation S33}$$

Following similar assumptions and math as before, then

$$\frac{\left[A_3^-\right]}{\left[A_1^-\right]} = \frac{k_3}{k_1}\frac{\left[N_3\right]}{\left[N_1\right]} + \frac{1}{2}\left(k_{31} + \frac{k_2 k_{32}}{k_1}\right)\left[N_2\right]t + \frac{1}{6}k_{21}k_{31}\left[N_1\right]^2 t^2 \qquad \textbf{Equation S34}$$

This IIC model is the method used to correct measured signals of N_2 and larger clusters for IIC bias [*Chen et al.*, 2012; *Hanson and Eisele,* 2002]. However, this model assumes no depletion of the neutral cluster concentrations and neglects possible contributions of ion decomposition. Deviations from this model provide insights into what other processes are affecting the formation of ions.

5.12.3 Positive Ion Cluster of Sulfuric Acid and Various Bases

Protonated water clusters were produced by passing water vapor over a Po-210 alpha source and were used to positively charge sulfuric acid clusters containing basic molecules. In the sulfuric acid+DMA system, the Cluster CIMS detected DMA^+, $A_1{\bullet}DMA_2^+$, $A_2{\bullet}DMA_2^+$, $A_2{\bullet}DMA_3^+$, $A_3{\bullet}DMA_4^+$, $A_4{\bullet}DMA_4^+$. These clusters are different than the ones reported in Bianchi et al. [2014] as they did not observe positive ion clusters with equal numbers of sulfuric acids and DMA molecules. Since we chemically ionize neutral clusters and can control the ion drift time, we are able to detect very short lived ions whereas Bianchi et al. sampled pre-existing ions that have achieved steady state. Ions with short lifetimes will not be observed in the long time scales of the CLOUD chamber experiments.

Our observed positive ion dimers and trimers are likely the evaporation products of larger ions. Ortega et al. [2014] predicts that sulfuric acid will evaporate from these positively charged clusters. For example, $A_1{\bullet}DMA_1^+$ will quickly evaporate into A_1 and DMA^+ (100 s^{-1}) and $A_2{\bullet}DMA_2^+$ will evaporate into $A_1{\bullet}DMA_2^+$ (1 s^{-1}). Therefore, we cannot conclude if the dimers observed in our positive ion data were initially neutral dimers.

We hypothesize that sulfuric acid will evaporate more slowly from sulfuric acid+diamine positive ion clusters than with DMA due to the additional amine group of a diamine. The observed positive ion cluster types are given in Table S4. In contrast to sulfuric acid and DMA, the positive ion clusters with diamine show either equal or more

acid molecules than base molecules. This supports our hypothesis that the both amine groups of the diamine have significant interactions with sulfuric acid.

Table S4 List of positive ion cluster types detected by the Cluster CIMS

Cluster Size, Base	DMA	EDA	Put	TMEDA
N_1	$A_1 \bullet DMA_2^+$	$A_1 \bullet EDA^+$ $A_1 \bullet EDA_3^+$	$A_1 \bullet Put^+$	$A_1 \bullet TMEDA^+$ $A_1 \bullet TMEDA_2^+$
N_2	$A_2 \bullet DMA_2^+$ $A_2 \bullet DMA_3^+$	$A_2 \bullet EDA^+$ $A_2 \bullet EDA_2^+$	$A_2 \bullet Put^+$ $A_2 \bullet Put_2^+$	$A_2 \bullet TMEDA^+$ $A_2 \bullet TMEDA_2^+$
N_3	$A_3 \bullet DMA_4^+$	$A_3 \bullet EDA^+$ $A_3 \bullet EDA_2^+$ $A_3 \bullet EDA_4^+$	$A_3 \bullet Put_2^+$ $A_3 \bullet Put_3^+$	$A_3 \bullet TMEDA_2^+$
N_4	$A_4 \bullet DMA_4^+$	$A_4 \bullet EDA_3^+$ $A_4 \bullet EDA_4^+$	$A_4 \bullet Put_3^+$	$A_4 \bullet TMEDA_2^+$
N_5		$A_5 \bullet EDA_3^+$		

Figure S25 shows the differences in $[N_1]$ and $[N_2]$ detected by acetate, nitrate, and protonated water cluster ions. If we assume sulfuric acid does not evaporate from these ion clusters, then protonated water is able to ionize the more chemically basic portion of the N_1 and N_2 population. $[N_1^+]$ represents ~1% of the overall $[N_1]$ whereas $[N_2^+]$ is about equal to the $[A_2^-]$ detected by nitrate CI. The difference between acetate $[N_2]$ and nitrate $[N_2]$ is approximately equal to the water $[N_2]$, perhaps indicating that acetate is able to chemically ionize the cluster types seen in positive spectra. We require more computational chemistry studies on the behavior of positive and negative sulfuric acid+diamine ion clusters to understand why nitrate detected $[N_1]$ and $[N_2]$ are lower than the concentrations measured using acetate CI.

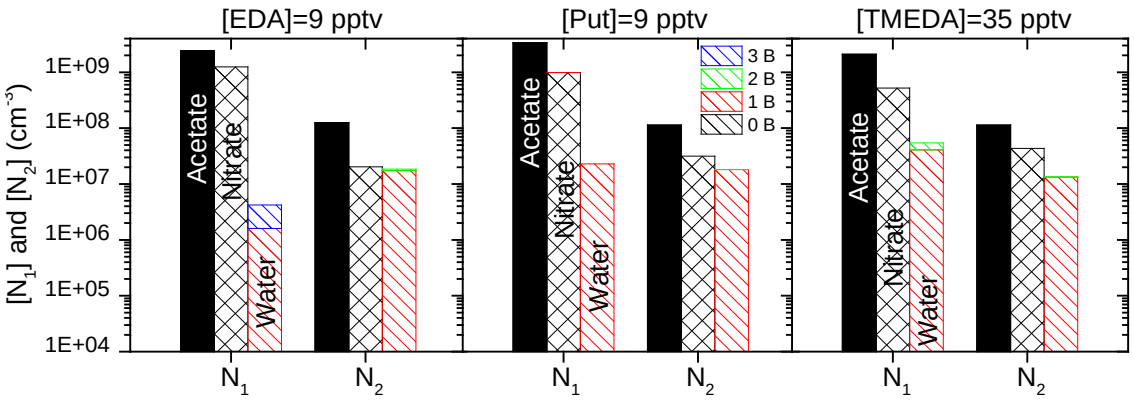

Figure S25 Monomer and dimers detected via acetate (solid), nitrate (hashed), and protonated water clusters (diagonal stripes) chemical ionization. Each color represents the number of base molecules with EDA shown on the left, Put center, and TMEDA right.

5.12.4 Modeled Reactions

The modeled reactions, listed in [table] can be divided into three categories: neutral cluster formation, chemical ionization and ion decomposition, and IIC. The neutral cluster forward rate constants, *k*, were assumed to be 4×10^{-10} cm^3 s^{-1}, and the ion forward rate constants, k_c, were taken to be 2×10^{-9} cm^3 s^{-1}. To constrain the number of parameter, we set all the evaporation rates except E_1 to zero. Rate constants listed as *fast* were assumed to be instantaneous and the intermediate products do not form in appreciable quantities.

Table S5 Summary of all the reactions modeled in this study

Neutral cluster formation	CI and ion decomposition reactions	IIC reactions
$A_1 + B \underset{E_1}{\overset{k}{\rightleftarrows}} AB$	$A_2B_2 + NO_3^- \xrightarrow{k_c} A_2B_2^- \xrightarrow{fast} A_2^-$	$A_1^- + A_1 \xrightarrow{k_c} A_2^-$
$AB + A_1 \xrightarrow{k} A_2B$	$AB + NO_3^- \xrightarrow{k_c} AB^- \xrightarrow{fast} A_1^-$	$A_2^- + A_1$ or $AB \xrightarrow{k_c} A_3^-$
$AB + AB \xrightarrow{k} A_2B_2$	$A_1 + NO_3^- \xrightarrow{k_c} A_1^-$	$A_1^- + A_2B \xrightarrow{k_c} A_3B^-$
$A_2B + B \xrightarrow{k} A_2B_2$	$A_2B + NO_3^- \xrightarrow{k_c} A_2B^- \xrightarrow{fast} A_2^-$	$A_1^- + A_3B \xrightarrow{k_c} N_4^-$
$A_2B + A_1 \xrightarrow{k} A_3B$	$A_3B + NO_3^- \xrightarrow{k_c} A_3B^- \xrightarrow{E_{A_3B^-}} A_3^-$	$A_1^- + A_2B_2 \xrightarrow{k_c} A_3B_2^-$
$A_3B + B \xrightarrow{k} A_3B_2$	$N_4 + NO_3^- \xrightarrow{k_c} N_4^-$	$A_1^- + AB \xrightarrow{k_c} A_2B^- \xrightarrow{fast} A_2^-$
$A_2B_2 + A_1 \xrightarrow{k} A_3B_2$	$A_3B_3 + NO_3^- \xrightarrow{k_c} A_3B_3^- \xrightarrow{fast} A_3B_2^-$	
$A_2B + AB \xrightarrow{k} A_3B_2$	$A_3B_2 + NO_3^- \xrightarrow{k_c} A_3B_2^- \xrightarrow{E_{A_3B_2^-}} A_3B^-$	
$A_2B_2 + AB \xrightarrow{k} A_3B_3$		
$A_3B_2 \xrightarrow{E_{A3B2}} A_2B_2 + A_1$		
A_3B or A_3B_2 or $A_3B_3 + AB \xrightarrow{k} N_4$		
A_3B_2 or $A_3B_3 + A_1 \xrightarrow{k} N_4$		
$A_2B_2 \xrightarrow{E_2} AB + AB$		
$A_2B_2 \xrightarrow{E_2} A_2B + B$		
$A_3B \xrightarrow{E_{A3B}} A_2B + A_1$		

5.12.5 Acetate Detected S_{195}/S_{160} for TMEDA and Put

Figure S26 provides acetate measured S_{195}/S_{160} as a function of CI reaction time for TMEDA and Put. The S_{195}/S_{160} values are higher than those seen for the diamines in Figure 21. The trends seen for acetate detected Put match closely with nitrate detected DMA where IIC produced A_2^- is negligible compared to $[N_2]$. Since nitrate detected S_{195}/S_{160} for Put (given in Figure S27) closely resembles that of EDA from Figure 21 of the main paper, we conclude that IIC is negligible for acetate detected $[N_2]$ of sulfuric acid+diamines.

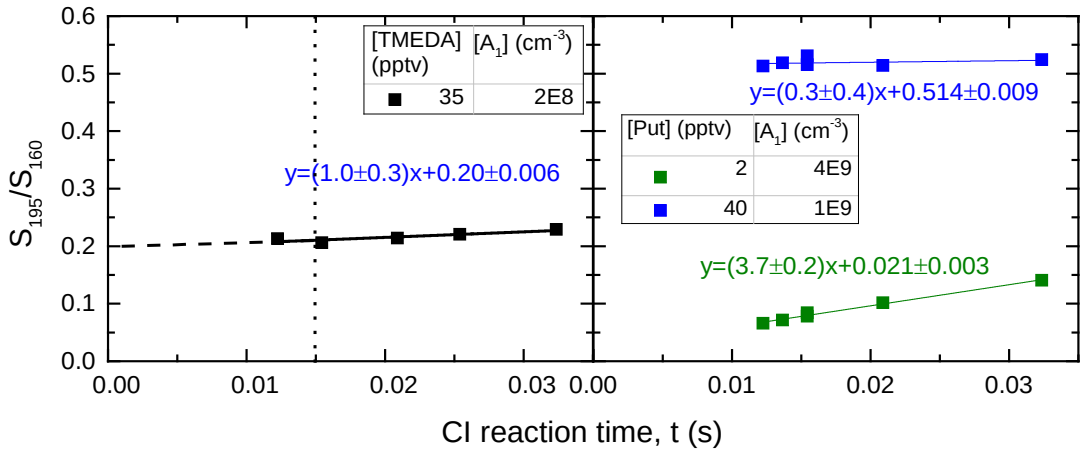

Figure S26 Acetate detected S_{195}/S_{160} as a function of CI reaction time for one [TMEDA] and two [Put]. The inset table provides the measured $[A_1]$.

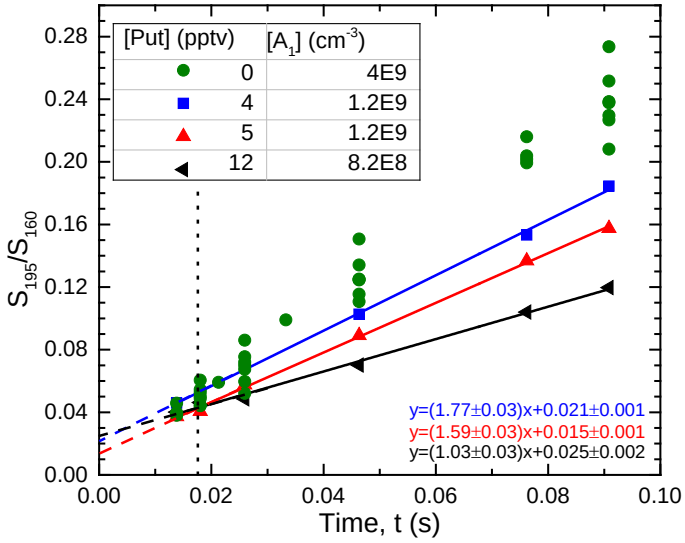

Figure S27 Nitrate detected S_{195}/S_{160} as a function of CI reaction time for Put. The inset table lists the corresponding measured $[A_1]$ and the equations provide the parameters of the fitted linear model.

Chapter 6. Conclusions and Recommendations for Future Work

6.1 Summary of Discoveries

The work presented in this dissertation improves our understanding on the chemical reactions behind atmospheric nucleation and on the instrumentation used to measure freshly formed clusters and particles. Chapter 3 investigates how various basic gases, such as ammonia and amines, stabilize sulfuric acid dimer clusters. I show that dimethylamine and trimethylamine stabilize dimers the most, leading to dimer concentrations approaching the collision-controlled limit. Building upon previous work from our group, I propose a revised acid-base chemical reaction model to describe atmosphereic nucleation, based on measurements in a laboratory flow reactor. This model was used to obtain dissocation rates of sulfuric acid+base clusters, which combined with observations, suggest that ammonia<methylamine<trimethylamine$\lesssim$dimethylamine at forming stable sulfuric acid dimers. Predicted nucleation rates are in the range of observed boundary layer nucleation rates for measurements conducted by our group and others worldwide.

Unlike dimer concentrations, concentrations of the larger clusters in ~1 nm in size are less certain due to measurement uncertainties, but accurate measurements of these larger clusters are needed to improve calculated evaporation rates and the acid-base reaction model. To better identify and understand these uncertainties, I developed a new method to compare number concentrations measured by these two fundamentally different instruments: a chemical ionization mass spectrometer (Cluster CIMS) and a scanning mobility particle spectrometer equipped with a diethylene glycol condensation particle counter (DEG SMPS). The smallest particles that can be detected by the DEG SMPS overlap with the largest clusters that can be detected with the Cluster CIMS. Comparison between these two instruments reveals that nitrate ions do not chemically ionize all types of clusters formed between reactions of sulfuric acid and dimethylamine. Acetate chemical ionization detected higher concentrations and more types of clusters than nitrate chemical ionization, leading to improved agreement between the Cluster

CIMs and the DEG SMPS. In addition, the number concentrations measured by the DEG SMPS in a pure sulfuric acid environment (with water but no base) were higher than predicted, suggesting that either ion-induced particle formation occurs in the charger of the mobility classifier or sulfuric acid reacts with DEG in the condenser and forms particles. Number concentrations in the smallest size bins of the DEG SMPS (~1 nm geometric diameter) may be biased high as a result.

After identifying possible uncertainties in the particle measurements, the DEG SMPS was used to show that reactions of sulfuric acid with atmospherically relevant diamines produce more particles than has been observed with any monoamines (e.g. dimethylamine and methylamine) and ammonia. Little is known about the abundance or chemical behavior of these diamines, and my thesis is the first to examine their role in nucleation. My measurements show that diamines are the most potent nucleating agents discovered to date and can react with sulfuric acid to produce 10-100 times more particles than monoamines in the flow reactor. Putrescine and cadaverine concentrations (both naturally occurring diamines formed via biological decomposition of proteins and other organic matter) were also measured in rural Oklahoma during spring, 2013. Their concentrations (10-100 pptv) were equal to or greater than the measured concentrations of dimethylamine at this site; thus these diamines likely significantly contribute to atmospheric nucleation.

Formation of larger clusters from reactions of sulfuric acid and various monoamines and atmospherically-relevant diamines were investigated in Chapter 5. However, to understand the cluster types and concentrations measured by the Cluster CIMS requires deeper insights into neutral cluster formation, chemical ionization, ion-induced clustering, and ion decomposition than was previously assumed. Ion behavior was studied by varying the chemical ionization reaction time. The results show that ion decomposition occurs and evaporation rates inferred from my measurements qualitatively agree with the cluster types predicted to decompose in computational chemistry simulations. A model was developed to describe these four processes using a series of

cluster balance equations to further interpret the observed trends in measured cluster signals as a function chemical ionization reaction time. The model suggests that certain sulfuric acid+diamine monomers and dimers cannot be ionized by nitrate. Thus, all previous atmospheric measurements of sulfuric acid clusters using nitrate chemical ionization may not be detecting the true cluster concentrations, reinforcing conclusions from Chapter 3.

6.2 Future Work in Nanocluster and Particle Instrumentation

The results presented in Chapters 3 and 5 answer questions regarding the measurement of clusters with the DEG SMPS and the Cluster CIMS. However, many more questions remain. Below is a list knowledge gaps that must be addressed in the future:

1) I show in Chapters 3 and 5 that nitrate is does not chemically ionize all types of clusters. My measurements show that the larger clusters (trimer and larger) are most affected by poor nitrate CI efficiency. In contrast, the DEG SMPS, with its alpha emitting Po-210 source, is able to ionize and detect these neutral clusters. This naturally leads to the question of how does the DEG SMPS charge ~1 nm clusters. The identity of charger reagent ion(s) remains unknown and likely depends heavily on the compounds in the sample flow. Better characterization of the charging ions will provide clues into which particle compositions are being charged and detected by the DEG SMPS. Alternatively, chemical ionization with known ions could be used instead of the Po-210 charger to better control the cluster types detected by the DEG SMPS. Using the method I lay out in Chapter 5, the resulting number concentrations can then be compared to concentrations measured by the Cluster CIMS. This comparison would provide more information on possible sources of uncertainty (e.g. charging efficiency and IIC) of the DEG SMPS which I have not studied.
2) In the same chapters, I show that more types of sulfuric acid+base clusters can be detected if acetate, rather than nitrate, is used at the CI reagent ion. Acetate is a

stronger conjugate base than nitrate and thus can ionize more chemically neutral clusters. Unfortunately as a consequence, acetate is also able to chemically ionize background compounds that will interfere with the signals of sulfuric acid clusters. Due to the vast number of compounds in the atmosphere, the background signals of acetate CI would be too high to meaningfully measure sulfuric acid clusters in the field. Identifying a reagent ion that is capable of ionizing the clusters of interest but without the high background would improve measurements. Alternatively, a higher resolution mass spectrometer could be used with acetate CI to detected sulfuric acid clusters in the field. The higher mass resolution would allow for definitive separation between peaks of interest and background signals.

3) Currently, computational chemistry simulations (primarily conducted by the Vehkamäki group) predict that nitrate is able to chemically ionize near chemically neutral clusters up to two sulfuric acids and two dimethylamines (no results have been published for larger clusters) [*Kupiainen-Määttä et al.*, 2013]. These simulations should be extended to larger clusters and clusters composed of sulfuric acid and diamines. These results can then be compared to measurements presented in Chapters 3 and 5 to determine the validity of the simulation's underlying assumptions (e.g. no energy barriers to proton transfers or molecular rearrangement inside a cluster and charge always resides on the bisulfate ion [*Kupiainen-Määttä et al.*, 2013]).

4) Throughout the studies detailed in this dissertation, the CI reaction time has been calculated based upon inlet dimensions, mobility of the reagent ion, and the electric field. This method assumes gas flows do not affect the CI reaction. The Cluster CIMS samples gas containing the neutral vapors and clusters of interest at a flow rate that can be varied, and a second, much smaller flow is perpendicularly injected into the sample flow (see Figure 1 in Chapter 2) to introduce the reagent ions. Empirical measurements using the Cluster CIMS suggest that these flows play a non-negligible role in the signal intensities and therefore the CI reaction time. Computational fluid dynamic modelling should be done on the sampling region and

mass spectrometer inlet to determine how fluid flow affects CI reaction time and ultimately the calculated cluster concentrations. It is possible that an alternative inlet design might allow for better characterization and reduce the sensitivity to flow.

5) The mass dependent sensitivity for the Cluster CIMS inlet, octopole, quadrupole, and detector has been experimentally measured (see SI of Chapter 5). However, electric fields that control the CI reaction time likely also mass discriminate. A similar mass-dependent sensitivity curve can be experimentally determined for the entire sampling region and mass spectrometer if a high enough concentration (above 10^6 cm^{-3}) of mono-mobile ions could be produced and introduced into the sample tube of the Cluster CIMS. The ions would then be simultaneously counted by the Cluster CIMS and an electrometer. The Cluster CIMS mass-dependent sensitivity is the ratio of its signal response to the ion concentration measured by the electrometer.

6.3 Future Work for the Chemical Reaction Model of Atmospheric Nucleation

Chapters 2, 4, and 5 presented experimental evidence supporting the acid-base chemical reaction model for nucleation. A second generation heuristic model was developed in Chapter 2 and significantly expanded in Chapter 5 to include formation of specific types of clusters using assumptions based upon computational chemistry results for sulfuric acid+dimethylamine clusters. Diamines and sulfuric acid were also shown to produce more particles than monoamines. Overall the results presented here are significant and advance our understanding on the identities of potent nucleation agents and the chemical mechanisms behind nucleation. However, questions remain.

1) Diamines and sulfuric acid produce markedly different cluster compositions and more particles than monoamines. I hypothesize that both amine groups of the diamine react with sulfuric acid to form a more stable cluster. Computational chemistry studies need to be done to test this hypothesis and explore evaporation rates of these clusters. Such work would also help experimentalists interpret their

data. Developing a more comprehensive understanding of sulfuric acid+diamine neutral cluster formation will require coordination between experimental and theoretical research.

2) In addition to neutral cluster formation pathways for sulfuric acid+diamines, the ion behavior of these clusters needs to be studied to better interpret the results presented in Chapter 5. Similar to the sulfuric acid+dimethylamine case, computational chemistry could provide ion decomposition rates of sulfuric acid+diamine clusters that can be used to determine the original identity of the neutral cluster.

3) The focus of this work is on a two component, acid-base system (with water implicitly included). Previous studies have shown that sulfuric acid in the presence of two bases will produce particle concentrations that are much higher than a single base system, where the concentrations approaches levels observed with sulfuric acid+diamine systems [*Glasoe et al.*, 2015; *Yu et al.*, 2012]. The Cluster CIMS was used to measure this synergistic effect between ammonia/methylamine and ammonia/dimethylamine (unpublished results not presented in my thesis). However, the 3 s acid-base reaction time was too short to observe noticeable differences in cluster composition and concentration when compared to a single base system. Likely, the synergistic effect requires more than 3 s to occur at measurable levels. More measurements using the Cluster CIMS should be done at longer reaction times to continue studying this effect. The challenge for these flow reactor experiments will be to minimize wall losses at longer reaction times so that the cluster concentrations are high enough for detection.

4) Relative humidity and temperature also play a large role in nucleation and were not explored in this dissertation. Constant relative humidity was chosen for convenience, and room temperature was chosen to prevent natural convection swirling in the flow reactor/Cluster CIMS sample tube. Relative humidity in the flow reactor can be adjusted by changing the flow rate of humidified nitrogen injected into the reactor. The temperature of the reactor is controlled by an exterior

water jacket. Modifications will need to be done to the Cluster CIMS sample tube (which is directly connected to the flow reactor) to attach it to the flow reactor temperature control system. Natural convection swirling will likely be suppressed by holding the Cluster CIMS sample tube at the same temperature as the walls of the flow reactor.

5) The studies detailed here are the most wide ranging cluster concentration measurements from various sulfuric acid+base environments that have been reported to date. Using these cluster concentrations, evaporation rates for specific cluster types can be calculated using comprehensive cluster balance equations that include neutral cluster formation, chemical ionization, IIC, and ion decomposition. This is similar to the approach taken in Chapter 5 but instead fits all the evaporation rates in addition to E_1. However, the challenge is that all these evaporation rates are interdependent and thus require a complex fitting method to determine them more accurately. Future work should identify a possible fitting method and to use it to estimate evaporation rates from measured cluster concentrations.

References

Almeida, J., et al. (2013), Molecular understanding of sulphuric acid-amine particle nucleation in the atmosphere, *Nature*, *502*(7471), 359-363, doi:10.1038/nature12663.

Ball, S. M., D. R. Hanson, F. L. Eisele, and P. H. McMurry (1999), Laboratory studies of particle nucleation: Initial results for H_2SO_4, H_2O, and NH_3 vapors, *Journal of Geophysical Research: Atmospheres*, *104*(D19), 23709-23718, doi:10.1029/1999JD900411.

Becker, R., and W. Döring (1935), Kinetische behandlung der Keimbildung in übersättigten Dämpfen, *Annalen der Physik*, *5*(24).

Benson, D. R., M. E. Erupe, and S. H. Lee (2009), Laboratory-measured H_2SO_4-H_2O-NH_3 ternary homogeneous nucleation rates: Initial observations, *Geophysical Research Letters*, *36*(15), L15818, doi:10.1029/2009GL038728.

Berresheim, H., T. Elste, C. Plass-Dülmer, F. L. Eisele, and D. J. Tanner (2000), Chemical ionization mass spectrometer for long-term measurements of atmospheric OH and H_2SO_4, *International Journal of Mass Spectrometry*, *202*(1–3), 91-109, doi:10.1016/s1387-3806(00)00233-5.

Bianchi, F., et al. (2014), Insight into Acid–Base Nucleation Experiments by Comparison of the Chemical Composition of Positive, Negative, and Neutral Clusters, *Environmental Science & Technology*, *48*(23), 13675-13684, doi:10.1021/es502380b.

Chen, M., et al. (2012), Acid–base chemical reaction model for nucleation rates in the polluted atmospheric boundary layer, *Proceedings of the National Academy of Sciences*, *109*(46), 18713-18718, doi:10.1073/pnas.1210285109.

Coffman, D. J., and D. A. Hegg (1995), A preliminary study of the effect of ammonia on particle nucleation in the marine boundary layer, *Journal of Geophysical Research: Atmospheres*, *100*(D4), 7147-7160, doi:10.1029/94JD03253.

Dawson, M. L., M. E. Varner, V. Perraud, M. J. Ezell, R. B. Gerber, and B. J. Finlayson-Pitts (2012), Simplified mechanism for new particle formation from methanesulfonic acid, amines, and water via experiments and ab initio calculations, *Proceedings of the National Academy of Sciences*, *109*(46), 18719-18724, doi:10.1073/pnas.1211878109.

DePalma, J. W., B. R. Bzdek, D. J. Doren, and M. V. Johnston (2011), Structure and Energetics of Nanometer Size Clusters of Sulfuric Acid with Ammonia and Dimethylamine, *The Journal of Physical Chemistry A*, *116*(3), 1030-1040, doi:10.1021/jp210127w.

Eisele, F. L. (1983), Direct tropospheric ion sampling and mass identification, *International Journal of Mass Spectrometry and Ion Processes*, *54*(1–2), 119-126, doi:10.1016/0168-1176(83)85011-3.

Eisele, F. L., and D. R. Hanson (2000), First Measurement of Prenucleation Molecular Clusters, *The Journal of Physical Chemistry A*, *104*(4), 830-836, doi:10.1021/jp9930651.

Eisele, F. L., and D. J. Tanner (1993), Measurement of the gas phase concentration of H_2SO_4 and methane sulfonic acid and estimates of H_2SO_4 production and loss in the atmosphere, *J. Geophys. Res.*, *98*(D5), 9001-9010, doi:10.1029/93jd00031.

Erupe, M. E., A. A. Viggiano, and S. H. Lee (2011), The effect of trimethylamine on atmospheric nucleation involving H_2SO_4, *Atmos. Chem. Phys.*, *11*(10), 4767-4775, doi:10.5194/acp-11-4767-2011.

Freshour, N., K. Carlson, Y. A. Melka, S. Hinz, and D. R. Hanson (2014), Quantifying Amine Permeation Sources with Acid Neutralization: AmPMS Calibrations and Amines in Coastal and Continental Atmospheres, *Atmos. Meas. Tech.*, *7*, 3611-3621, doi:10.5194/amt-7-3611-2014.

Ge, X., A. S. Wexler, and S. L. Clegg (2011), Atmospheric amines – Part I. A review, *Atmospheric Environment*, *45*(3), 524-546, doi:http://dx.doi.org/10.1016/j.atmosenv.2010.10.012.

Glasoe, W. A., K. Volz, B. Panta, N. Freshour, R. Bachman, D. R. Hanson, P. H. McMurry, and C. Jen (2015), Sulfuric Acid Nucleation: An Experimental Study of the Effect of Seven Bases, *Journal of Geophysical Research: Atmospheres*, 2014JD022730, doi:10.1002/2014JD022730.

Gross, J. H. (2010), Mass spectrometry a textbook, edited, pp. 1 online resource (xxiv, 753 p.), Springer,, Berlin ; London.

Hanson, D. R., J. B. Burkholder, C. J. Howard, and A. R. Ravishankara (1992), Measurement of hydroxyl and hydroperoxy radical uptake coefficients on water and sulfuric acid surfaces, *The Journal of Physical Chemistry*, *96*(12), 4979-4985, doi:10.1021/j100191a046.

Hanson, D. R., and F. L. Eisele (2002), Measurement of prenucleation molecular clusters in the NH_3, H_2SO_4, H_2O system, *J. Geophys. Res.*, *107*(D12), 4158, doi:10.1029/2001jd001100.

Hanson, D. R., F. L. Eisele, S. M. Ball, and P. M. McMurry (2002), Sizing Small Sulfuric Acid Particles with an Ultrafine Particle Condensation Nucleus Counter, *Aerosol Science and Technology*, *36*(5), 554-559, doi:10.1080/02786820252883793.

Hanson, D. R., and E. R. Lovejoy (2006), Measurement of the Thermodynamics of the Hydrated Dimer and Trimer of Sulfuric Acid, *The Journal of Physical Chemistry A*, *110*(31), 9525-9528, doi:10.1021/jp062844w.

Hanson, D. R., P. H. McMurry, J. Jiang, D. Tanner, and L. G. Huey (2011), Ambient Pressure Proton Transfer Mass Spectrometry: Detection of Amines and Ammonia, *Environmental Science & Technology*, *45*(20), 8881-8888, doi:10.1021/es201819a.

Hiemenz, P. C., and T. P. Lodge (2007), *Polymer Chemistry, Second Edition*, Taylor & Francis.

Iida, K., M. R. Stolzenburg, and P. H. McMurry (2009), Effect of working fluid on sub-2 nm particle detection with a laminar flow ultrafine condensation particle counter, *Aerosol Science and Technology*, *43*(1), 81-96, doi:10.1080/02786820802488194.

IPCC (2014), *Climate Change 2014: Impacts, Adaptation, and Vulnerability. Part A: Global and Sectoral Aspects. Contribution of Working Group II to the Fifth Assessment Report of the Intergovernmental Panel on Climate Change [Field,*

C.B., V.R. Barros, D.J. Dokken, K.J. Mach, M.D. Mastrandrea, T.E. Bilir, M. Chatterjee, K.L. Ebi, Y.O. Estrada, R.C. Genova, B. Girma, E.S. Kissel, A.N. Levy, S. MacCracken, P.R. Mastrandrea, and L.L. White (eds.)], 1132 pp., Cambridge University Press, Cambridge, United Kingdom and New York, NY, USA.

Jen, C. N., D. R. Hanson, and P. H. McMurry (2015), Towards Reconciling Measurements of Atmospherically Relevant Clusters by Chemical Ionization Mass Spectrometry and Mobility Classification/Vapor Condensation, *Aerosol Science and Technology, ARL*, *49*(1), i-iii, doi:10.1080/02786826.2014.1002602.

Jen, C. N., P. H. McMurry, and D. R. Hanson (2014), Stabilization of sulfuric acid dimers by ammonia, methylamine, dimethylamine, and trimethylamine, *Journal of Geophysical Research: Atmospheres*, *119*(12), 2014JD021592, doi:10.1002/2014JD021592.

Jiang, J., M. Attoui, M. Heim, N. A. Brunelli, P. H. McMurry, G. Kasper, R. C. Flagan, K. Giapis, and G. Mouret (2011a), Transfer Functions and Penetrations of Five Differential Mobility Analyzers for Sub-2 nm Particle Classification, *Aerosol Science and Technology*, *45*(4), 480-492, doi:10.1080/02786826.2010.546819.

Jiang, J., M. Chen, C. Kuang, M. Attoui, and P. H. McMurry (2011b), Electrical Mobility Spectrometer Using a Diethylene Glycol Condensation Particle Counter for Measurement of Aerosol Size Distributions Down to 1 nm, *Aerosol Science and Technology*, *45*(4), 510-521, doi:10.1080/02786826.2010.547538.

Jiang, J., J. Zhao, M. Chen, F. L. Eisele, J. Scheckman, B. J. Williams, C. Kuang, and P. H. McMurry (2011c), First Measurements of Neutral Atmospheric Cluster and 1–2 nm Particle Number Size Distributions During Nucleation Events, *Aerosol Science and Technology*, *45*(4), ii-v, doi:10.1080/02786826.2010.546817.

Jokinen, T., M. Sipilä, H. Junninen, M. Ehn, G. Lönn, J. Hakala, T. Petäjä, R. L. Mauldin Iii, M. Kulmala, and D. R. Worsnop (2012), Atmospheric sulphuric acid and neutral cluster measurements using CI-APi-TOF, *Atmos. Chem. Phys.*, *12*(9), 4117-4125, doi:10.5194/acp-12-4117-2012.

Kirkby, J., et al. (2011), Role of sulphuric acid, ammonia and galactic cosmic rays in atmospheric aerosol nucleation, *Nature*, *476*(7361), 429-433, doi:http://www.nature.com/nature/journal/v476/n7361/abs/nature10343.html#supplementary-information.

Kuang, C., P. H. McMurry, and A. V. McCormick (2009), Determination of cloud condensation nuclei production from measured new particle formation events, *Geophysical Research Letters*, *36*(9), L09822, doi:10.1029/2009GL037584.

Kuang, C., P. H. McMurry, A. V. McCormick, and F. L. Eisele (2008), Dependence of nucleation rates on sulfuric acid vapor concentration in diverse atmospheric locations, *Journal of Geophysical Research: Atmospheres*, *113*(D10), n/a-n/a, doi:10.1029/2007jd009253.

Kulmala, M., H. Vehkamäki, T. Petäjä, M. Dal Maso, A. Lauri, V. M. Kerminen, W. Birmili, and P. H. McMurry (2004), Formation and growth rates of ultrafine atmospheric particles: a review of observations, *Journal of Aerosol Science*, *35*(2), 143-176, doi:http://dx.doi.org/10.1016/j.jaerosci.2003.10.003.

Kupiainen-Määttä, O., T. Olenius, T. Kurtén, and H. Vehkamäki (2013), CIMS Sulfuric Acid Detection Efficiency Enhanced by Amines Due to Higher Dipole Moments: A Computational Study, *The Journal of Physical Chemistry A*, *117*(51), 14109-14119, doi:10.1021/jp4049764.

Kupiainen, O., I. K. Ortega, T. Kurtén, and H. Vehkamäki (2012), Amine substitution into sulfuric acid - ammonia clusters, *Atmos. Chem. Phys.*, *12*(8), 3591-3599, doi:10.5194/acp-12-3591-2012.

Kürten, A., et al. (2014), Neutral molecular cluster formation of sulfuric acid–dimethylamine observed in real time under atmospheric conditions, *Proceedings of the National Academy of Sciences*, doi:10.1073/pnas.1404853111.

Kurtén, T., et al. (2011), The effect of H_2SO_4 & amine clustering on chemical ionization mass spectrometry (CIMS) measurements of gas-phase sulfuric acid, *Atmos. Chem. Phys.*, *11*(6), 3007-3019, doi:10.5194/acp-11-3007-2011.

Kurtén, T., L. Torpo, M. R. Sundberg, V. M. Kerminen, H. Vehkamäki, and M. Kulmala (2007), Estimating the NH3:H2SO4 ratio of nucleating clusters in atmospheric conditions using quantum chemical methods, *Atmos. Chem. Phys.*, *7*(10), 2765-2773, doi:10.5194/acp-7-2765-2007.

Larriba, C., and C. J. Hogan (2013a), Free molecular collision cross section calculation methods for nanoparticles and complex ions with energy accommodation, *Journal of Computational Physics*, *251*(0), 344-363, doi:http://dx.doi.org/10.1016/j.jcp.2013.05.038.

Larriba, C., and C. J. Hogan (2013b), Ion Mobilities in Diatomic Gases: Measurement versus Prediction with Non-Specular Scattering Models, *The Journal of Physical Chemistry A*, *117*(19), 3887-3901, doi:10.1021/jp312432z.

Larriba, C., C. J. Hogan, M. Attoui, R. Borrajo, J. F. Garcia, and J. F. de la Mora (2011), The Mobility–Volume Relationship below 3.0 nm Examined by Tandem Mobility–Mass Measurement, *Aerosol Science and Technology*, *45*(4), 453-467, doi:10.1080/02786826.2010.546820.

Leopold, K. R. (2011), Hydrated Acid Clusters, *Annual Review of Physical Chemistry*, *62*(1), 327-349, doi:doi:10.1146/annurev-physchem-032210-103409.

Leverentz, H. R., J. I. Siepmann, D. G. Truhlar, V. Loukonen, and H. Vehkamäki (2013), Energetics of Atmospherically Implicated Clusters Made of Sulfuric Acid, Ammonia, and Dimethyl Amine, *The Journal of Physical Chemistry A*, *117*(18), 3819-3825, doi:10.1021/jp402346u.

Lovejoy, E. R., and J. Curtius (2001), Cluster Ion Thermal Decomposition (II): Master Equation Modeling in the Low-Pressure Limit and Fall-Off Regions. Bond Energies for HSO_4-$(H_2SO_4)_x(HNO_3)_y$, *The Journal of Physical Chemistry A*, *105*(48), 10874-10883, doi:10.1021/jp012496s.

McGrath, M. J., T. Olenius, I. K. Ortega, V. Loukonen, P. Paasonen, T. Kurtén, M. Kulmala, and H. Vehkamäki (2012), Atmospheric Cluster Dynamics Code: a flexible method for solution of the birth-death equations, *Atmos. Chem. Phys.*, *12*(5), 2345-2355, doi:10.5194/acp-12-2345-2012.

McMurry, J. (2008), *Organic Chemistry*, 7th ed., Thomson Brooks/Cole.

McMurry, P. H. (1980), Photochemical aerosol formation from SO_2: A theoretical analysis of smog chamber data, *Journal of Colloid and Interface Science*, *78*(2), 513-527, doi:http://dx.doi.org/10.1016/0021-9797(80)90589-5.

McMurry, P. H. (1983), New particle formation in the presence of an aerosol: Rates, time scales, and sub-0.01 μm size distributions, *Journal of Colloid and Interface Science*, *95*(1), 72-80, doi:http://dx.doi.org/10.1016/0021-9797(83)90073-5.

Murphy, D. M., and D. W. Fahey (1987), Mathematical treatment of the wall loss of a trace species in denuder and catalytic converter tubes, *Analytical Chemistry*, *59*(23), 2753-2759, doi:10.1021/ac00150a006.

Olenius, T., O. Kupiainen-Määttä, I. K. Ortega, T. Kurtén, and H. Vehkamäki (2013), Free energy barrier in the growth of sulfuric acid–ammonia and sulfuric acid–dimethylamine clusters, *The Journal of Chemical Physics*, *139*(8), -, doi:doi:http://dx.doi.org/10.1063/1.4819024.

Ortega, I. K., O. Kupiainen, T. Kurtén, T. Olenius, O. Wilkman, M. J. McGrath, V. Loukonen, and H. Vehkamäki (2012), From quantum chemical formation free energies to evaporation rates, *Atmos. Chem. Phys.*, *12*(1), 225-235, doi:10.5194/acp-12-225-2012.

Ortega, I. K., T. Olenius, O. Kupiainen-Määttä, V. Loukonen, T. Kurtén, and H. Vehkamäki (2014), Electrical charging changes the composition of sulfuric acid–ammonia/dimethylamine clusters, *Atmos. Chem. Phys.*, *14*(15), 7995-8007, doi:10.5194/acp-14-7995-2014.

Ouyang, H., S. He, C. Larriba-Andaluz, and C. J. Hogan (2015), IMS–MS and IMS–IMS Investigation of the Structure and Stability of Dimethylamine-Sulfuric Acid Nanoclusters, *The Journal of Physical Chemistry A*, doi:10.1021/jp512645g.

Paasonen, P., et al. (2012), On the formation of sulphuric acid - amine clusters in varying atmospheric conditions and its influence on atmospheric new particle formation, *Atmos. Chem. Phys.*, *12*(19), 9113-9133, doi:10.5194/acp-12-9113-2012.

Panta, B., W. A. Glasoe, J. H. Zollner, K. K. Carlson, and D. R. Hanson (2012), Computational Fluid Dynamics of a Cylindrical Nucleation Flow Reactor with Detailed Cluster Thermodynamics, *The Journal of Physical Chemistry A*, *116*(41), 10122-10134, doi:10.1021/jp302444y.

Petäjä, T., M. Sipilä, P. Paasonen, T. Nieminen, T. Kurtén, I. K. Ortega, F. Stratmann, H. Vehkamäki, T. Berndt, and M. Kulmala (2011), Experimental Observation of Strongly Bound Dimers of Sulfuric Acid: Application to Nucleation in the Atmosphere, *Physical Review Letters*, *106*(22), 228302.

Pöschl, U., M. Canagaratna, J. T. Jayne, L. T. Molina, D. R. Worsnop, C. E. Kolb, and M. J. Molina (1998), Mass Accommodation Coefficient of H_2SO_4 Vapor on Aqueous Sulfuric Acid Surfaces and Gaseous Diffusion Coefficient of H_2SO_4 in N_2/H_2O, *The Journal of Physical Chemistry A*, *102*(49), 10082-10089, doi:10.1021/jp982809s.

Premnath, V., D. Oberreit, and C. J. Hogan (2011), Collision-Based Ionization: Bridging the Gap between Chemical Ionization and Aerosol Particle Diffusion Charging, *Aerosol Science and Technology*, *45*(6), 712-726, doi:10.1080/02786826.2011.556683.

Riipinen, I., et al. (2007), Connections between atmospheric sulphuric acid and new particle formation during QUEST III-IV campaigns in Heidelberg and Hyytiälä, *Atmos. Chem. Phys.*, *7*(8), 1899-1914, doi:10.5194/acp-7-1899-2007.

Rosser, S., and J. F. de la Mora (2005), Vienna-Type DMA of High Resolution and High Flow Rate, *Aerosol Science and Technology*, *39*(12), 1191-1200, doi:10.1080/02786820500444820.

Schobesberger, S., et al. (2013), Molecular understanding of atmospheric particle formation from sulfuric acid and large oxidized organic molecules, *Proceedings of the National Academy of Sciences*, *110*(43), 17223-17228, doi:10.1073/pnas.1306973110.

Seinfeld, J. H., S. N. Pandis (2006), *Atmospheric Chemistry and Physics- From Air Pollution to Climate Change*, John Wiley and Sons, Inc, Hoboken, NJ.

Slocum, R. D., and H. E. Flores (1991), *Biochemistry and Physiology of Polyamines in Plants*, Taylor & Francis.

Su, T., and M. T. Bowers (1973), Theory of ion-polar molecule collisions. Comparison with experimental charge transfer reactions of rare gas ions to geometric isomers of difluorobenzene and dichloroethylene, *The Journal of Chemical Physics*, *58*(7), 3027-3037, doi:doi:http://dx.doi.org/10.1063/1.1679615.

Titcombe, M. E. (2012), New particle formation: sulfuric acid and amine chemical nucleation, photochemical reaction chamber studies and the laboratory cluster-CIMS, Ph.D thesis, University of Minnesota - Twin Cities, Minneapolis, MN.

Ude, S., and J. F. de la Mora (2005), Molecular monodisperse mobility and mass standards from electrosprays of tetra-alkyl ammonium halides, *Journal of Aerosol Science*, *36*(10), 1224-1237, doi:10.1016/j.jaerosci.2005.02.009.

Viggiano, A. A., J. V. Seeley, P. L. Mundis, J. S. Williamson, and R. A. Morris (1997), Rate Constants for the Reactions of $XO_3^-(H_2O)_n$ (X = C, HC, and N) and $NO_3^-(HNO_3)_n$ with H_2SO_4: Implications for Atmospheric Detection of H_2SO_4, *The Journal of Physical Chemistry A*, *101*(44), 8275-8278, doi:10.1021/jp971768h.

Weber, R. J., J. J. Marti, P. H. McMurry, F. L. Eisele, D. J. Tanner, and A. Jefferson (1996), Measured atmospheric new particle formation rates: implications for nucleation mechanisms, *Chemical Engineering Communications*, *151*(1), 53-64, doi:10.1080/00986449608936541.

Weber, R. J., P. H. McMurry, L. Mauldin, D. J. Tanner, F. L. Eisele, F. J. Brechtel, S. M. Kreidenweis, G. L. Kok, R. D. Schillawski, and D. Baumgardner (1998), A study of new particle formation and growth involving biogenic and trace gas species measured during ACE 1, *Journal of Geophysical Research: Atmospheres*, *103*(D13), 16385-16396, doi:10.1029/97JD02465.

Woo, K. S., D. R. Chen, D. Y. H. Pui, and P. H. McMurry (2001), Measurement of Atlanta Aerosol Size Distributions: Observations of Ultrafine Particle Events, *Aerosol Science and Technology*, *34*(1), 75-87, doi:10.1080/02786820120056.

Yu, H., R. McGraw, and S.-H. Lee (2012), Effects of amines on formation of sub-3 nm particles and their subsequent growth, *Geophysical Research Letters*, *39*(2), L02807, doi:10.1029/2011GL050099.

Zhang, Y., P. H. McMurry, F. Yu, and M. Z. Jacobson (2010), A comparative study of nucleation parameterizations: 1. Examination and evaluation of the formulations, *Journal of Geophysical Research: Atmospheres, 115*(D20), D20212, doi:10.1029/2010JD014150.

Zhao, J., F. L. Eisele, M. Titcombe, C. Kuang, and P. H. McMurry (2010), Chemical ionization mass spectrometric measurements of atmospheric neutral clusters using the cluster-CIMS, *J. Geophys. Res., 115*(D8), D08205, doi:10.1029/2009jd012606.

Zhao, J., J. N. Smith, F. L. Eisele, M. Chen, C. Kuang, and P. H. McMurry (2011), Observation of neutral sulfuric acid-amine containing clusters in laboratory and ambient measurements, *Atmos. Chem. Phys., 11*(21), 10823-10836, doi:10.5194/acp-11-10823-2011.

Zollner, J. H., W. A. Glasoe, B. Panta, K. K. Carlson, P. H. McMurry, and D. R. Hanson (2012), Sulfuric acid nucleation: power dependencies, variation with relative humidity, and effect of bases, *Atmos. Chem. Phys., 12*(10), 4399-4411, doi:10.5194/acp-12-4399-2012.